

## Electrical and thermal properties of high aspect ratio carbon-based polymer nanocomposites.

A research and development in polymer nanocomposites

Master's thesis in Materials Science

EMIL ALISKANOVIC

MASTER'S THESIS 2018:XX

# Electrical and thermal properties of high aspect ratio carbon-based polymer nanocomposites

A research and development in polymer nanocomposites

EMIL ALISKANOVIC



**CHALMERS**  
UNIVERSITY OF TECHNOLOGY

Department of Industrial and Materials Science  
Division of Materials Science  
Polymeric materials and composites

CHALMERS UNIVERISY OF TECHNOLOGY  
Gothenburg, Sweden 2018

Electrical and thermal properties of high aspect ratio carbon-based polymer nanocomposites.  
A research and development in future conductive polymers.  
EMIL ALISKANOVIC

© EMIL ALISKANOVIC, 2018

Examiner: Roland Kádár, Department of Industrial and Materials Science, Chalmers University of  
Technology  
Company supervisor: Thomas Gkourmpis, Borealis AB Stenungsund

Master's thesis 2018:XX  
Department of Industrial and Materials Science  
Division of Materials Science  
Polymeric materials and composites  
Chalmers University of Technology  
SE-412 96 Gothenburg  
Telephone: +46 31 722 10 00

Cover: Graph representing electrical conductivity as function of filler concentration in a polymer matrix according to percolation theory with pictures representing a general microstructure of each region.

Typeset: Times New Roman

## Abstract

This project is a part of a collaboration of Borealis AB Stenungsund with Chalmers University of Technology. The objective of this project is to conduct an experimental study on the effect of different carbon based high aspect ratio fillers and different polymer architectures on the resulting thermal, electrical and morphological properties.

A literature review was performed on the methods of analytical characterization, results of thermal and electrical properties for similarly used materials in this project. A deeper analysis has been made on the percolation theory which is the quintessential driving factor of the high aspect ratio fillers on the electrical properties.

Parameters like filler type, polymer matrix, dispersion method, filler ratios and blend ratios are evaluated with respect to their impact on percolation threshold, degree of crystallinity, thermal stability, melting and crystallization temperature.

Regarding the electrical properties of hybrid filler composites, it showed to have a synergetic effect when substituting 10 wt.% with another type of filler with different dimensionality. This was shown to be the case for three different hybrid systems. The degree of crystallinity was observed to have a parabolic trend where when combining certain fillers with each other. It was found that at equal parts of two different fillers, there was a maximum in the degree of crystallinity. Substituting 10 wt.% of a certain filler type showed to improve electrical properties that may be used in commercial applications to lower the cost of certain products. For further studies, a more in-depth analysis of the relationship between the different fillers could perhaps result in a better hybrid composite.

## Acknowledgements

Firstly, I want to thank Borealis AB Stenungsund for supplying me with materials and for funding this thesis project. A special thanks goes to Dr. Thomas Gkourmpis, who has been my supervisor. I am very thankful for all the support, guidance and experience you have given me for this unique opportunity to research in the field of nanocomposites.

A big thanks to my examiner Senior lecturer Roland Kádár, who has supported me throughout the project. I want to thank you for all the help and advice you have given me in order to think critically, structure my work and thesis in a professional way.

I want to thank PhD. Karolina Gaska who has been my mentor during my thesis work. I am thankful for all the discussions we have had and the instructions of the equipment that has been used on Chalmers University of Technology.

Many thanks to Andrei Ionasc who has been collaborating with me the first half of the project with a focus on the mechanical and rheological properties of the materials that were studied.

I also want to thank Roger Sagdahl and Håkan Millqvist for the helping me with the instruments in the materials processing lab and for installing the equipment needed for the electrical testing.

Finally, I want to thank the Department of Industrial and Materials Science, the Department of Chemistry and Chemical Engineering at floor eight, and the Department of Applied Physics for letting me use your equipment.

Emil Aliskanovic, Gothenburg, June 2018

# Contents

Abstract .....	iii
Acknowledgements .....	iv
Contents .....	v
1. Introduction .....	4
2.1 Theoretical background .....	5
2.2 Carbon based nanomaterial .....	5
2.2.1 Graphene/Graphite nanoplatelets .....	6
2.2.2 Carbon Nano Tubes (CNT) .....	6
2.2.3 Carbon Black .....	7
2.3 Thermoplastic matrices .....	7
2.3.1 Thermal properties of polymer nanocomposites .....	8
2.3.2 Crystallization and melting .....	8
2.3.3 The glass transition temperature .....	9
2.4 Thermo-analytical methods .....	10
2.4.1 Differential Scanning Calorimeter, (DSC) .....	10
2.4.2 Thermogravimetric Analysis, (TGA) .....	11
2.5 Electrical properties of polymer nanocomposites .....	11
2.5.1. Percolation theory .....	12
2.5.1.1 Lattice model .....	13
2.5.1.2 Continuum Model .....	15
2.5.2 Electrical conductivity mechanisms .....	16
2.5.3 Nanofiller parameters affecting electrical conductivity .....	17
2.5.3.1 Aspect ratio .....	18
2.6 Dispersion methods of nanofillers in nanocomposites .....	19
2.6.1 Melt mixing .....	19
2.6.2 Solution mixing .....	20
2.6.3 In-situ polymerization .....	20
3. Methods .....	21
3.1 Material preparation .....	21
3.2 Compounding .....	22
3.3 Compression moulding .....	23
3.4 Sample preparation .....	24
3.5 Analytical characterization .....	24
3.5.1 DC conductivity .....	24
3.5.2 Differential Scanning Calorimetry, (DSC) .....	24
3.5.3 Thermogravimetric Analysis, (TGA) .....	25
3.6 Morphological characterization .....	25
4. Results and Discussion .....	27

4.1 Polyethylene composites .....	27
4.1.1 PE1/F1 .....	27
4.1.2 PE2/F1 .....	29
4.1.3 PE2/F4 .....	32
4.1.4 PE3/F1 .....	34
4.1.5 PE4/F1 .....	35
4.1.6 PE5/F1 .....	36
4.1.7 Summary of polyethylene composites .....	37
4.2 Polypropylene composites .....	39
4.2.1 PP1/F1.....	39
4.2.2 PP2/F1.....	41
4.2.3 Summary of polypropylene composites.....	42
4.3 Electrical properties of PE and PP nanocomposites.....	44
4.4 Hybrid composites .....	45
4.4.1 PP1/F1/F2 .....	45
4.4.2 PP1/F1/F3 .....	47
4.4.3 PE2/F1/F4.....	50
4.5 Blend composites .....	52
4.5.1 PE1/PP1/F1 Method A.....	52
4.5.2 PE1/PP1/F1 Method B.....	53
4.5.3 PE1/PP1/F1 Method C.....	54
Sources of error .....	55
5. Conclusion.....	56
Future work .....	57
Bibliography.....	58

## List of Figures

Figure 1, Schematic model of a spherulite .....	9
Figure 2, (a) Visual representation of DSC with surface contacts inside a furnace in a controlled atmosphere. (b) A typical DSC curve of heat flow as a function of temperature with distinctive transitional peaks of a general thermoplastic.....	10
Figure 3, (a) A visual representation of a typical TGA furnace with a balance. (b) A typical TGA degradation curve of mass as a function of temperature and time. ....	11
Figure 4 Visual representation of the microstructure of a nanocomposite containing a nanofiller which are represented as doth. With increased filler concentration there is an increase amount of electrically conductive pathways that are formed.....	12
Figure 5 A graph representing electrical conductivity as a function of filler concentration according to the percolation power law dependency. ....	12
Figure 6 Lattice model.....	13
Figure 7, (a) Visual representation of a Hard-core with soft shell rod like and spherical particles. (b) Visual representation of a Hard-core rod like and spherical particles. ....	15
Figure 8, A visual representation of a cross section of an internal chamber mixer with two counter rotating rotors.....	20
Figure 9, Flow chart of the protocol for incorporating and testing the nanocomposites.....	21
Figure 10, Glovebox with an intermediate chamber connected to a ventilation system. Image courtesy of Roland Kádár.....	21
Figure 11, Powder dispenser. Image courtesy of Roland Kádár. ....	22
Figure 12, Internal mixing chamber of compounder. ....	22
Figure 13, DC setup of power supply, safety box with crocodile clamps and multimeter. Image courtesy of Roland Kádár.....	24
Figure 14, Numbered samples mounted on a sample holder. ....	26
Figure 15, (a) DSC curve where heatflow is in a function of sample temperature, showing crystallization peaks of different compositions of PE1 with filler F1. (b) DSC curve where heatflow is in a function of sample temperature, showing melting peaks of different compositions of PE1 with filler F1.....	27
Figure 16, (a) TGA curves of the degradation of different compositions of PE1 with filler F1 (b) Calculated onset temperatures for PE1/F1 in a function of filler loading. ....	27
Figure 17, (a) SEM picture of pure PE1 at a magnification of 1000x (b) SEM picture of PE1/0,5wt.% F1 at a magnification of 1000x.....	28
Figure 18, (a) SEM picture of PE1/2wt.%F1 at a magnification of 1000x (b) SEM picture of PE1/4wt.%F1 at a magnification of 1000x.....	28
Figure 19, The electrical conductivity as a function of. filler loading of PE1/F1 with a fitted curve according to the percolation threshold powerlaw equation.....	29
Figure 20, (a) DSC curve of melting peaks of different compositions of PE2 with filler F1, (b) DSC curve of crystallization peaks of different compositions of PE2 with filler F1 .....	29
Figure 21, TGA curve of the degradation of PE2 with 5wt.% of filler F1 .....	30
Figure 22, (a) SEM of pure PE2 at a magnification of 1000x, (b) SEM of PE2/1,5%F1 at a magnification of 1000x .....	31
Figure 23, Electrical conductivity as a function of filler loading of PE2 with filler F1 .....	31
Figure 24, (a) DSC curve of melting peaks of different compositions of PE2 with filler F4, (b) DSC curve of crystallization peaks of different compositions of PE2 with filler F4 .....	32
Figure 25, (a) SEM of PE2/0,125wt.%F4 at a magnification of 1000x, (b) SEM of PE2/0,15wt.%F4 at a magnification of 1000x.....	32
Figure 26, SEM of PE2/1wt.%F4 at a magnification of 1000x.....	33
Figure 27, Electrical conductivity as a function of filler loading of PE2 with filler F4 .....	33
Figure 28, (a) DSC curve of crystallization peaks of different compositions of PE3 with filler F1, (b) DSC curve of melting peaks of different compositions of PE3 with filler F1. ....	34
Figure 29, (a) DSC curve of crystallization peaks of different compositions of PE4 with filler F1, (b) DSC curve of melting peaks of different compositions of PE3 with filler F1 .....	35
Figure 30, (a) DSC curve of crystallization peaks of different compositions of PE4 with filler F1, (b) DSC curve of melting peaks of different compositions of PE3 with filler F1 .....	36

Figure 31, Electrical conductivity as a function of filler loading of PE5 with filler F1 .....	36
Figure 32, Crystallization temperature as a function of filler of polyethylene composites with fillers F1 & F4 .....	37
Figure 33, Melting temperature as a function of filler of polyethylene composites with fillers F1 & F4.....	37
Figure 34, Degree of crystallinity as a function of filler of polyethylene composites with fillers F1 & F4.....	38
Figure 35, (a) DSC curve of melting peaks of different compositions of PP1 with filler F1, (b) DSC curve of crystallization peaks of different compositions of PP1 with filler F1. ....	39
Figure 36, (a) TGA curves of the degradation of different compositions of PP1 with filler F1, (b) Onset temperature calculated from the TGA of the different compositions of PP1/F1.....	39
Figure 37, (a) SEM picture of pure PP1 at a magnification of 993x, (b) SEM picture of PP1/0,5%F1 at a magnification of 1000x.....	40
Figure 38, Electrical conductivity as a function of filler loading of PP1 with filler F1 .....	40
Figure 39, (a) DSC curve of crystallization peaks of different compositions of PP1 with filler F1, (b) DSC curve of melting peaks of different compositions of PP1 with filler F1. ....	41
Figure 40, Electrical conductivity as a function of filler loading of PP2 with filler F1 .....	41
Figure 41, Crystallization temperature as a function of filler of polypropylene composites with filler F1 .....	42
Figure 42, Melting temperature as a function of filler of polypropylene composites with filler F1 .....	42
Figure 43, Degree of crystallinity as a function of filler of polypropylene composites with filler F1 .....	43
Figure 44, Electrical conductivity of all single filler and single polymer composites .....	44
Figure 45, (a) DSC curve of melting peaks of different compositions of PP1 with fillers F1&F2, (b) DSC curve of melting peaks of different compositions of PP1 with fillers F1&F2.....	45
Figure 46, (a) SEM picture of PP1 with 4wt.% of filler F2 at a magnification of 1000x, (b) SEM picture of PP1 with 4wt.% of fillers 90wt.%F1 & 10wt.%F2 at a magnification of 1000x. ....	45
Figure 47, Electrical conductivity as a function of filler loading of PP2 with filler F1 & F2 and reduced mass fraction of F1 represented as hollow symbols. ....	46
Figure 48, (a) DSC curve of melting peaks of different compositions of PP1 with fillers F1&F3, (b) DSC curve of crystallization peaks of different compositions of PP1 with fillers F1&F3. ....	47
Figure 49, (a) SEM picture of PP1 with 4wt% of filler F3 at a magnification of 1000x, (b) SEM picture of PP1 with 4wt% of fillers 90wt.%F1 & 10wt.%F3 at a magnification of 1000x.....	47
Figure 50, (a) Melting and crystallization temperatures as a function of filler ratio between the fillers F1&F2&F3, (b) Degree of crystallinity as a function of filler ratio between the fillers F1&F2&F3.....	48
Figure 51, Electrical conductivity as a function of filler loading of PP2 with filler F1 & F3 and reduced mass fraction of F1 represented as hollow symbols. ....	49
Figure 52, (a) DSC curve of melting peaks of different filler ratios of PP1 with 1wt.% of fillers F1&F4, (b) DSC curve of crystallization peaks of different filler ratios of PP1 with 1wt.% of fillers F1&F4.....	50
Figure 53, (a) SEM picture of PE2 with 1wt% of fillers 90%F1 & 10%F4, (b) SEM picture of PE2 with 1wt% of fillers 10%F1 & 90%F4. ....	50
Figure 54, (a) DSC curve of melting peaks of different filler ratios of PP1 with 0,1wt.% of fillers F1&F4, (b) DSC curve of crystallization peaks of different filler ratios of PP1 with 0,1wt.% of fillers F1&F4.....	51
Figure 55, Electrical conductivity as a function of filler loading of PE2 with filler F1 & F4 and reduced mass fraction of F4 represented as hollowed symbols. ....	51
Figure 56, (a) DSC of a two polymer blend composites where one consisting of 90% PE1 and 10% PP1 and the other has 5wt% of filler F1 in the 10% PP1 phase. The manufacturing method was dry mixing, (b) DSC of a two polymer blend composites where one consisting of 9 .....	52
Figure 57, (a) SEM picture of a polymer blend of 90% PE1 10% (PP1/5wt% F1). The manufacturing method was dry mixing, (b) SEM picture of a polymer blend of 90% PP1 10% (PE1/5wt% F1). The manufacturing method was dry mixing. ....	52
Figure 58, (a) DSC of a two polymer blend composites where one consisting of 90% PP1 and 10% PE1 and the other has 5wt% of filler F1 in the 10% PE1 phase. The manufacturing method was liquid mixing, (b) DSC of a two polymer blend composites where one consisting o .....	53
Figure 59, DSC curves of 90:10 and 10:90 blends of PE1 and PP1 with 5wt% of F1 in the 10% of respective phase.....	54
Figure 60, (a) SEM picture of a polymer blend of 90%PE1 10% (PP1/5wt% F1). The manufacturing method was chunk mixing., (b) SEM picture of a polymer blend of 90%PP1 10% (PE1/5wt% F1). The manufacturing method was chunk mixing.....	54

## List of Tables

Table 1, Filler residue calculated from the TGA of the different compositions of PE1/F .....	28
Table 2, Table of calculated residue from TGA of PE2 with F1 compared to desired filler loading of F1 .....	30
Table 3, Table of calculated residue from TGA of PE1 with F1 compared to desired filler loading of F1 .....	39
Table 4, Table of all percolation thresholds of single filler composites of PP and PE .....	44

# 1. Introduction

This project is part of a collaboration between Chalmers and Borealis on the commercially and scientifically important field of polymer nanocomposites. Borealis is a world leader of innovative plastics materials and have intensive research activities in many fields ranging from high voltage power cables to automotive parts and films used in the food industry, covering the entire range from polymer design and catalysis to processing and mechanical performance. Chalmers is recognized as a world-leading centre of excellence in material science ranging from fundamental to applied research.

The objective of this student project is to conduct an experimental study on the effect of different carbon based high aspect ratio fillers and different polymer architectures have on the resulting electrical, thermal and morphological properties. Different polymer compounds on different polymeric types with a variety of filler loadings will be made and optimized. These compounds were then being tested, and their overall performance was assessed with respect to their electrical properties.

Some of questions that are central for the understanding of these phenomena that this project will aim to address are:

- How different processing conditions affect the overall dispersion of high aspect ratio fillers?
- How the chain conformation affects the resulting electrical performance?
- What is the effect of the different fillers on the overall crystallization behaviour and resulting morphology?

Lastly, the limitations of the projects' characterization methods were restricted to the availability of equipment at Chalmers University of Technology. The characterization methods were focusing on retrieving information of the electrical, thermal and morphological properties. The work was mainly based on the Department of Industrial and Material Science but support and equipment from the Department of Applied Physics and Chemistry and Chemical Engineering will also be available.

## 2.1 Theoretical background

Polymer nanocomposites is a combination of a polymer matrix with either an organic or inorganic material where at least one of its dimensions are in the nanoscale. The typical way of classifying nanomaterials is to identify them in relation to their dimensionality where they can be classified as either zero-dimensional, one-dimensional, two-dimensional or sometimes even three-dimensional. The term “nano” in nanocomposites usually stands for the smallest scale of fillers that are used in composites. Their size of nanoparticles are usually considered to be below 100 nm, at least in one of its dimensions [1],[2]. Because the fillers size, it establishes an interaction down to the size of an individual polymer chain. Hence, this may give a possibility to control different mechanisms which in turn results in an influence on the micro scale.

Zero-dimensional nanomaterials are materials where all of its dimensions are below 100 nm. One-dimensional differs from zero-dimensional by having one dimension that is outside the nanoscale, e.g. of materials could be nano- wires, tubes or rods. Two-dimensional nanomaterials are harder to classify since some materials are classed as two-dimensional simply because of its internal structure being two-dimensional. Nevertheless, two-dimensional materials are materials where two of its dimensions are not confined in the nanoscale [3].

Many application fields use material in its pure form; however, it is more likely that engineering materials are used as hybrid materials where the combined materials give new materials with tailored properties. One such field is polymer nanocomposites where a nanomaterial is introduced to a polymer matrix giving new material properties that was not achievable for each separate constituent.

Polymer nanocomposites have shown promising results in different applications. The critical part of making a successful application of the composite is to understand the impact the nanofiller has on the entire composite. These impacts might be an increase in mechanical, electrical, rheological, thermal etc. Many research groups have narrowed their studies in chemistry and morphology of the polymer matrix in combination with the fillers surface chemistry, shape, and size in order to further understand the enhanced properties the nanofillers grant. The secret in understanding of nanocomposites lies in understanding the intersecting mechanisms or interactions of physics, chemistry, materials science and continuum mechanics between filler and polymer [1].

The terms “agglomerate” and “aggregate” will be used in this work to define the assemblages of the particles in the polymer melt. Each term has its unique meaning, which has very often been described incorrectly in literature. A review of the terms has been scrutinized by G. Nichols et.al. (2002) [4], and they concluded that the terms are currently used interchangeably without any consideration of their meanings. They have proposed the following definitions for each word as; The term agglomerate is used when one describes the particle assemblage. Hard and soft agglomerates can be determined where hard agglomerates are described as brittle agglomerates which can be fractured by applying extensive force. The term aggregate should be used only to describe the prenucleation of the structure that arises from the supramolecular structures which later way develop into agglomerates [4].

## 2.2 Carbon based nanomaterial

Carbon based nanomaterials are widely used in different applications due to their unique properties when combined with other materials such as improving electrical conductivity, thermal conductivity, corrosion resistance, mechanical properties, surface chemistry, tribological properties, etc. Depending on the type of filler, the properties can vary. The nanofiller with most desired effects suitable for an application must be chosen. The shape of the filler is one of the most influencing parameters when it comes the interaction between the particle and the matrix. The aspect ratio is such a parameter that can quantify the level of interaction between the two systems. The aspect ratio is the ratio between an objects longest dimension to its shortest. The particles can broadly be classified as, [5]:

- (Quasi-) Spherical particles
- Whiskers and rods particles
- Platelets (lamellar) particles

### 2.2.1 Graphene/Graphite nanoplatelets

Graphene is an allotrope of carbon arranged in a two-dimensional honeycomb lattice with a  $sp^2$ -hybridized bonding. Since its recent discovery it has received enormous attention in academia due to its exceptional mechanical, thermal, and electrical properties. Polymer nanocomposites containing graphene is one field that has attracted attention due to its promising enhancements to a polymer matrix compared to other fillers that requires much higher filler loadings to achieve same results [6]. Graphene possesses in general a high surface area and high aspect ratio which results in increase in electrical and thermal conductivity, tensile modulus and gas barrier properties when incorporated into a polymer matrix. A single graphene sheet has a Young's modulus of 1 TPa and an ultimate tensile strength of 130 GPa. It has a specific area of  $2600 \text{ m}^2/\text{g}$  and electric conductivity of  $6 \cdot 10^5 \text{ S/m}$  [7]. Incorporating graphene into a polymer matrix can be complex due to some polymers' nonpolar nature and the fact that the nanofiller tends to be thermodynamically driven to aggregate. There are different methods that can improve the compatibility between the graphene and the polymer however by increasing the interfacial adhesion, however they usually require further modification or functionalization of the graphene which not only makes the process more difficult but also tends to disrupt the honeycomb structure of the graphene resulting in a decrease in electrical conductivity [8].

The synthesis of graphene in large scales has been a challenge. Today there are different synthesis methods, but they are usually classified into three routes of processing which are:

- Mechanical exfoliation
- Chemical exfoliation
- Chemical vapor deposition

Mechanical exfoliation is a top-down method which means that pyrographic graphite, which is the raw material, is stripped down to its essential component, which are single layers of graphene, by physically peeling of layer by layer mechanically. This was initially done by using scotch tape but today there are more complex systems. The yield of filler is too low to be used as a composite by this method. An alternative for large scale production is to chemically oxidize the graphite which later is exfoliated by ultrasonication. However, this method implies the use of a solvent which furthermore complicates the preparation process.

Similarly, chemical exfoliation is also a top-down method. In chemical exfoliation the graphite is put into a mixture of acids where and oxidation of the surface initiates cleavage of the layers. The separation of the layers usually goes down to 4-5 layers of graphene, however with additional steps it is possible to increase the yield by rapidly evaporating the acids. The drawback with this method is that the surface can have defects on them thus changing the physical properties once incorporated into a matrix. There are methods which includes a mix between mechanical and chemical exfoliation for higher yields.

Chemical vapor deposition or CVD is a bottom-up method where a monolayer of graphene is synthesized by decomposing the carbon which is fed into the system into atomic carbon. Then by using catalysts, the atomic carbon can be rearranged on a surface into a graphene lattice system [9].

The terminology of graphene in research has been used in a generic manner and often not represented correctly since graphene is a single layer of carbon, while some research papers have used the word graphene for few layered graphene or even graphite nanoparticles which consists of several layers of graphene it is actually incorrect to call it graphene if it does not consist of a single layer of carbon.

### 2.2.2 Carbon Nano Tubes (CNT)

CNT is essentially a graphene sheet rolled into a cylinder making the morphological structure resemble rods or whiskers. There are two types of CNT's: Single walled carbon nanotubes (SWCNT) and multiple walled carbon nanotubes (MWCNT). They also have three types of lattice structure: zigzag, armchair, and chiral lattice structure. The properties of the CNT's are strongly dependent on the length, diameter, number of walls and what type of structure. In electrical perspective the CNT can either be conductive or semi-conductive due to the lattice structure [9].

Due to the CNT's elongated structure, they are desired for enhancing both mechanical and electrical properties.

The synthesis of CNT can be carried out by several different preparation methods such as: arc evaporation, chemical vapor deposition, electrolysis, laser ablation etc. The most common methods are arc evaporation, CVD, and laser ablation. The arc evaporation method creates CNT in a plasma between graphite electrodes in the presence of a gas. The CVD synthesis of CNT is like the graphene synthesis however the geometry of the catalyst is what decides what type of morphology the end product will have. Laser ablation utilizes lasers to vaporize a carbon source doped with small amounts of metal catalysts in the presence of an inert gas at high pressures [9].

### **2.2.3 Carbon Black**

Carbon black is a carbon-based filler that is usually divided into subgroups of thermal-, furnace-, channel- and acetylene blacks. The material consists of elemental amorphous carbon in quasi-spherical particles coalesced into aggregates and agglomerates [10]. The processing method dictates what kind of carbon black will be produced but the essential technique is the same which is the thermal decomposition of hydrocarbons [11]. Thermal blacks are produced by the thermal decomposition of natural gas while acetylene black is thermally decomposed acetylene in the absence of oxygen. The characteristics carbon black differs from the processing method thus influencing the particle properties in polymer compounds. Carbon blacks are electrically conductive however when incorporated into a high resistance polymer matrix as a composite it acts as semiconductor. The compound conductivity however depends on the grade of carbon black and the filler load. The particle aggregate size is on average 10nm in lower filler loadings. [10].

## **2.3 Thermoplastic matrices**

Thermoplastics consists of long polymer molecules with a repeating unit of its monomer. Generally, they are not cross-linked and can be repeatedly melted. Compared to thermoset plastics, thermoplastics does not undergo any chemical change when it cures. The main advantage of thermoplastics is that they are easier to process due to their softening and ability to flow upon heating. Compared to thermoset plastics, thermoplastics lack covalent bonding between the chain, they instead rely heavily on intermolecular forces such as Van der Waals forces to hold the chains together. The degree of crystallinity often contributes to higher mechanical strength and the amorphous part contributes elasticity and impact strength [2]. Thermoplastics have in general high impact strength due to their toughness [12].

Thermoplastics are most often provided in the form of pellets, granulates or powder. Different forms are preferable over others depending on what application of moulding method is used.

### 2.3.1 Thermal properties of polymer nanocomposites

Heat can be defined as atoms or molecules in motion. In solid materials heat is presented as vibration in their local position. The temperature is higher when the molecules vibrate in a higher amplitude. This is the basis of understanding the fundamentals of solids thermal properties such as heat capacity, expansion coefficient, conductivity, and melting and glass transition temperatures.

Heat affects other material properties such as mechanical, electrical and optical. With an increase of temperature, the material expands and as a result, mechanical property such as the elastic modulus decreases, tensile strength decreases and is more prone to creep. The properties will continually decrease the more one approaches the melting temperature.

The two fundamental reference temperature points that need to be covered are the melting point  $T_m$  and the glass transition temperature  $T_g$ . Crystalline solids like metals have a sharp melting point while non-crystalline materials such as amorphous polymers usually don't have. The melting temperature  $T_m$  is the highest temperature where crystalline structures can exist in a polymer. If the temperature of a polymer sample exceeds this value, the polymer can be considered to be a viscous or viscoelastic liquid [13]. The glass transition temperature describes the characteristic transition from being a solid to a viscous liquid [14]. When mixing two immiscible polymers, two glass transition temperatures will be observed [13].

Adding heat to a material costs energy, this energy is called the heat capacity or the specific heat  $C_p$  at constant pressure. It is defined as energy amount to heat 1 kg of a material heated by 1 K, therefore the unit being in the form of  $J/kg K$  where heat is measured in Joules, J. The method of measuring the heat capacity is done by a technique called calorimetry.

A measured energy quantity is added into a sample with a known mass. The increased energy content results in an elevated temperature of the sample which is also measured thus giving the calculated value of the heat capacity [14].

### 2.3.2 Crystallization and melting

Crystallization of a polymer occurs when a polymer melt is cooled below the melt temperature  $T_m$ . Due to polymolecularity of polymers a 100% crystallization is impossible to achieve. Polymer crystallization is dominated of the phenomena that untangled molecules straighten out and then attach themselves to a crystal face. This process is slow and is accelerated by rapidly cooling the polymer [2]. Consequently, these polymers are referred to be semi-crystalline. Therefore, it is assumed that semi-crystalline structures occur in small regions where crystallites are connected to the amorphous molecules. Crystallization is initiated at different points in the melts often by impurities. The impurity acts as a nucleation site for the melt. There are various existing crystalline structures that have been recognized [15]:

*Single crystals.* Forms usually in solutions in order to study crystal formation.

*Spherulites.* The spherulite growth is the growth of several folded crystal lamellae. The direction of lamella growth is in the radial direction from the nucleus centre of the spherulite. The growth will stop until the spherulite meets a neighbouring spherulite. Amorphous polymer that do not stack to the crystalline lamellae is left in between. Some linear polymers can undergo a second crystallization due to the fact that the macromolecules of those polymers are identical to those which have crystallized. Secondary crystallization is slow and the primary is rapid. This proceeds the spherulite to become more solid, however if the polymer consists of irregularities such as branches, co-polymer units, crosslinked or having atactic arrangements, these types will be rejected by the crystallizing lamellae and will be left in the amorphous phase, thus having an overall increased concentration of the amorphous fraction.

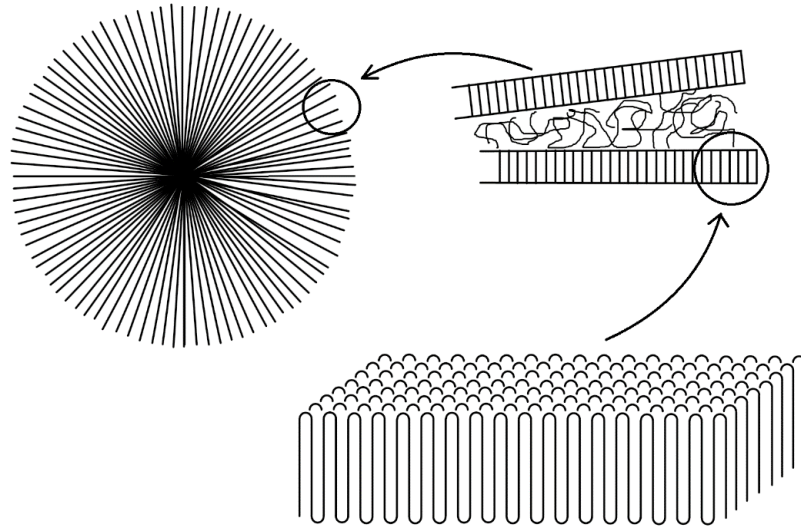


Figure 1, Schematic model of a spherulite with crystalline lamellas and amorphous as structural components.

*Deformed crystals.* If the polymer is deformed while crystallizing spherulites, they will instead form oriented lamellae.

*Shish-kebab.* Shish-kebabs, like the name suggests, contains groups of oriented fibrils, the shish in the kebab, and crystallized polymer lamellae are attached to the shish, which are the kebabs. [13], [15].

Crystallization associates with both diffusion and nucleation of the polymer. Diffusion occurs faster in short ranges and in elevated temperatures. Below the glass transition temperature, virtually all molecules in a polymer are completely frozen when it comes to diffusive processes. When a polymer chain diffuses it forms a stable nucleus when it reaches a crystal boundary. The surface energies provide an increase in the free energy which results from the fact that below the equilibrium melting point, the crystallization free energy is negative thus resulting as decreased energy when nucleating on a surface:

$$\Delta G = \Delta g V_{crystal} + \sum_i A_i \sigma_i \text{ [J]} \quad (2.1)$$

Where  $\Delta G$  is the free energy,  $\Delta g$  the change in specific free energy,  $V_{crystal}$  is the volume of the nucleus and  $A_i \sigma_i$  is the specific surface energy with the area of  $i$ . [16]

The existence of a nanofiller inside a polymer matrix will therefore complicate the matter of crystallization since the nucleation of the polymer depends on the specific surface energy that the nanofiller provides.

The crystallization of polymers such as polyethylene and polypropylene is generally found to nucleate a given number of spherulites for a given volume at an isothermal temperature close to the melting temperature. There is a higher nucleation of spherulites if the crystallization temperature is reduced. Adding nucleating agents such as a nanofiller may increase the crystallization temperature thus increasing the degree of crystallinity to the polymer [2].

### 2.3.3 The glass transition temperature

Those polymers that does not crystallize below the crystallization temperature even when cooled very slowly from the molten state are called amorphous polymers. The main effect of cooling the melt is that the amplitude and frequency of the molecular vibration is decreasing. The polymer which consists of long molecules if cooled sufficiently will start to behave more like a tangled liquid yet still being extremely sluggish. This is known as the glassy state of a polymer. It differs from the liquid state only in one respect which is the immobility of the molecular backbones [15].

A noticeable change in properties of the polymer of the polymer is in its specific volume. When an amorphous polymer is heated and approaches the glass transition temperature, a sudden increase in the specific volume can be observed. This is due to thermal expansion in the glassy state that increases the separation of crumbled

yet immobile molecules. They do not change their local position, only their distance from one another. Only if the amorphous polymer is heated surpassed the glass transition temperature is when it starts to behave more like a liquid [15]. The elastic modulus below and above the  $T_g$  can have a difference in a factor of 1000 [16].

## 2.4 Thermo-analytical methods

Modern analytical instruments make it possible to measure thermal properties of polymer with a high degree of accuracy. In order to execute precise calculations and simulations of polymer properties the accuracy is a necessity.

### 2.4.1 Differential Scanning Calorimeter, (DSC)

Differential Scanning Calorimeters are used to determine the thermal transitions of polymers usually in a range between  $-180\text{ }^\circ\text{C}$  and  $+600\text{ }^\circ\text{C}$  [13]. Most usually they are used to observe both crystallization and melting. Samples are placed inside containers, usually called pans, then set inside a chamber that contains two stages of placement which have embedded thermocouples. One stage for the pan with the sample inside and another stage for a reference pan. The thermocouples contact the container from the outside, usually the bottom area. Figure 2a shows a simple schematic of DSC furnace setup.

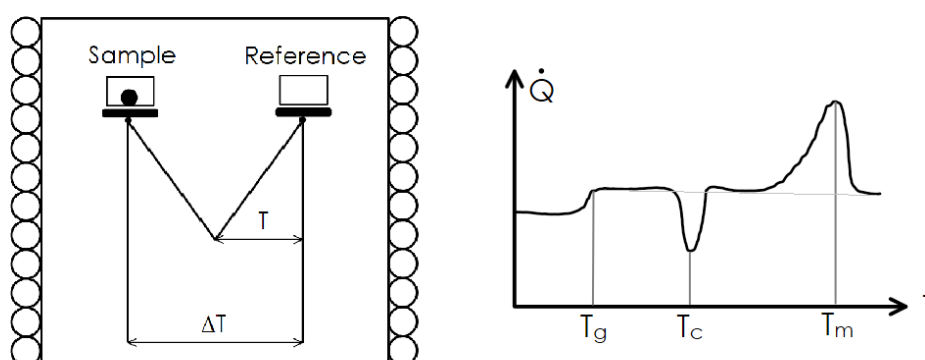


Figure 2, (a) Visual representation of DSC with surface contacts inside a furnace in a controlled atmosphere. (b) A typical DSC curve of heat flow as a function of temperature with distinctive transitional peaks of a general thermoplastic.

The machine scans through the range of temperatures while simultaneously collecting data and measuring differential temperature between the sample and the reference pans. The DSC analysis usually requires that samples are below 10mg.[13]

Figure 2b shows a typical endothermic melting of a semicrystalline polymer undergoing a glass-, a re-crystallization and a melting transition on a heat flow vs. temperature diagram. When reaching the glass transition an increase in the heat flow, also called an endothermic reaction, is observed. When the temperature is cooling down from the melt temperature and approaching the crystallization temperature, an exothermic reaction is taking place. This is due to the crystalline state is giving off heat when going to a lower state of energy. In contrast to crystallization, the melting peak is an endothermic reaction since it takes energy in order to transition to a molten state [13], [16].

Since the change value is measured in heat flow, the area under the curve integrated to the trend baseline in a function of time would naturally be the amount of heat. The area, or the heat, under the peaks are called enthalpies. They can be formulated as following:

$$\Delta H_f^0 = \int_{T_1}^{T_m^0} \Delta C_{p,c} dt \text{ [J/g]} \quad (2.2)$$

where  $\Delta C_{p,c}$  is the specific heat difference between the liquid and crystalline phase,  $T_m^0$  is the equilibrium melting temperature,  $\Delta H_f^0$  is the theoretical 100% crystalline value of heat of fusion.

The degree of crystallinity  $\chi$  is defined as the ratio between the heat of fusion of a polymer sample  $\Delta H_f$  and the heat of fusion of for a 100% crystalline polymer  $\Delta H_f^0$ .

$$\chi = \frac{\Delta H_f}{\Delta H_f^0} * 100 \text{ [%]} \quad (2.3)$$

The value of  $\Delta H_f^0$  differs in different polymers. Polyethylene has been found to be  $\Delta H_f^0 = 294.2 \text{ J/g}$  at equilibrium temperature according to P.Cebe et.al (2017) [17]. Polypropylene has a 100% theoretical heat of fusion of  $\Delta H_f^0 = 206.8 \text{ J/g}$  according to Springer Materials database [18],[19].

### 2.4.2 Thermogravimetric Analysis, (TGA)

A thermogravimetric analyser measures the change in weight of less than  $10 \mu\text{g}$  as a function of time and/or temperature [13]. The analysis is used to observe derived values such as; thermal stability, decomposition behaviour, sample composition (e.g. ratio between filler and polymer) amongst other values. Measurement are performed in either isothermal conditions or programmed temperature sweeps where the instrument permits a continuous measurement of weight as a function of temperature and time [16]. The atmosphere can be controlled by pumping a flow of various gases inside the furnace chamber. Usually inert gases such as argon or nitrogen are used to avoid oxidation. The maximum sample weight during TGA are around  $500 \text{ mg}$  [13]. If the sample is too large it may develop thermal gradients within the specimen, in other words, a temperature deviation from the set temperature. Instead, finer powders are recommended for quantitative analysis [16].

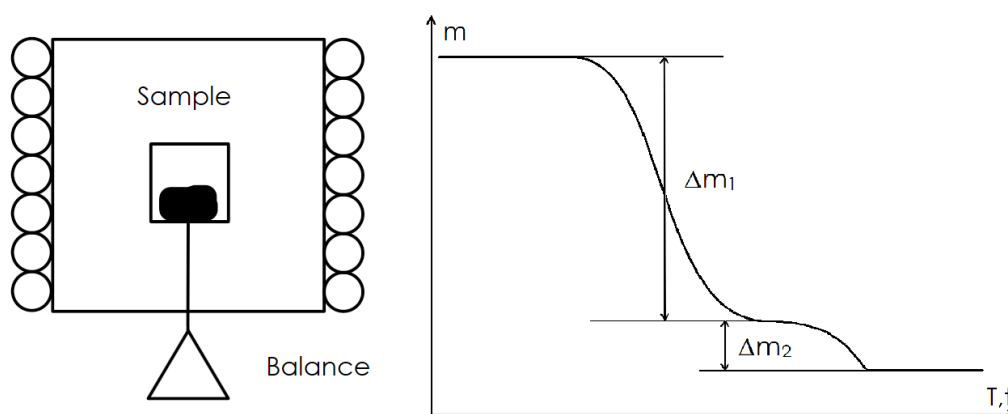


Figure 3, (a) A visual representation of a typical TGA furnace with a balance.  
(b) A typical TGA degradation curve of mass as a function of temperature and time.

Figure 3 above shows a general case of a polymer containing a filler. The figure shows the transitions where different components of the specimen undergoes decomposition. During these transitions a reduction in mass is observed. This change in mass is measured and can be used to calculate the proportion of each composition. The change in mass  $\Delta m_1$  from Figure 3 is the mass difference in the decomposition of the polymer, while  $\Delta m_2$  is the decomposition of the filler material which decomposes at an elevated temperature.

## 2.5 Electrical properties of polymer nanocomposites

Most polymers are intrinsically insulating in nature since they lack delocalized electrons compared to metals. However, it is possible to make an insulating polymer semi-conductive or perhaps even conductive by introducing a conductive nanomaterial to its matrix. Having a connectivity and spatial arrangements of the conductive nanofiller within an isolating matrix can result in a macroscopic effect which increases the overall electrical conductivity dramatically. This effect of sudden increase in conductivity when introducing nanofillers is called percolation theory. The basic principle of the step phenomena can be explained by when dispersing nanofiller into a polymer, the nanoparticles tend to agglomerate and thus form “pathways” where the particles connect, thereby making the composite conductive. There are many theories trying to explain the electrical percolation phenomena by incorporating some parameters such as filler concentration, filler distribution, filler shape, filler/matrix interaction and the processing technique involved [20]. Most theories try

to explain how and why the nanofiller are arranging in such a way that they result in a macroscopic electrical connectivity. It is believed that the physical driving forces are most likely to be statistical, geometrical, thermodynamic and quantum tunnelling in origin [21].

### 2.5.1. Percolation theory

Percolation models have been successful to various degrees when trying to explain the electrical behaviour of polymer nanocomposites. Experimental and theoretical predictions have established that the sharp insulation-conductor transition can be explained by a fitting of a power-law dependence curve, which is as followed:

$$\sigma = \sigma_0(\varphi - \varphi_c)^t, \quad \varphi > \varphi_c \text{ [S/m]} \quad (2.4)$$

$$\sigma = \sigma_i(\varphi_c - \varphi)^{-s}, \quad \varphi < \varphi_c \text{ [S/m]} \quad (2.5)$$

where  $\sigma$  is the bulk conductivity,  $\sigma_0$  and  $\sigma_i$  is the conductivity of the filler,  $\varphi$  and  $\varphi_c$  are the filler fraction and the critical filler concentrations and the exponents  $t$  and  $s$  determine the power of the conductivity increase [20]. Figure 5 below shows a generalized percolation curve where conductivity increases with increased filler content. As the figure shows there are three different regions of a percolation curve; 1: The isolating region, 2: the percolation region and 3: the conductive region.

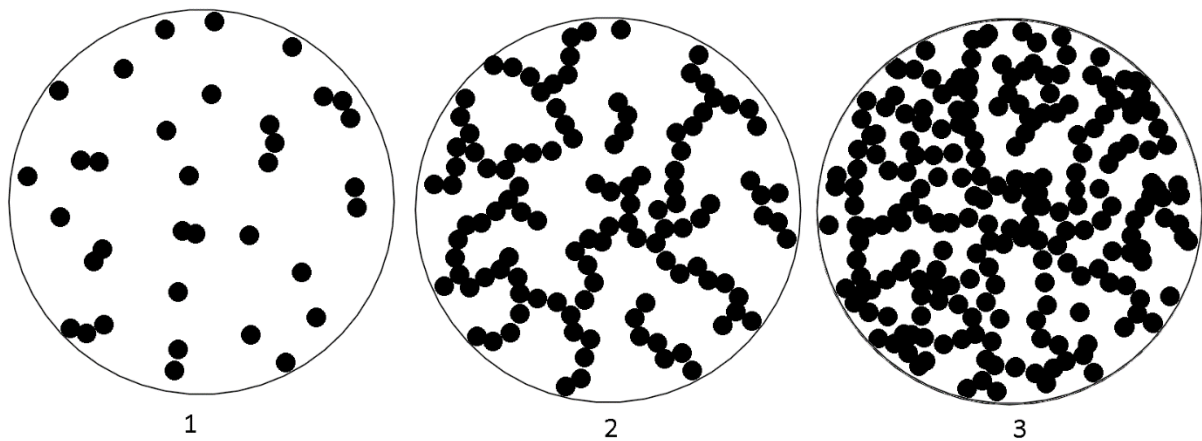


Figure 4 Visual representation of the microstructure of a nanocomposite containing a nanofiller which are represented as doth. With increased filler concentration there is an increase amount of electrically conductive pathways that are formed.

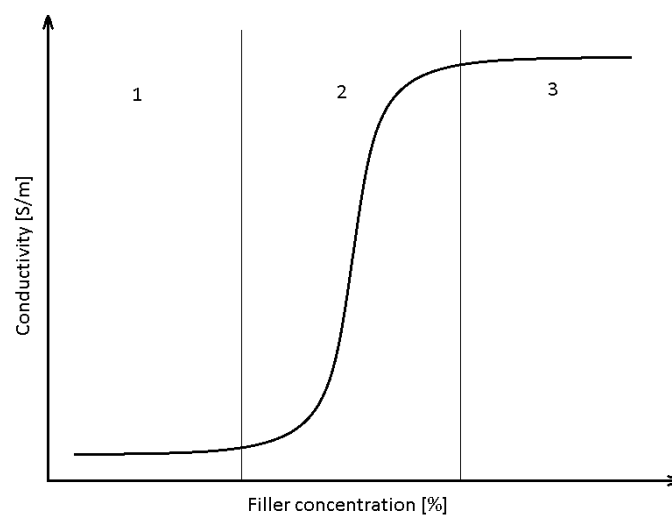


Figure 5 A graph representing electrical conductivity as a function of filler concentration according to the percolation power law dependency.

Figure 4 above illustrates a microscopic image of the composite where the black circles are representing a conductive nanoparticle and the white background illustrates the insulating polymer matrix. At low concentrations, the filler particle density is low and there are not enough particles that connect with each other in order to create a network so that current may flow. In this region, the conductivity is mainly governed by the matrix. The conductivity close to the percolation threshold have sufficient particles to form a network capable of carrying a current, thus the conductivity is following a sharp increase. Lastly in the conductive region, the particles have created multiple connections in the network thus increasing the conductivity even more up till a point where it has a stable but lower increase in conductivity with increased concentration. In other words, the value of the conductivity is determined by the number of pathways and density of conductive particles on a macroscopic scale.

One thing that should be mentioned is that there remains a conductivity even though if there is a lack of nanofillers in the network. This is because the conductivity is governed by trapped charge carriers and polarization effects that is generally influenced by morphology and polarity of the polymer matrix. Additionally, the influence of frequency dependence of the nanocomposite will result in different electrical measurements for AC and DC.

For theoretical explanations to fit in with the practical, the percolation threshold should have a very sharp cut off on the percolation threshold. This is where the last particles would make a full circuit. We can see that this does not happen. The reason for percolation models not being able to accurately predict the percolating behaviour is not well understood since the most probable cases of deviation are due to the surface chemistry of the nanofiller and the possibility of electrons tunnelling between particles in close distance to each other [20],[22].

In general, the conductivity of the nanocomposites is influenced by different parameters such as filler distribution, filler shape/size, filler/matrix interaction and the processing technique. Statistical, geometric and thermodynamic models have tried to explain the conductivity behaviour on the basis of these parameters [20].

This study will limit the electrical properties of the nanocomposite by only taking the direct current measurements into consideration. The following chapter will explain basic models of the percolation theory to try to understand the conductivities' dependence on the filler concentration.

#### 2.5.1.1 Lattice model

In order to simplify the percolation theory, consider having a two-dimensional square lattice illustrated as Figure 6 below. This system represents empty sites as black coloured dots and occupied sites as red coloured dots. Assuming the probability  $p$  that a site is occupied, and two neighbouring occupied sites are connected, represented as a red line between the sites. The figure below shows several sites being connected in a so called "cluster" which is defined by each site in the ensemble has at least another occupied site nearby which it connects to.

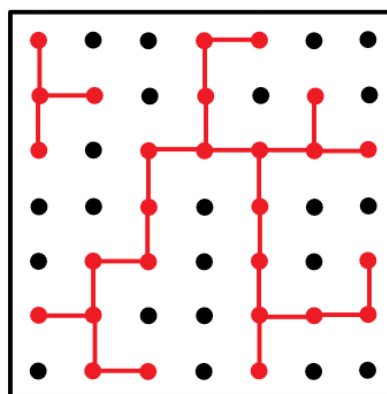


Figure 6 Lattice model with connected sites represented in red dots and lines while empty sites as black dots.

In Figure 6 we can see that a cluster connects the opposite sides of the lattice system, this type of cluster is called a "spanning cluster" which spans across the whole system. The figure above illustrates a 7x7 lattice system, but to appreciate the percolation theory, an infinite lattice system needs to be applied to the system.

Naturally one would think that with increased probability of a site occupation, the number and size of the spanning clusters would increase. However, there is a critical probability value  $p_c$  known as the percolation threshold of this system which states that when  $p \geq p_c$  only then can there exist a spanning cluster in the system. Power law functions can adequately describe these properties, for an example; the average geometrical size of the finite clusters described as their effective radius  $\lambda$ , defines the scale of the percolating system.

$$\lambda \propto |p - p_c|^{-\nu} \quad (2.6)$$

The critical exponent  $\nu$  is dependent on the dimensionality  $D$  that is also known as universality. The well-known values of  $\nu$  being 1.33 and 0.88 when  $D$  is equal to 2 and 3 dimensions correspondingly.

Each connection between the occupied sites are considered to be resistors when there is an electrical current passing through only if the sites are connected to the spanning cluster. The bonds that actually carry the current are called the backbone of the spanning cluster since branches that deviate from the backbone and are not connected to any other sites are called dead ends.

In an infinite lattice system, sites that are connected in the backbone by more than one bond are called blobs. Topologically, they can be viewed as square or cubic network of links with a length of  $\lambda$  that connect the sites. If the sample size is  $L$ , there would be an average of  $L/\lambda$  links that connect two opposite sides of the system thus giving a parallel of  $(L/\lambda)^{D-1}$  number of such series. If each link has a resistance of  $R_\lambda$  and the whole system has a resistance of  $R_L$ , the correlation between the dimensionality and the number of links will give the following equation:

$$R_L = R_\lambda (\lambda/L)^{D-2} \quad (2.7)$$

The remaining parameter that needs to be estimated is the value of  $R_\lambda$ . The perfect scenario of a system that percolates would be if every site was connected through a single bond connection. The lowest possible value of  $R_\lambda$  would be  $R_\lambda = r_0 L_1$  where  $r_0$  is the resistance of a single bond and  $L_1$  is the number of single bond connections. Naturally, it is hard to achieve a perfect scenario therefore the blobs included in the equation its expected that  $R_\lambda > r_0 L_1$ . As stated by I. Balberg (2012)[23], an argument can show that  $L \propto -(p - p_c)^{-1}$ , which gives  $R_\lambda \propto -(p - p_c)^{-\zeta}$ , where  $\zeta$  is represented as a diminishing number of blobs as the number of sites approaches the critical percolation threshold where the value of  $\zeta$  being 1.3 and 1.1 when  $D$  is equal to 2 and 3 dimensions correspondingly. The global conductivity of the lattice system can now be summarized by the previous equation into a unified simplification and explanation of the conductivity dependence of the number of site location as:

$$\sigma = \sigma_{0p} (p - p_c)^t \quad (2.8)$$

Where  $\sigma_{0p}$  is the characteristic conductivity of the system and  $t$  is the critical exponent that is gained from [23]:

$$t = (D - 2)\nu + \zeta \quad (2.9)$$

The traditional method of approximating the percolation threshold was done by simulating the distinct position of a lattice system using the Monte Carlo method which utilizes a stochastic algorithm which generates random positions for the lattice system. Despite its usefulness, this method showed to be a poor representation of reality. This in turn led to further research and development to the continuum model [2], [23], [24].

### 2.5.1.2 Continuum Model

In contrast to the previously covered lattice model of the percolation theory, the system in continuum percolation does not have occupied or non-occupied sites, instead objects are varying in shape, size and are placed randomly in space. If the shape and size are nonisotropic the orientation should also be taken into consideration. Since the physical parameters vary so does the bonding between two objects.

The continuum percolations model's volume fraction,  $x$ , can be correlated to the lattice model's  $p$ , the probability of a site being occupied, however the random nature of the objects position in continuum percolation models makes it hard to take the different models to get along any further. Continuum models are in a way a more realistic approach for describing the object's position in space. The main types of continuum models are classified as following:

#### *Soft-core system:*

Particles are assumed to be fully interpenetrating and are considered to be bonded when overlapping.

#### *Hard-core system:*

Particles cannot overlap, they bond when in direct contact.

#### *Hard-core with soft shell-system:*

Particle geometry is not the only governing parameter for its ability to bond. The tunnelling distance between them is taken into account as well. It is a mix between the hard- and soft core system.[2], [23]

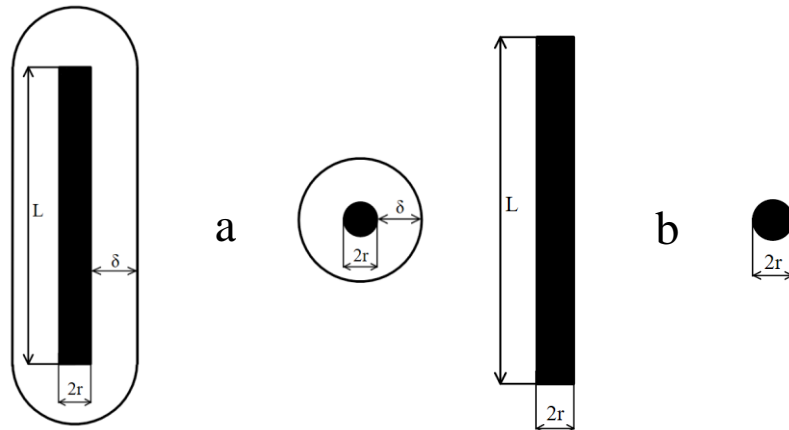


Figure 7, (a) Visual representation of a Hard-core with soft shell rod like and spherical particles.  
(b) Visual representation of a Hard-core rod like and spherical particles.

#### *Soft-core system*

Simulating a system that contains particles with high aspect ratio draws a great deal of computational power. One way to simplify the task is to treat the excluded volume that the particle is replacing in the system. Through this way it is possible to represent the critical number of particles,  $N_c$  required to form a conductive network by taking the excluded volume,  $V_{excl}$  into account.

$$N_c \propto \frac{1}{V_{ex}} \quad (2.10)$$

Since the number of particles is directly proportional to true volume of the particle, the critical volume fractional percolation threshold,  $\varphi_c$  can be expressed as:

$$\varphi_c \propto \frac{V}{V_{ex}} \quad (2.11)$$

A spherical object where its excluded volume is considered to be the interaction volume can be expressed as:

$$\varphi_c = 1 - \exp\left(\frac{-B_c V}{V_{ex}}\right) \quad (2.12)$$

where  $B_c$  is the critical concentration of bonds per sphere and  $V$  the volume of the sphere.

For non-spherical objects such as a cylinder, a permeable “soft” shell is covering the cylinder, or a so called spherocylinder [25], with a length of  $L$  and radius of  $r$  where the volume of the cylinder would be:

$$V = \frac{4\pi}{3}r^3 + \pi r^2 L \quad (2.13)$$

And the excluded volume;

$$V_{ex} = \frac{32\pi}{3}r^3 + 8r^2 L + 4rL^2 \sin \theta \quad (2.14)$$

where  $\sin \theta$  is the average of orientation of the distribution of cylinders in the system. The critical fractional volume of a spherocylinder is derived from the equations above and gives:

$$\varphi_c = \frac{V}{V_{ex}} = \frac{\frac{4\pi}{3}r^3 + \pi r^2 L}{\frac{32\pi}{3}r^3 + 8\pi r^2 L + 4\pi r L^2} \quad (2.15)$$

The driving parameters for achieving a low percolation threshold is the aspect ratio,  $L/r$  which is the ratio between an objects size of dimensions [2], [23],[25].

#### *Hard-core soft-shell system*

The hard-core-soft-shell systems has particles with impenetrable core with radius of  $r$  and a soft shell covering it with a radius of  $r + \delta$ . The parameter  $t$  is the ratio of the radius of the hard core with the soft shell

$$t = \frac{r}{r+\delta} \quad (2.16)$$

Soft-core systems ratio would be  $t = 0$  and hard-core ratio would be  $t = 1$ . Hardcore with soft shell would then obviously be  $t > 1$ . The excluded volume of the hard-core soft-shell systems would be expressed as the excluded volume of the soft-shell subtracted by the inner hard-core excluded volume, thus giving the following expression of the total excluded volume for a spherocylindrical particle.

$$V_{ex} = \frac{32\pi}{3}r^3 \left[ (1 - t^3) + \frac{3}{4} \left(\frac{L}{r}\right) (1 - t^2) + \frac{3}{32} \left(\frac{L}{r}\right)^2 (1 - t) \right] \quad (2.17)$$

Clearly the governing parameter is the outer shell radius, however, it is hard to determine without knowing the radius of the inner hard-core [25].

Most models are used in a statistical manner by the use of a simulation simulations, in most cases the Monte Carlo method. However, even though simulations are useful in explaining how the particles effect the properties of the percolation, they are not realistic representations because the experimental data does not coincide with the use of different polymer matrices [2].

### **2.5.2 Electrical conductivity mechanisms**

One of the most well-known approaches explaining the percolation behaviour of interparticle conduction has been assuming that conduction is not only carried when two particles are interconnected, but also as a function of tunnelling. This approach however cannot be predicted by the standard power law fitting that is commonly used.

When tunnelling, or hopping as it is also called [23], occurs, electrons that are carried by the conductive particle medium has a slight possibility to tunnel through a barrier that it usually cannot overcome, in this case; tunnelling across a two different conductive particles in a nonconductive polymer medium. To understand the phenomena of a particle trying to overcome a potential barrier, a metaphor of ball attempting to roll over a hill can be used as well. In order for the ball to roll over the hill it must have a certain energy to surpass the potential barrier. However instead of the ball rolling over the hill, imagine that the ball is digging through the hill over to the other side to successfully crossing the potential barrier.

The possibility of tunnelling between the particles decays exponentially with the distance between the particles, expressed as the following equation:

$$g = g_0 \exp\left(\frac{-2\delta_{ij}}{\xi}\right) \quad (2.18)$$

where  $g$  is the interparticle conductance,  $\delta_{ij}$  is the minimum distance between the surface of particle  $i$  and  $j$  and  $\xi$  is the quantum wavefunction decay of the electron outside the conducting particle it belonged to [2],[23], [25].

There are two extreme cases which govern the conductive behaviour of the composite. If we consider that the particles are spheres and the centre-to-centre distance is  $r_{ij}$  thus the tunnel distance results in  $\delta_{ij} = r_{ij} - D$ , where  $D$  is the diameter of the sphere. The resulting extreme cases would be either if that the particles are so large that  $\xi/D \rightarrow 0$  resulting from equation 2.18, that conductivity between particles only occurs if the particles are in direct contact. This would lead a conductivity behaviour more alike equation (2.4) thus giving the critical exponent  $t \cong 2$ . The second extreme case is if  $D/\xi \rightarrow 0$  where the particles would be randomly dispersed throughout the medium. In this case the site density  $\rho$  would not change the connectivity, only the decaying wavefunction  $\delta_{ij}$  would be the governing parameter [23], [28].

I. Balberg et al. (2012)[23] presented a numerical analysis where they used the Global Tunnelling Network (GTN) model, introduced from an earlier paper of theirs, where conductive particles forms a global network of connectivity through quantum tunnelling [28]. The study presented cases of impenetrable particles where spherical particles and anisotropic particles of different aspect ratios  $a/b$  were used to simulate a numerical percolation threshold  $\varphi_c$ . They obtained results indicate that the conductivity as a function of filler content  $\sigma(\varphi)$ , had a strong dependence the aspect ratio  $a/b$  of the filler which they later on formulated as the equation:

$$\sigma \cong \sigma_0 \exp \left[ \frac{-2\delta_c(\varphi, a, b)}{\xi} \right] \quad (2.19)$$

where  $\delta_c$  is the geometrical critical distance of connection between particles through electron tunnelling [28]. The percolation threshold as mentioned would vary on the shape of the filler. For prolate, oblate and spherical particles the threshold would be expressed as:

$$\sigma \cong \sigma_0 \exp \left[ \frac{-2D}{\xi} \frac{\gamma(b/a)^2}{\varphi} \right] \quad (2.20)$$

$$\sigma \cong \sigma_0 \exp \left[ \frac{-2D}{\xi} \left[ \frac{0,15(a/b)}{\varphi} \right]^{4/3} \right] \quad (2.21)$$

$$\sigma \cong \sigma_0 \exp \left[ \frac{-2D}{\xi} \frac{1,65(1-\varphi)^3}{12\varphi(2-\varphi)} \right] \quad (2.22)$$

Conductive behaviour explained by tunnel mechanisms between particles have been shown to be successful because it does not follow the regular sharp cut off in the percolation region from the powerlaw equation. Instead, the findings made by I. Balberg et.al (2012)[23] suggest that tunnelling and geometrical connectivity of semi-penetrable particles shows an effective description of understanding the problem of conductivity in polymer nanocomposites [28].

Nanofillers in a polymer matrix in reality has more parameters than just shape and random orientation. The fillers are also affected by entanglements, agglomeration and interaction with the polymer [2].

### 2.5.3 Nanofiller parameters affecting electrical conductivity

Filler size, shape and aspect ratio are one of the main influencing geometric parameters on the electrical conductivity and percolation behaviour.

A study done by C.W Nan et.al (1993) [29], concluded statistically that if two kinds of spherical particles with different sizes of  $R_1$  and  $R_2$ , where randomly distributed in a polymer matrix, the percolation threshold  $\varphi_c$  followed a general relation of

$$\begin{cases} \frac{R_1}{R_2} \leq 1, \varphi_c \geq 0.16 \\ \frac{R_1}{R_2} \gg 1, \varphi_c \ll 0.16 \end{cases} \quad (2.23)$$

This relation has been observed in other studies experimentally [25]. Just the size difference of filler particles changes the percolative behaviour of the nanocomposite. However, as A. Celzard et.al (1996), [30] pointed out in a study that the aspect ratio is the most dominating parameter according to experimental and theoretical models for carbon-fibre and GNP nanocomposites.

#### 2.5.3.1 Aspect ratio

High aspect ratio fillers form conductive networks in lower concentrations compared to spherical or other low aspect ratio fillers. The reason being that high aspect ratio has covering a larger area thus providing a higher possibility of contact with other objects. Fillers with high aspect ratios usually decreases the percolation threshold and according to some studies the percolation threshold is directly proportional to the inverse value of the aspect ratio in respect to the excluded volume theory [25]. Not only is the aspect ratio of importance, the length of the filler also shows impact on the percolation threshold.

## 2.6 Dispersion methods of nanofillers in nanocomposites

In order to produce a nanocomposite, one must first introduce the nanomaterial into the polymer matrix. The method that is used to disperse the filler inside the matrix vastly affects the overall properties of the finished composition. Due to the different dispersion methods having such different results, depending on the degree of dispersity, application and commercial aspect of the finished product, different choices of preparation methods are more desired than others.

However, though there are different reasons for choosing an appropriate method of dispersion, one of the main issues with polymer nanocomposites is the fact that random dispersity is hard to achieve since the nanofillers tendency to create agglomerates. This is believed to be due to the weak attractive forces between the fillers. [31]

Generally, there are three types of methods for preparing polymer nanocomposites: melt mixing, in-situ polymerization and solution mixing.

### 2.6.1 Melt mixing

Melt mixing or melt compounding is an effective and cost-effective method of incorporating nanofillers into a polymer melt. It involves mixing nanoparticles in a polymer melt with the presence of shearing. The processes can be done in many forms and most often solvent-free [32], [33]. The advantage with this technique is that the filler can be directly dispersed into the matrix without any chemical modification. Also, this method is preferred in industrial facilities since it is easily scalable. Many studies has been made concerning the dispersity of conductive nanofillers in various types of polymers using the melt mixing method [33],[34],[35]. As mentioned before, the fact that particles have interactions that makes them cluster and agglomerate makes it difficult to disperse a nanofiller homogenously in a polymer matrix. Fillers usually come in the form of powder which means that there is a pre-existing agglomeration before the filler is even processed. Some studies have been made on the effect of processing conditions on the filler dispersion. Depending on different parameters such as filler-matrix interaction, size, viscosity of the matrix, mixing speed and time of mixing, it has been observed to play an important role on the dispersity of the particles [13], [33].

The fundamental mechanisms of melt mixing methods are to understand the difference of two major key factors which are the dispersiveness and distributiveness. Dispersive mixing is the reduction of clusters of nanoparticles and distributive mixing is the process of spreading the particles in the compound. The two mechanisms can either occur simultaneously or step-wise depending on the process method. In mixing equipment such as an internal mixing chamber provides a complex flow pattern of shear flow and elongational flow. The incorporation of the filler material into a liquid polymer occurs four main steps:

1. *The incorporation of the filler into the liquid.*
2. *The wetting of the solid phase by the liquid phase.*
3. *The fragmentation of the solid agglomerates, which can be divided into to different processes: the erosion and the break up. The former is a low energy fracture and it prevails in the low shear regions, whereas the latter is the high energy fracture and it prevails in the big shear regions of the mixer.*
4. *The agglomeration of the dispersed particles due to the cohesive forces between the particles provoked by the particle-particle collisions (cited from J. Keith Nelson, (2010) [5])*

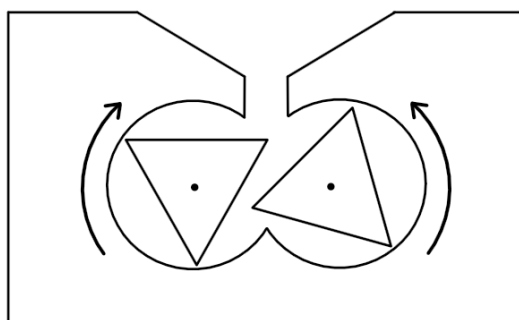


Figure 8, A visual representation of a cross section of an internal chamber mixer with two counter rotating rotors.

Internal mixing chambers is commonly used in small batch sizes often in research where high intensity mixing of low volumes are needed. Figure 8 above displays a simple schematic of an internal mixing chamber with two counter rotating rotors. The mixing in internal mixing chambers generate complex shearing and elongation flows that are well suited for dispersing solid particle agglomerates within a polymer matrix. The dispersion of the filler is strongly influenced by the mixing time, chamber temperature, rotor speed and rotor blade geometry.[13]

### 2.6.2 Solution mixing

While physical melt mixing is a great mixing technique which can be scalable, however as mentioned before the local dispersion are often non-homogenous due to the fillers agglomeration and entanglement of some fillers. Hence, other techniques such as solution mixing could be a solution to homogenously disperse a filler throughout a matrix. Solution mixing usually involves mixing soluble nanomaterial in a solution by dissolving the desired polymer with the nanomaterial. Shear mixing of the solution results in the polymer possibly intercalating and encapsulating the filler when it precipitates. This solution can then be processed further by either extracting and drying the solution or directly cast into a mould and later remove the solvent. The latter case may however cause an increase in aggregation of the nanomaterial hence potentially decreasing the composites properties [35]. Solution mixing works well for intercalating the polymer when the filler has little or no polarity [5].

### 2.6.3 In-situ polymerization

In situ polymerization is a rather simple technique where the building blocks of the polymer, called monomers, are diluted with the desired nanomaterial. Here the monomers can penetrate some types of filler to exfoliate them. Then, the monomers in the solution are polymerized by either a catalyst, radiating the solution or heat. The polymerization causes the monomers to polymerize long polymer chains resulting in a intercalated composite [5]. This method can be applied in both thermosets and thermoplastics. Although in-situ polymerization provides an excellent dispersion of nanofiller, it is however an expensive method and not desirable for largescale production facilities.

### 3. Methods

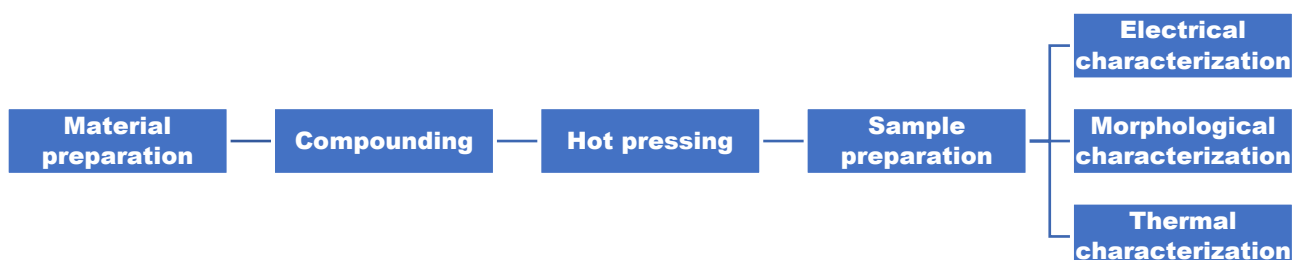


Figure 9, Flow chart of the protocol for incorporating and testing the nanocomposites.

This chapter covers the methodology of the project and the preparation of the materials for the specific characterization methods. Figure 9 above shows a flowchart of the steps needed to conduct the different characterization methods which will be elaborated more in the following chapter.

#### 3.1 Material preparation

The polymers prepared for processing was done by weighing each component using an ordinary glass beaker and a scale. The polymer was in the forms of pellets. Due to safety issues the nanomaterial was enclosed inside a glovebox compartment with ventilation system attached to. The potential long-term health risks of nanomaterials in this class have not been thoroughly investigated thus extreme precaution is necessary. Particle gas masks, latex gloves and safety clothing were used at all times. The glovebox container was equipped with an intermediate airlock to ensure that no particles leaves the glovebox.



Figure 10, Glovebox with an intermediate chamber connected to a ventilation system. Image courtesy of Roland Kádár.

The nanomaterial was weighed inside the glovebox, as seen in Figure 10, fitted with a sensitive scale onto a beaker. When the correct amount of nanomaterial was weighed, it was then transferred to a special made glass burette enclosing the nanofiller inside, seen in Figure 11 below. The burette is made in such a way that it was possible to transfer the nanomaterial directly inside the mixing chamber with the use of an adaptor. This equipment was used to ensure that no nanomaterial was released into the atmosphere and as a precaution, a ventilation extension arm was placed directly above internal mixing chamber.



Figure 11, Powder dispenser. Image courtesy of Roland Kádár.

### 3.2 Compounding

The processing of the nanocomposites was conducted by dispensing the nanofiller from the burette directly into the polymer melt which was added inside the heated mixing chamber. The temperature of the mixing chamber was adjustable by a digital display installed to the mixing chamber. The chamber had two rotational screws with adjustable rotational speeds. When equipped with the rotors that was used, the internal chamber had a volume of 50 cm<sup>3</sup>. The total added mass in the chamber should be in the respect of the density for the specific polymer. For polyethylene based matrices the chamber temperature was set to 160 °C and 200 °C for polypropylene based matrices. Figure 12 below shows the chamber of the internal mixing chamber.



Figure 12, Internal mixing chamber of compounder.

The compounding was performed by first adding the polymer pellets into the properly heated mixing chamber with a low rotational speed. Two thirds of the weighed polymer were added into the chamber. After it was given time to melt, the rotational speed was adjusted to a rotational speed recommended by the company. Next, the nanomaterial inside the glass burette was mounted onto the mixing chamber and then slowly added the nanomaterial inside the chamber with molten polymer. After the burette was emptied, the other third of the polymer was added into the chamber.

Later when everything was added inside, the chamber was closed with a clamp that has a 5 kg weight attached to it. This is to prevent the polymer from squeezing out of the chamber while mixing. Also by doing this, the chamber was somewhat separated to outside environments.

Lastly, the rotational speed was slowly increased to a desired rotational speed and mixing process was operated to a specified time, as recommended by the company. After the compounding, the material was removed by scraping it out with brass spatulas. The semi-molten plastic was then taken out and put on a ceramic plate too cool it down. While it was cooling, ridges were made on the plastic by the use of the brass spatulas. The pieces could later be broken into smaller pieces thus making the process more time efficient.

The polymer blends were prepared according to three different methods before the incorporation of the filler:

1. Method A: Mixing of two different polymer pellets inside a beaker.
2. Method B: Mixing of two different polymers by the use of an extruder equipped with a Saxton mixer element.
3. Method C: Mixing of two different polymers where one polymer component is already incorporated with a filler.

The blends from Method A & B are put inside the mixing chamber and filler are added as explained before.

### **3.3 Compression moulding**

When hot-pressing a material, the desired shape of the material should come in the form of small pellets. Having a large surface area for a constant mass makes the specimen undergo higher heat transfer which melts the pellets more quickly. The process could be much faster by using a pelletizer, however this would make it necessary to extrude the composite through a small circular die which would later then be pelletized. Therefore, this step was avoided.

The broken off pieces were pressed into square mould shapes by having a metal rim with an inner dimension of 100x100 mm and a thickness of either 2 mm or 0.1 mm. The metal mould was put between two Teflon sheets which in turn was put between two flat metal plates. With the plastic inside between, the moulding piece was put inside a hydraulic press. The desired force and temperature exerted on the mould was controlled by a small control unit on the press. Afterwards, the specimen was pressed by holding a two-button safety switch until the two pressing elements made contact which then initiated the automatic mode of the press. However, instead of directly going to automatic mode, the two plates were positioned a couple millimetres from the surface. This was done so that the plastic had time to melt before pressing, otherwise the specimen might deform, leak under the frame or damage the Teflon sheets.

After about 5-10 minutes, depending on the polymer matrix, the plastic had reached high enough temperature to undergo a compression with homogenous compression flow. The next step was to increase the pressure, which needed to be slow in the beginning otherwise the polymer might leak outside the frame. Later, when the pressure had reached the desired force, the press was in the high-pressure stage for 5 min. Afterwards the temperature was set to ambient temperature and the connected water-cooling system was turned on to cool down the mould. This process took approximately 10-15 minutes depending on how high the temperature was set. Lastly, the metal sheets were taken out of the press and the Teflon was separated from the rim with the moulded polymer plaque inside. The polymer plaque was then taken out and put into a labelled bag.

### 3.4 Sample preparation

To prepare the compounded and pressed material for the analytical characterization, different methods were used depending on the test.

For electrical analysis the pressed composite plaques were cut using a manual cutting press with cutting dies with a rectangular geometry with the dimensions of 50x10 mm.

The DSC samples were cut to a desired weight from the pressed plaque using a scalpel. The TGA samples were prepared in the same manner but with different weights.

For morphological analysis which were conducted by the use of a scanning electron microscope, cryogenic fracturing, etching and sputtering of the samples were needed before conducting the analysis.

### 3.5 Analytical characterization

#### 3.5.1 DC conductivity

To calculate the DC conductivity, Sorensen DCS 300-3.5 power supply was used to connect a two-point measurement setup, seen in Figure 13. The setup consisted of two crocodile clamps with flat surfaces that acted as a two-point measurement. The setup was installed in a safety glass box with a safety switch. The current was measured using a Fluke 8846A Precision Multimeter that could measure currents down to 0,01  $\mu\text{A}$ .

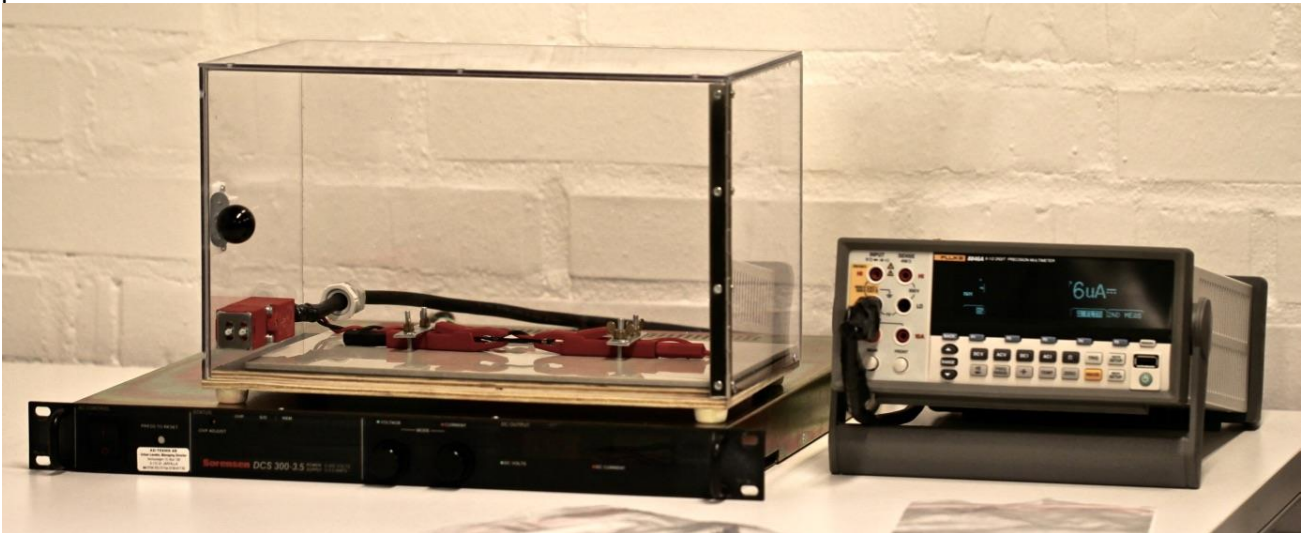


Figure 13, DC setup of power supply, safety box with crocodile clamps and multimeter. Image courtesy of Roland Kádár.

The conductivity was calculated using Pouillet's law, which is based from Ohm's law, in order to obtain the sample's volumetric resistivity which was then later inversed the value to get the sample's conductivity.

$$\rho = R \frac{A}{l}, \sigma = \frac{1}{\rho} \quad (2.21)$$

Where  $\rho$  is resistivity, R the samples' resistance, A the cross-section area, l the length of the specimen and  $\sigma$  the conductivity. [36]

Different mass fractions of the same composite type were measured for its conductivity. These values were later plotted as point values and a curve fitting of the percolation theory model was done. This was done to obtain the critical percolation threshold and the critical exponent.

#### 3.5.2 Differential Scanning Calorimetry, (DSC)

A Differential Scanning Calorimetry (DSC) is a thermoanalytical instrument that measures the amount of heat that is required to increase the temperature of a sample as a function of time and temperature. Measurements provide quantitative and qualitative information about physical changes by analysing the endothermic and exothermic transitions over a function of temperature and time. Such information can be used to study phase transitions, degree of crystallinity, melt temperatures, crystallization temperatures and cooling- and heating enthalpies. The experiments were carried out by a Mettler Toledo DSC+3.

The procedure of measuring the degree of crystallinity is done by drawing an arbitrary baseline from the first onset of melting to the last trace of crystallinity and by calculating the area under the measured curve one can obtain the heat of fusion for a specific sample. The degree of crystallinity can be obtained from equation (2.3)

Preparation of material for DSC analysis is simply done by cutting a small piece of the plastic, weighing it to approximately 5 mg then putting it in an aluminium pan that the DSC machine is calibrated to.

When using the DSC for measurement for quantitative information one must take the thermal history of the specimen into consideration. In order to avoid incorrect measurements induced by the thermal history, the samples were heated and cooled twice in a cycle. Polyethylene samples were cycled twice between -50 °C and 180 °C and polypropylene were cycled between -50 °C and 220 °C with a heating rate of either 1, 10, 20, 40 or 100 °C/min. When the sample is heated the first time, it stays in an isothermal state at maximum temperature for 1-3 minutes to erase the thermal history of the sample. Hence the next cycle should give a more accurate measurement. Afterwards when the experiment is finished, the aluminium pan of 40 µl is taken out and thrown in a recycling waste bag.

### 3.5.3 Thermogravimetric Analysis, (TGA)

A Thermogravimetric analysis (TGA) is an instrument used to measure the difference in mass measured over a time and temperature function. This method was used to determine properties such as thermal stability and thermal decomposition of polymer and filler. The obtained data was used to determine at what temperature the polymer started to degrade and to calculate the mass fraction of the filler since the carbon-based filler has a considerable higher temperature of degradation. The experiments were carried out by a Mettler Toledo TGA/DSC 3+

The TGA analysis was executed by similar means of the DSC analysis. Firstly, one measures the mass of the specimen to make sure adequate mass is achieved, which is about 5-10 mg. After this has been done, the weighed piece is put inside an alumina pan of 70 µl then later placed inside the TGA machine. Two pans are put inside the machine since one should be an empty one to act as a reference. The experiment method was programmed to go from ambient temperature to 900 °C with an atmosphere of nitrogen gas. When it had reached 900 °C the gas flow switched from nitrogen gas to air and stayed in an isothermal state for 10 min. This was done to make sure that all material that was inside the polymer composite has evaporated, degraded, or oxidized.

Quantitative and qualitative analysis of the obtained data from TGA and DSC was conducted using the software OriginPro 2016. For the DSC analysis, this was done through analysing the peaks of the time disposed heatflow vs. temperature curve. By calculating the area under the exothermic part of the normalized curve, one obtains the enthalpy or the heat of fusion for that sample. Calculating the degree of crystallinity is done by using the acquired enthalpy divided by the theoretical heat of fusion for a 100% pure crystalline polymer as mentioned in the theory.

The peaks were easily found by a tool in OriginPro 2016 that finds the maximum/minimum value. This maxima or minima are the crystallization temperature, the melt temperature or a possible third option which could be a co-crystallization temperature for two different polymers.

## 3.6 Morphological characterization

An SEM-Leo Ultra 55 was used to investigate the morphology of the polymer composites. The cut samples were cooled in liquid nitrogen and then fractured using a hammer in order to get a clean fracture. The cryogenic fracture is commonly used to expose the fillers in polymer nanocomposites when observing them under an SEM. Thereafter the samples were etched according to a modified etching procedure originally made by M. Shahin et.al, (1999) [37].

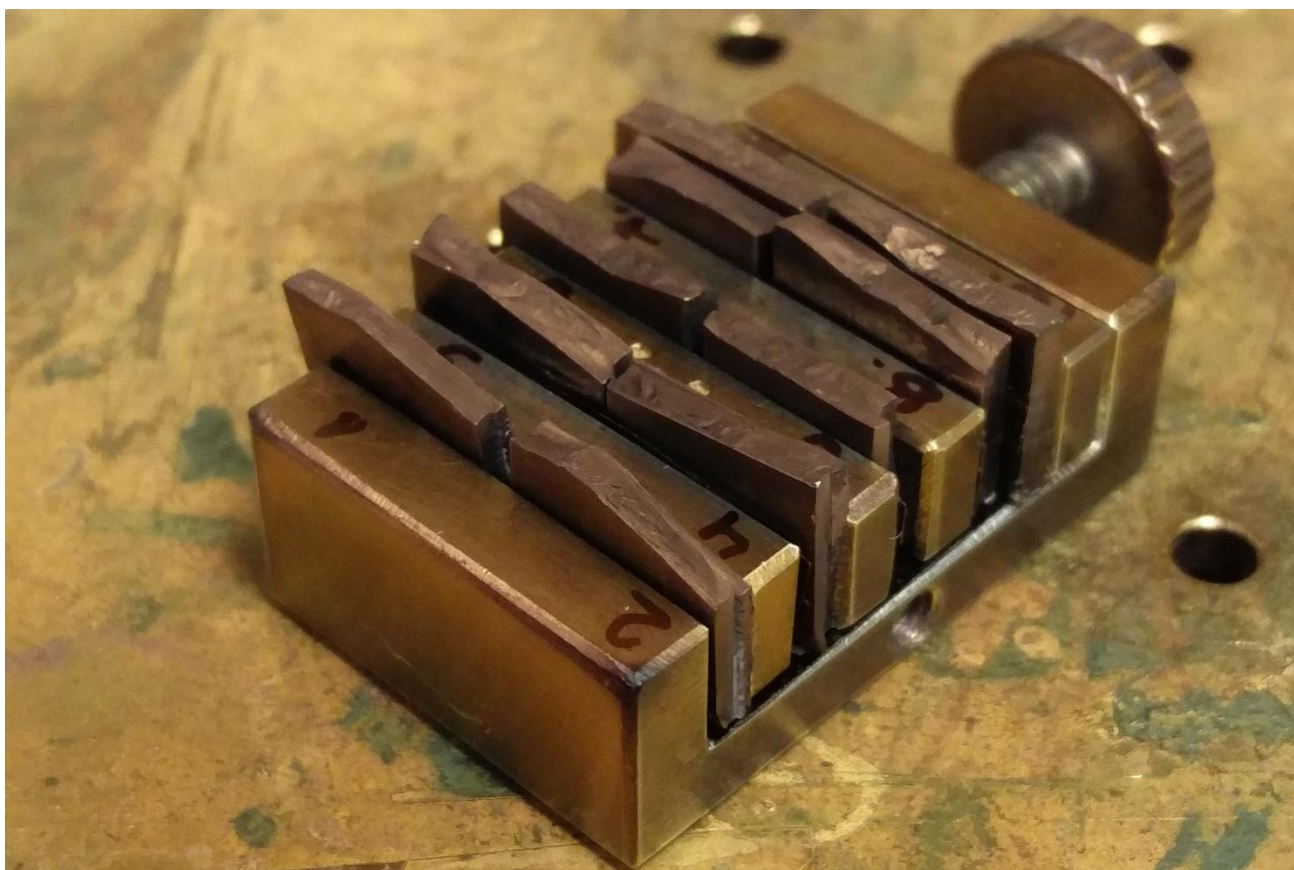


*Figure 14, Numbered samples mounted on a sample holder.*

After the etching procedure the samples were put on a metal holder which is to be placed inside the vacuum chamber of the SEM. Sample holder can be seen in Figure 14. Conductive tape was used to make sure there was a good contact between the samples and the holder. Afterwards, the holder together with the samples were put inside a Sputter Coater S150B, BOC Edwards, Crawley, UK chamber where it was coated with approximately 5 nm film of gold particles to make the surface conductive so that it is visible under the scanning electron beam.

## 4. Results and Discussion

### 4.1 Polyethylene composites

#### 4.1.1 PE1/F1

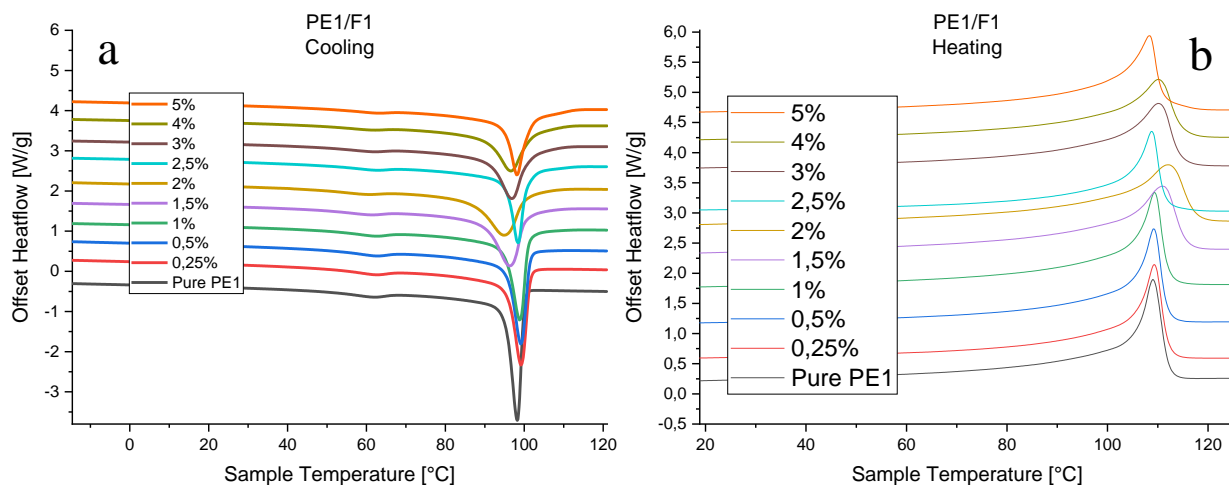


Figure 15, (a) DSC curve where heatflow is in a function of sample temperature, showing crystallization peaks of different compositions of PE1 with filler F1.

(b) DSC curve where heatflow is in a function of sample temperature, showing melting peaks of different compositions of PE1 with filler F1

Figure 15 shows a thermal analysis of PE1 with filler F1 showing heat flow vs. temperature. The values of the crystallization and the melting peaks,  $T_c$  and  $T_m$ , can be seen in Figure 32 & 33. The  $T_c$  and  $T_m$  shows a decreasing trend in temperature with increased filler loading. However, one should note that the difference is rather small. The reason why the peaks of the concentrations 1.5%, 2%, 3% and 4% look different was found out to be that the compounding temperatures of those concentrations were different which caused the polymer to have a different morphology thus resulting as a bit shifted peaks compared to the other concentrations. Overall, with increased filler amount, there was an observation of lower peak height. The average  $T_c$  and  $T_m$  shows a decrease in temperature with increased amount of filler. However, the degree of crystallinity shown in Figure 34 shows a trend of decreased degree of crystallinity with increased amount of filler.

Comparing the values of crystallinity from Figure 34 and the  $T_c$  and  $T_m$  from Figure 32 & 33 one can conclude that the fillers are inhibiting the crystallization kinetics by immobilizing the polymer chains in the vicinity of the filler.

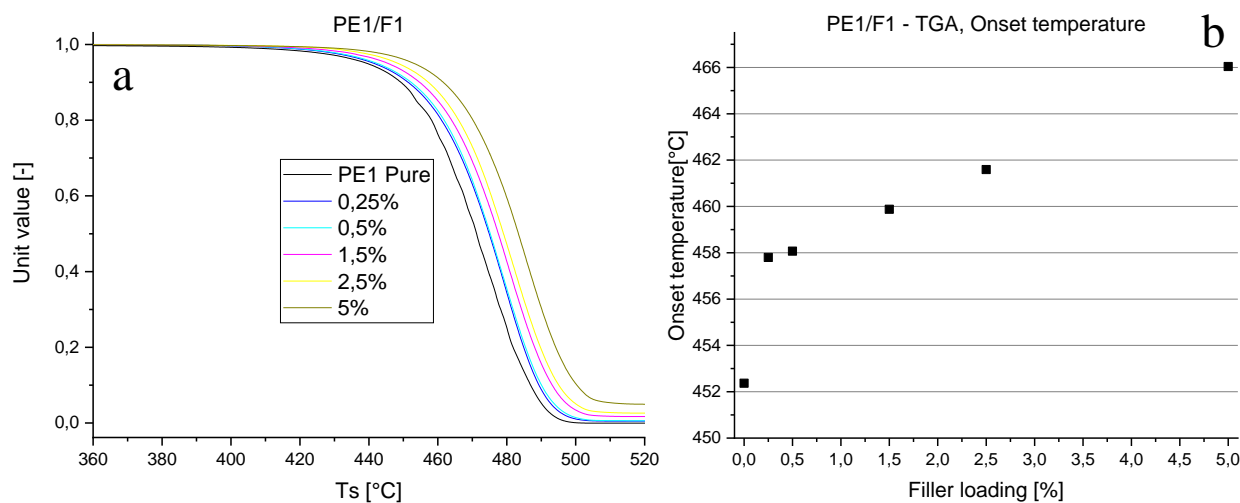


Figure 16, (a) TGA curves of the degradation of different compositions of PE1 with filler F1  
(b) Calculated onset temperatures for PE1/F1 in a function of filler loading.

Table 1, Filler residue calculated from the TGA of the different compositions of PE1/F1

PE1/F1 TGA Results						
Filler loading (wt.%)	0	0.25	0.5	1.5	2.5	5
Residue @ 550°C (wt.%)	~0	~0	0.59	1.68	2.59	4.93
Onset temperature (°C)	452.4	457.8	458.1	459.9	461.6	466

TGA was conducted in order to calculate if the desired filler content in the polymer matrix was reached, an analysis was made on several different concentrations of PE1 with filler F1. Figure 16a shows that the method of incorporating the filler into the polymer matrix was adequate enough to provide a desired accuracy of filler content. In Figure 16b, we can see that there is an increase in onset temperature with increased filler content in polymer PE1. This observation is from the manifestation of a shift in the onset temperature of degradation with increased filler content in the composites which indicates an improved thermal stability with increased filler content.

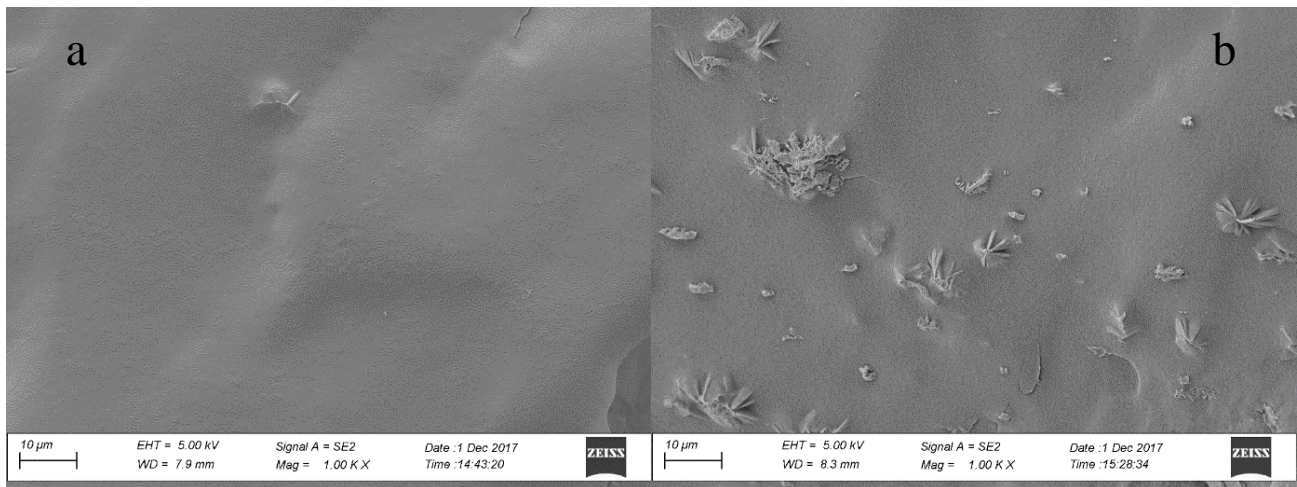


Figure 17, (a) SEM picture of pure PE1 at a magnification of 1000x. (b) SEM picture of PE1/0.5wt.% F1 at a magnification of 1000x.

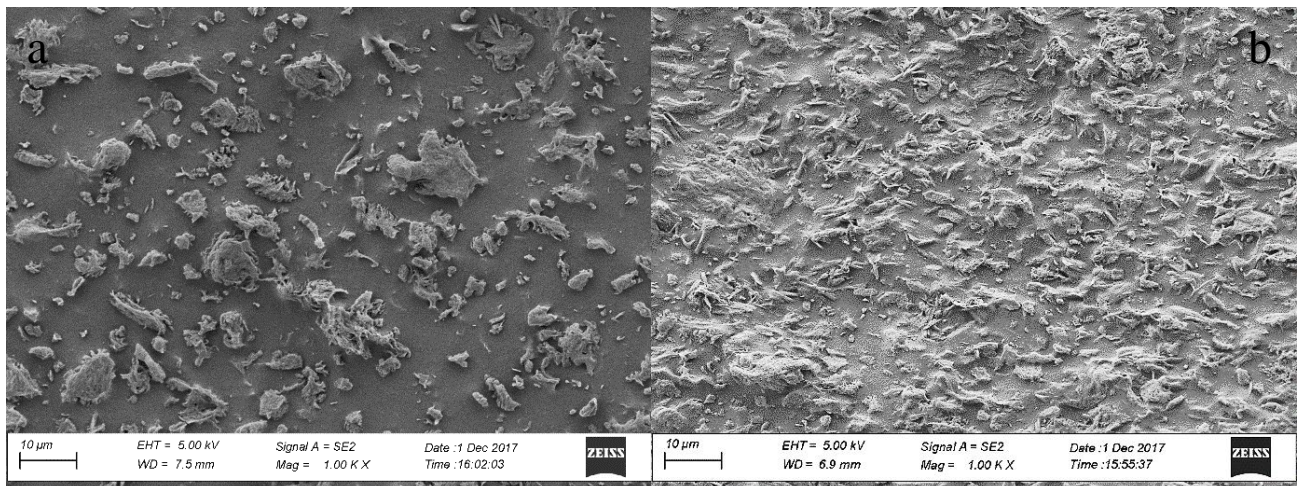


Figure 18, (a) SEM picture of PE1/2wt.%F1 at a magnification of 1000x (b) SEM picture of PE1/4wt.%F1 at a magnification of 1000x.

In Figure 17a, we can see very clearly spherulites in the pure PE1 SEM picture with little to no crystalline structure extruding from the surface, however in higher filler loadings we can observe an increase in crystalline structures protruding from the surface. In Figure 18, we can see PE1 with filler contents between 0.5% and 4% and that there is an increase of agglomerates as we increase the filler content. We can see that there is a high amount of interconnected agglomerate particles in the 4% concentration but not quite so in the lower 2% concentration.

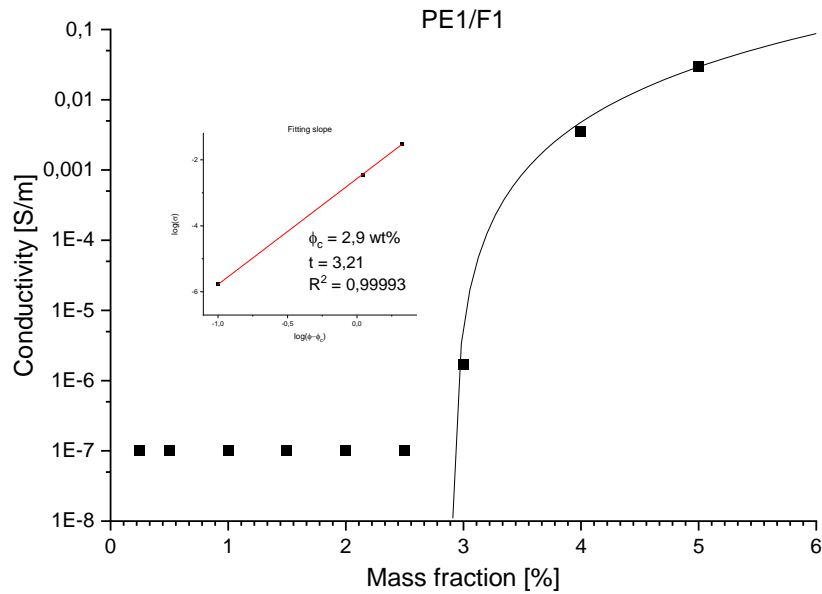


Figure 19, The electrical conductivity as a function of filler loading of PE1/F1 with a fitted curve according to the percolation threshold powerlaw equation

The higher amount of interconnect particles there is in a composite, the higher the electrical conductivity is. This is clearly visible by comparing the SEM pictures with the measured electrical conductivity in Figure 19. The measured electrical conductivity values from each composite concentration is plotted and fitted with an equation to the percolation power law. The acquired percolation threshold for PE1 with filler F1 was  $m_c = 2.9$  wt% with a slope value of  $t = 3.21$ . Comparing Figure 19 with (a) and (b) in Figure 18 we can see that it is between these two filler concentrations that we can observe a local interconnected network in the SEM picture. However, it should be noted that the particles do not need to be in direct physical contact as mentioned before due to the phenomena of tunnelling electrons between the conductive particles. At the 3% mark we see that there is a sudden increase of electrical conductivity compared to the lower concentrations. As this region is the percolation region, it is here where the global conductive networks are starting to form. One must be noted that the measured conductivity might not be entirely accurate since the lower conductivities are actually not at the measured value. This is due to the inaccuracy of the instrument which was used to measure the current of the sample. In reality, these values are much lower and perhaps some concentrations actually start to percolate even before the calculated percolation threshold but are not measurable by the used instrument.

#### 4.1.2 PE2/F1

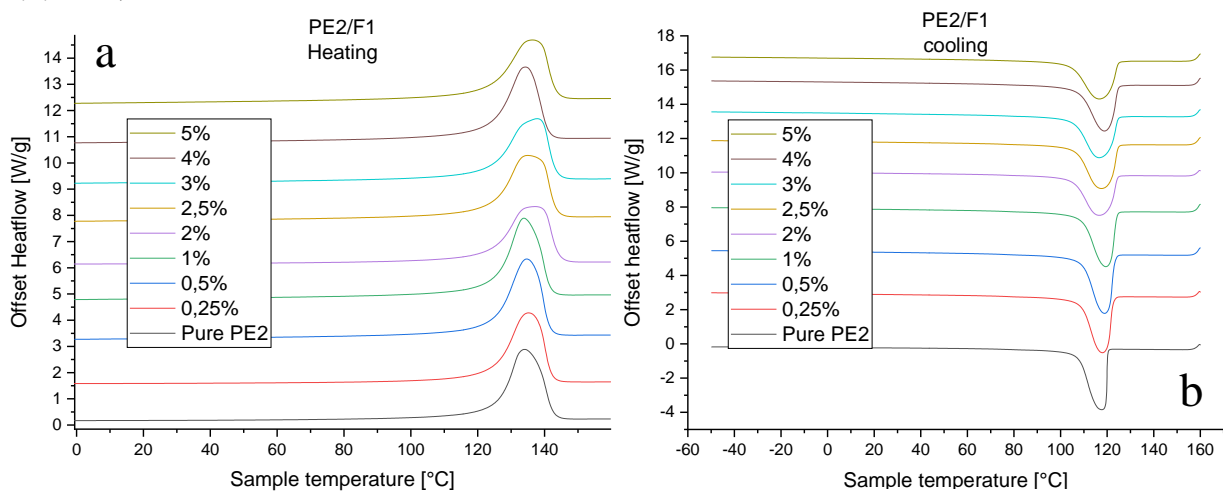


Figure 20, (a) DSC curve of melting peaks of different compositions of PE2 with filler F1, (b) DSC curve of crystallization peaks of different compositions of PE2 with filler F1.

Figure 20, shows a thermal analysis of PE2 with filler F1 showing heat flow vs. temperature. The values of the crystallization and the melting peaks,  $T_c$  and  $T_m$ , can be seen in Figure 32 & 33. The  $T_c$  and  $T_m$  shows an inconclusive trend with increased filler loading. Similar to PE1/F1 composite, the PE2/F1 manufacturing methods differed for some concentrations hence the reason why they look different. The crystallization temperature of PE2/F1 with increased filler load had an inconclusive trend. The melting temperature was observed to initially increase then slightly decrease. Comparing the cooling temperature with the degree of crystallinity seen in Figure 34, we can conclude that the fillers are acting as nucleating agents, lowering the activation energy needed to start the crystallization processes of PE2/F1. However, with increased filler load we can see a decrease in the degree of crystallinity due to the filler hindering the crystallization kinetics.

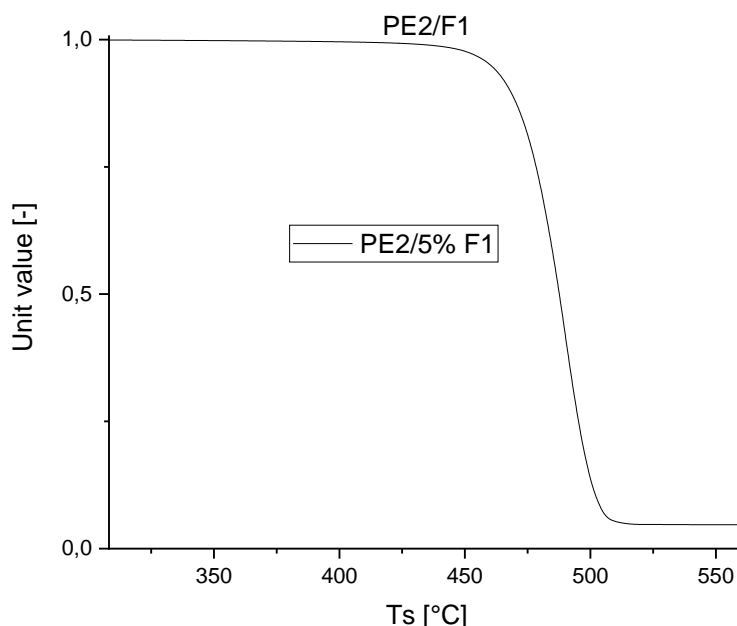


Figure 21, TGA curve of the degradation of PE2 with 5wt.% of filler F1.

Table 2, Table of calculated residue from TGA of PE2 with F1 compared to desired filler loading of F1.

PE2/F1 TGA Results	
Filler loading (wt.%)	5
Residue @ 550 °C (wt.%)	4,7
Onset temperature (°C)	471.5

The TGA results of PE2 with filler F1 showed an accurate weight of desired filler amount. Figure 21 shows the thermal degradation curve of PE2/5wt%F1 with a residue showcased in Table 2. It has to be noted that this method of calculating the residue is a rough approximation of the filler amount since the instrument is not accurate with low amounts of residue.

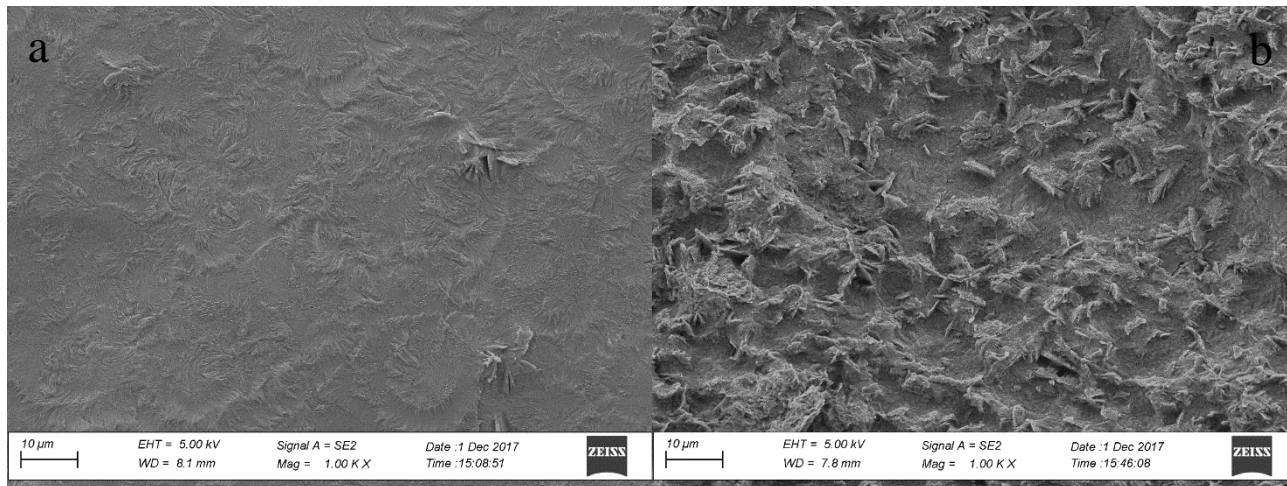


Figure 22, (a) SEM of pure PE2 at a magnification of 1000x, (b) SEM of PE2/1,5%F1 at a magnification of 1000x.

In Figure 22a, we can see the crystalline structures of pure PE2, while in Figure 22b, we can observe more protruding crystalline structures due to the filler acting as nucleation sites for the crystalline growth. The filler particles in Figure 22b is PE2/1,5wt%F1 shows a certain degree of interconnected particles because it is above the calculated percolation threshold, however it is visible that there are some gaps of pure polymer. This makes sense since 1.5 wt% is close to the percolation threshold of 1.3 wt%. At this concentration the conductive network just starts to form global pathways but are somewhat diffused.

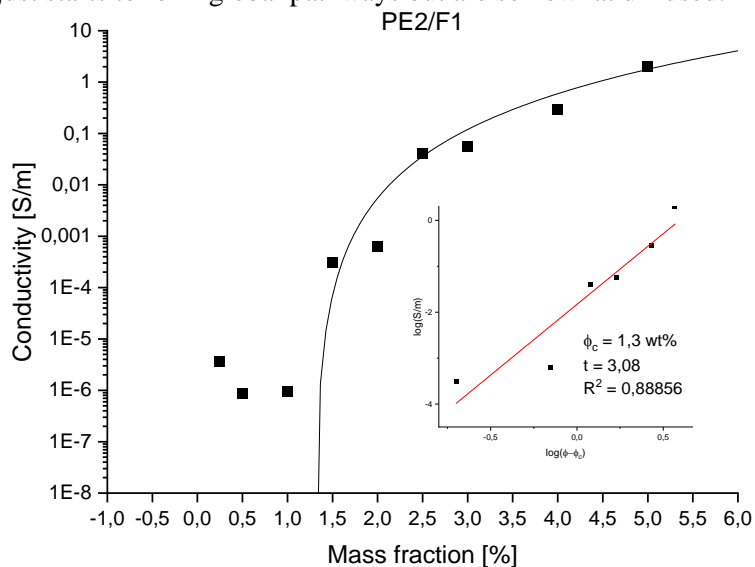


Figure 23, Electrical conductivity as a function of filler loading of PE2 with filler F1.

Comparing Figure 22 with Figure 21, we can see that the SEM sample of PE2/1.5 wt%F1 is close to the calculated percolation threshold. Comparing the conductive trend of PE2/F1 with PE1/F1, we can see that the conductivity at the same filler loads are higher when incorporated in PE2. This supports the theory that the filler behaves differently in different polymer matrices. Not only is the conductivity improved but also the percolation threshold is lower than that of PE1/F1.

#### 4.1.3 PE2/F4

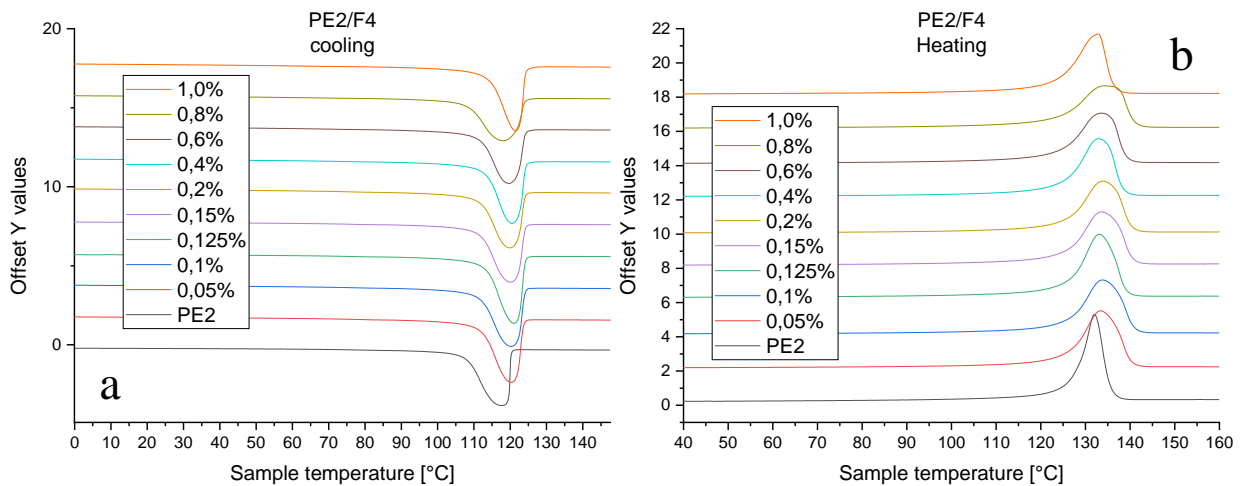


Figure 24, (a) DSC curve of melting peaks of different compositions of PE2 with filler F4, (b) DSC curve of crystallization peaks of different compositions of PE2 with filler F4.

Filler F4 is different from filler F1 in the sense that its dimensionality is different. We can see the difference of the different fillers effect on the polymer PE2 crystallization temperature in Figure 24. While filler F1 has little effect on PE2's crystallization temperature, F4 has much more profound affect even at 0.05 wt.%. Overall no conclusion could be drawn from the melting and crystallization temperature other than that the crystallization temperature is increased at a low filler content and stay stable with increased filler loading. The degree of crystallinity as seen in Figure 34 shows a strong nucleating effect even at 0.05 wt.% and later decreasing in crystallinity with increased filler content. In contrast to F1 in the same polymer matrix we can see a much stronger nucleating effect, however it is rapidly decreasing in crystallinity the more of filler F4 is added. This concludes that F4 also acts as a nucleating agent but inhibits the crystallization kinetics more than it nucleates at much lower filler contents.

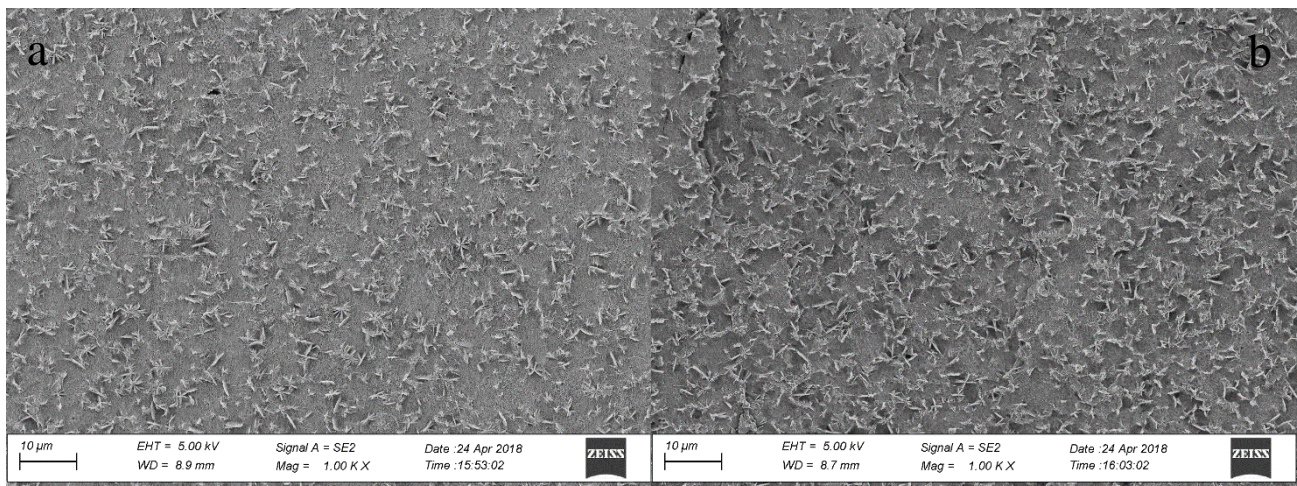


Figure 25, (a) SEM of PE2/0.125wt.%F4 at a magnification of 1000x, (b) SEM of PE2/0.15wt.%F4 at a magnification of 1000x.

Figure 25 shows PE2 with filler F4 of concentrations respectively 0.125 wt.% and 0.15 wt.%. We can see that the latter composition has a higher density of crystalline structures on the surface due to it having a higher filler loading. We can clearly see that this is the filler acting as a nucleation site for the crystallization of the polymer.

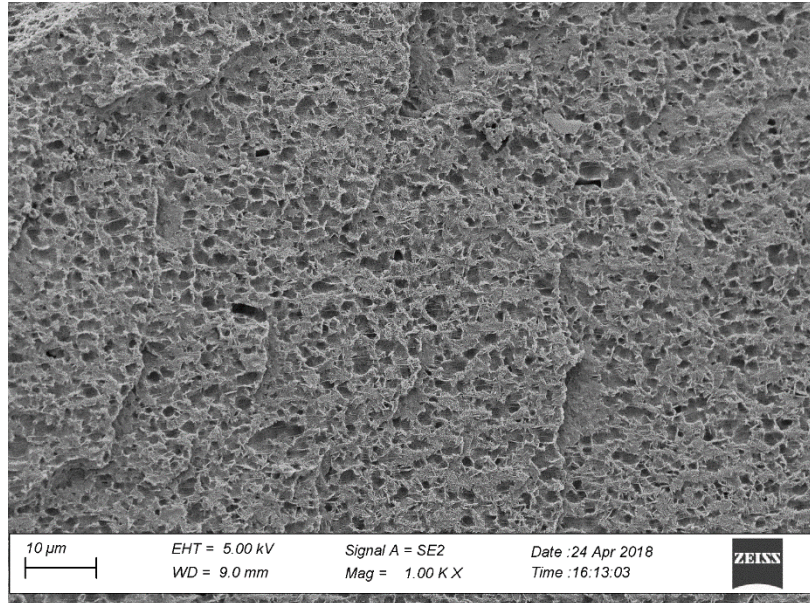


Figure 26, SEM of PE2/1wt.%F4 at a magnification of 1000x,

Figure 26 is PE2 with 1wt% of filler F4 which is substantially more in filler loading than the previous compositions in Figure 25. This is evident on the amount and the density of crystalline structures on the surface of the composite. At higher magnification, it was observed that the nanofiller tended to align parallel with the pressing direction from the hot pressing. This alignment could perhaps have an influence of the electrical conductivity since the electrical samples cut out from the plaque that was pressed had different conductivities depending on where it was cut on the sample. However, due to inaccuracy of pressing technique, there might be local regions which were subjected to higher squeeze flow due to distribution of the composite in the pressing mould thus resulting in an increase of particle alignment.

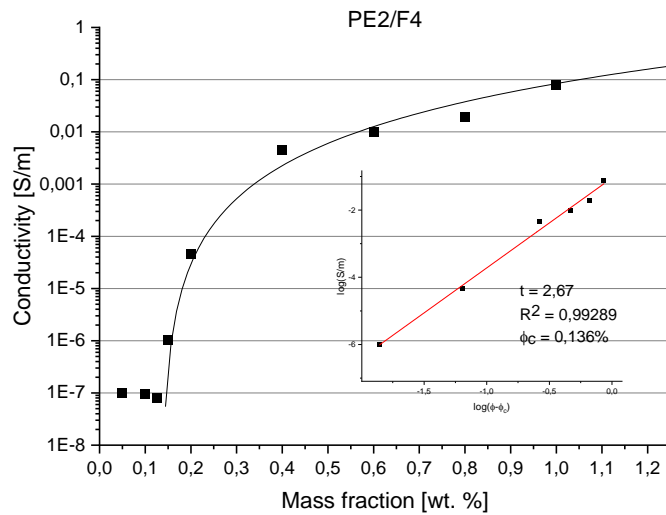


Figure 27, Electrical conductivity as a function of filler loading of PE2 with filler F4.

In Figure 27, we can see that the percolation threshold for the composite PE2/F4 was fitted to a value of  $m_c = 0,136\text{wt}\%$ . This critical concentration is significantly lower than that of PE2/F1 due to filler F4 having a different aspect ratio and molecular structure than filler F1. We can see that the degree of conductivity is the same order of magnitude when PE2/F4 is at 1 wt% and PE2/F1 is at 5 wt%.

#### 4.1.4 PE3/F1

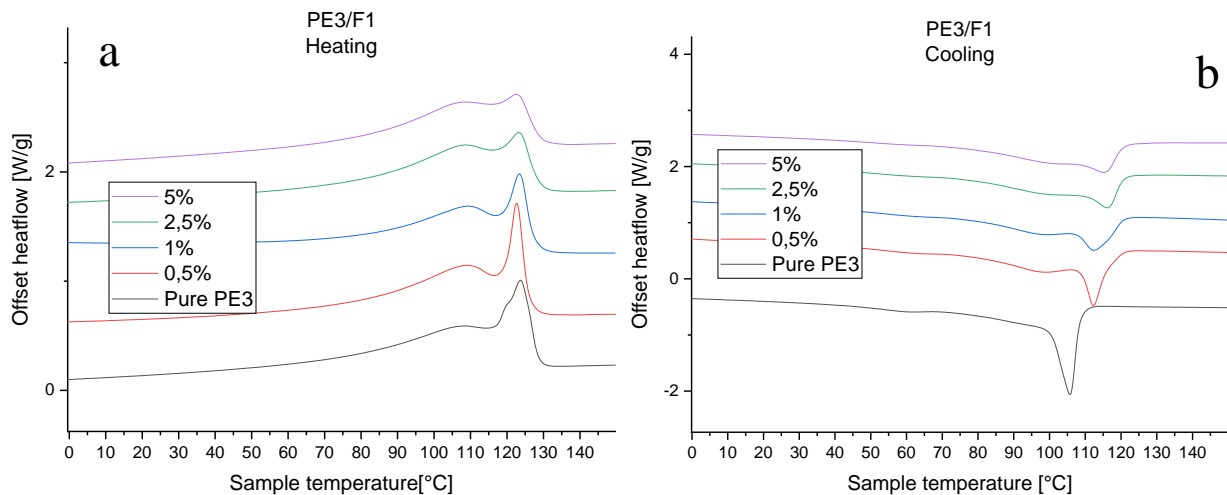


Figure 28, (a) DSC curve of crystallization peaks of different compositions of PE3 with filler F1, (b) DSC curve of melting peaks of different compositions of PE3 with filler F1.

In Figure 28a, we can see that the crystallization temperature is affected by the filler load. In pure PE3, we see that there are two crystallization peaks, one for primary crystallization and the other for secondary crystallization. It was observed that with increased filler loading the two different crystallization temperature shifted to a lower temperature. The secondary crystallization temperature shifted by roughly 37°C by adding 0.5 wt% of F1 while the primary shifted 7 °C. We can see in Figure 33 that the polymer's melting temperature is remaining approximately constant with increased filler loading while the polymers crystallization temperature seems to have strong nucleation affect even at low concentrations and continuously increasing in temperature to a certain point where it seems to be saturated. The degree of crystallinity seen in Figure 34 shows a steady decrease in crystallinity with increased filler loading. The degree of crystallinity of PE3/1wt%F1 seems to be an artefact in the calculation. Overall, we see a strong dependence of the interactions between the polymer PE3 with filler F1 by the means that the filler acts as a nucleating agent while inhibiting the crystallization kinetics.

#### 4.1.5 PE4/F1

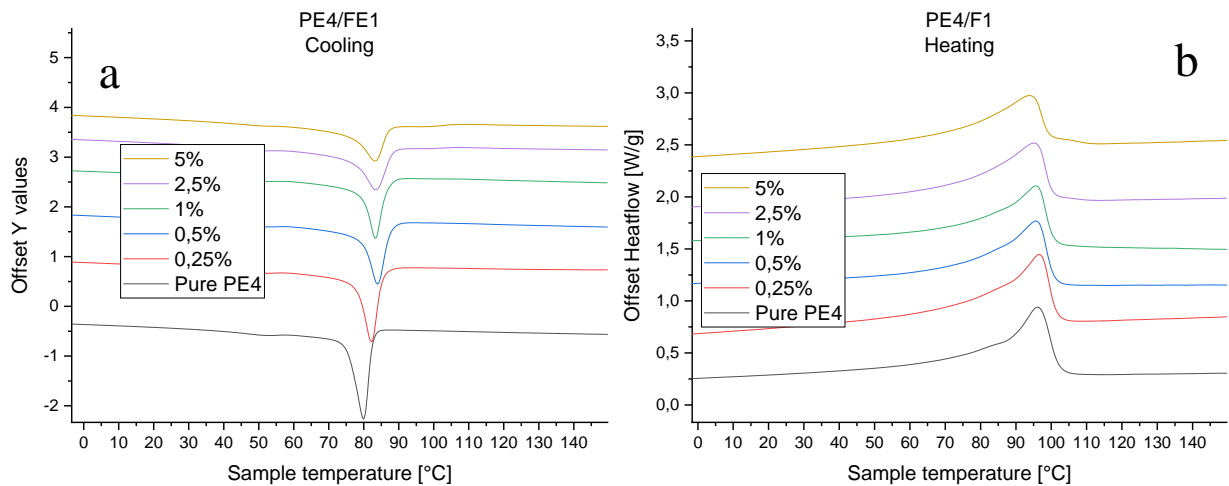


Figure 29, (a) DSC curve of crystallization peaks of different compositions of PE4 with filler F1, (b) DSC curve of melting peaks of different compositions of PE4 with filler F1

Similar to the previous mentioned polymer PE3, polymer PE4 has two distinctive peaks in both the crystallization and the melting temperature in Figures 29. In Figure 29a, the secondary melting peaks is less obvious to notice since it seems to merge with the bigger primary peak. In figure 32, we can see that the crystallization temperature is increasing with filler loading, while the melting temperature, seen in figure 33, is slightly decreasing with filler loading except for the composition with 0,25wt% where there is a slight increase in melting temperature. This could be due to inaccuracy of the instrument or the preparation method. The filler has a substantially lower effect on the melting temperature than that of the crystallization temperature. The degree of crystallinity was observed to increase in low filler loading but decrease in higher filler loadings. In Figure 34, we can see the crystallinity increases from 36% to 38% when adding 0.25 wt% of F1 into the polymer. The crystallinity remains at 38% for 0,5wt% but decreases down to 33% at 1 wt% filler loading.

#### 4.1.6 PE5/F1

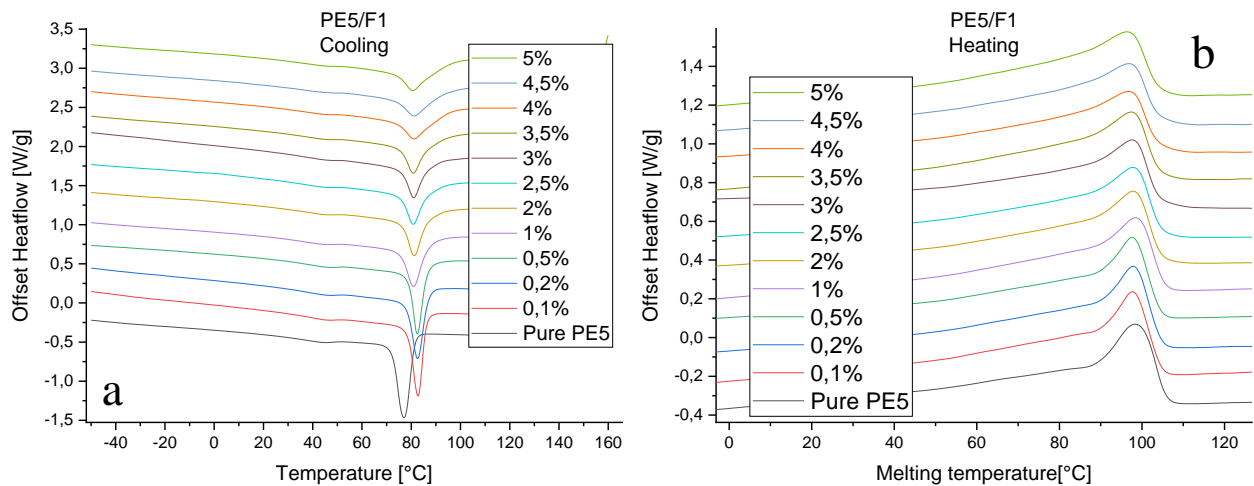


Figure 30, (a) DSC curve of crystallization peaks of different compositions of PE5 with filler F1, (b) DSC curve of melting peaks of different compositions of PE5 with filler F1.

In figure 30a we see cooling curves of PE5 with filler F1 with increasing filler loading. The crystallization temperature has a considerable increase in temperature at 0.1 wt% of filler F1. This temperature remains constant to 0.5 wt% and then drops down slightly at 1% and then remains constant up to 5 wt%. The melting temperature seen in figure 30b stays roughly the same but with a slight average decrease in melting temperature with increased filler loading. The degree of crystallinity seen in figure 34, shows an increase of crystallinity at lower filler content then a decrease in crystallinity at higher filler loading. As mentioned before, this is most probably caused by the filler acting as a nucleating agent but at the same time inhibiting the crystallization kinetics thus resulting in a decrease in crystallinity but an increase in crystallization temperature.

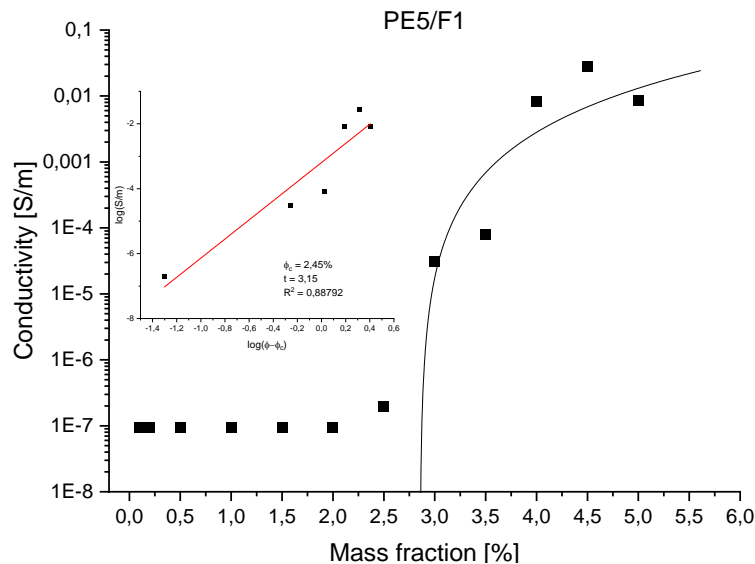


Figure 31, Electrical conductivity as a function of filler loading of PE5 with filler F1.

The percolation threshold of PE5 with filler F1 was calculated to be approximately  $m_c = 2.45$  wt%. The fitting accuracy was somewhat poor due to the electrical conductivity values not being consistent. This may be due to an error in calculating the correct weight fraction of the filler or that the processing parameters were changed. It is observed that the concentrations of 3 wt.% and 5 wt.% of filler F1 deviates from the other obtained values.

#### 4.1.7 Summary of polyethylene composites

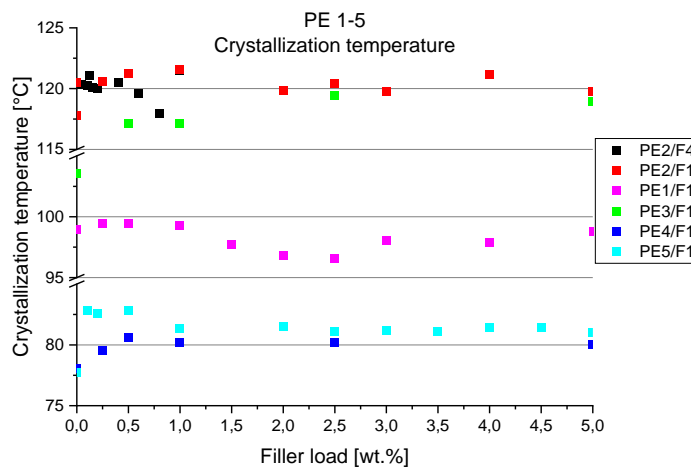


Figure 32, Crystallization temperature as a function of filler of polyethylene composites with fillers F1 & F4.

In Figure 32, we can see the crystallization temperatures of the polyethylene polymers with filler F1 and one composite with filler F4. The composites with filler F1 has a trend of initially increased crystallization temperature at low filler content and then a decreasing trend with increased filler amount. We can also observe that the polymers differ in their morphological structure even though they are all polyethylene based composites. The composites PE2/F4 has a more noticeable trend compared to the composites with the filler F1. This is due to the filler having a different aspect ratio.

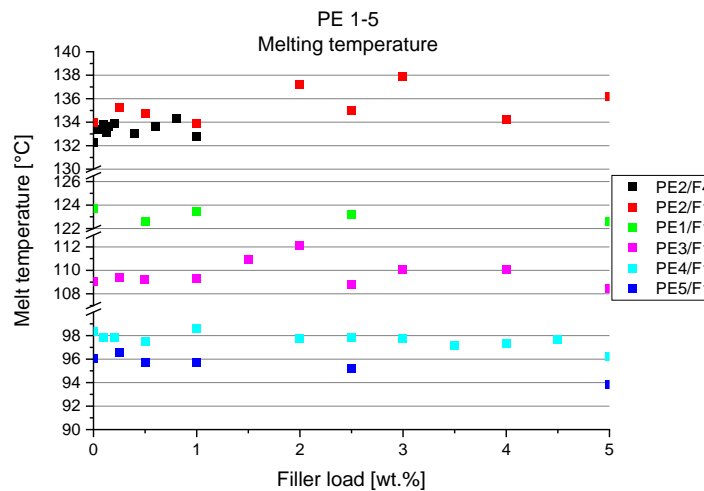


Figure 33, Melting temperature as a function of filler of polyethylene composites with fillers F1 & F4.

The overall conclusion of the melting temperature of polyethylene based composites is that it increases from their pure components while decreasing ever so slightly in temperature with increased filler content as seen in figure 33.

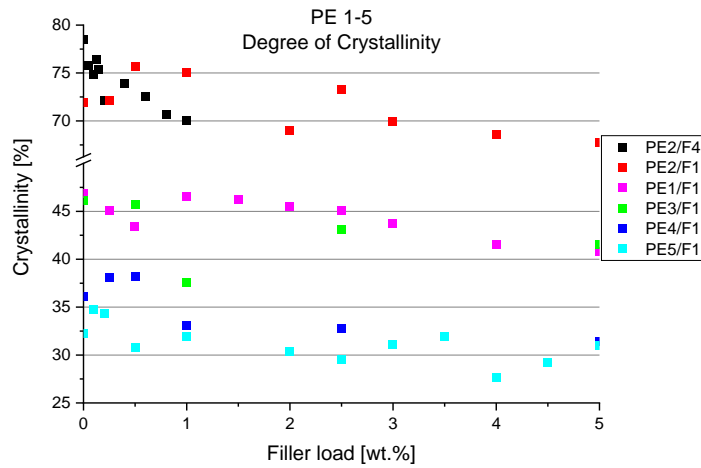


Figure 34, Degree of crystallinity as a function of filler of polyethylene composites with fillers F1 & F4

We can see a strong correlation of increased degree of crystallinity in low filler amount while in higher filler amount we see a steady decrease of the degree of crystallinity. In figure 34, we see polyethylene composites with filler F1 and filler F4 having a similar effect but in different filler concentrations.

## 4.2 Polypropylene composites

### 4.2.1 PP1/F1

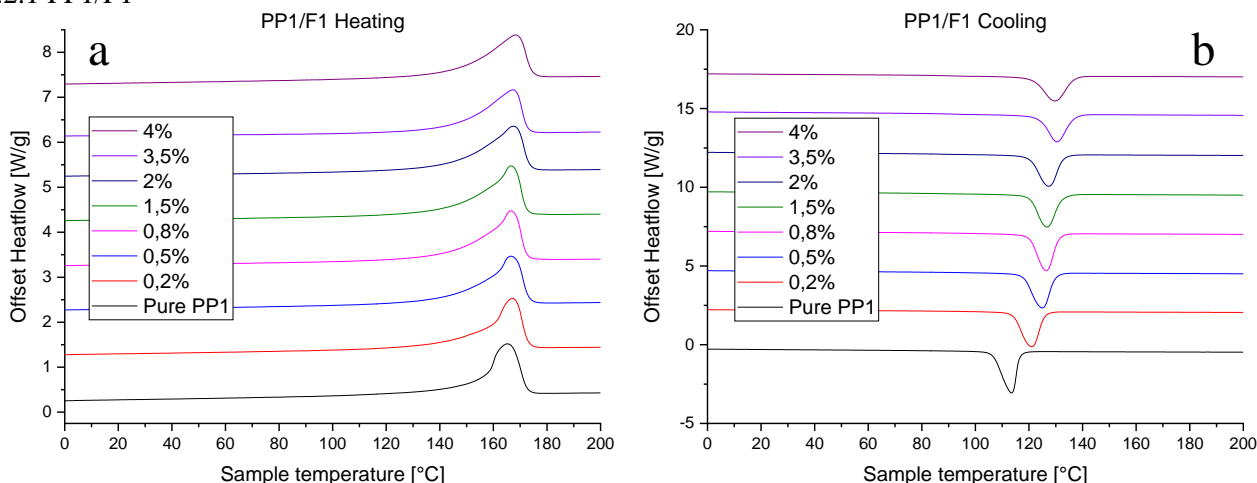


Figure 35, (a) DSC curve of melting peaks of different compositions of PP1 with filler F1, (b) DSC curve of crystallization peaks of different compositions of PP1 with filler F1.

Figure 35a shows the melting curves of PP1 with filler F1. We can see that there is little change in the melting temperature pure visually. If we look closer in Figure 42, we can see that there is a slight increase in temperature with increased filler content but only by a few degrees. There is a quite notable change in melting temperature. In Figure 35b, we can see that there is a strong effect of the filler on the melting temperature even at low filler concentration. The melting temperature is continually increasing but with less effect with increased filler loading. If we compare the degree of crystallinity, seen in figure 43, we can see that there is an initial increase in crystallinity and then a decrease with higher filler content. Again, as previously concluded, this is due to the fact that the filler acts as a nucleation agent but prevents the crystallization kinetics thus resulting in such a particular way.

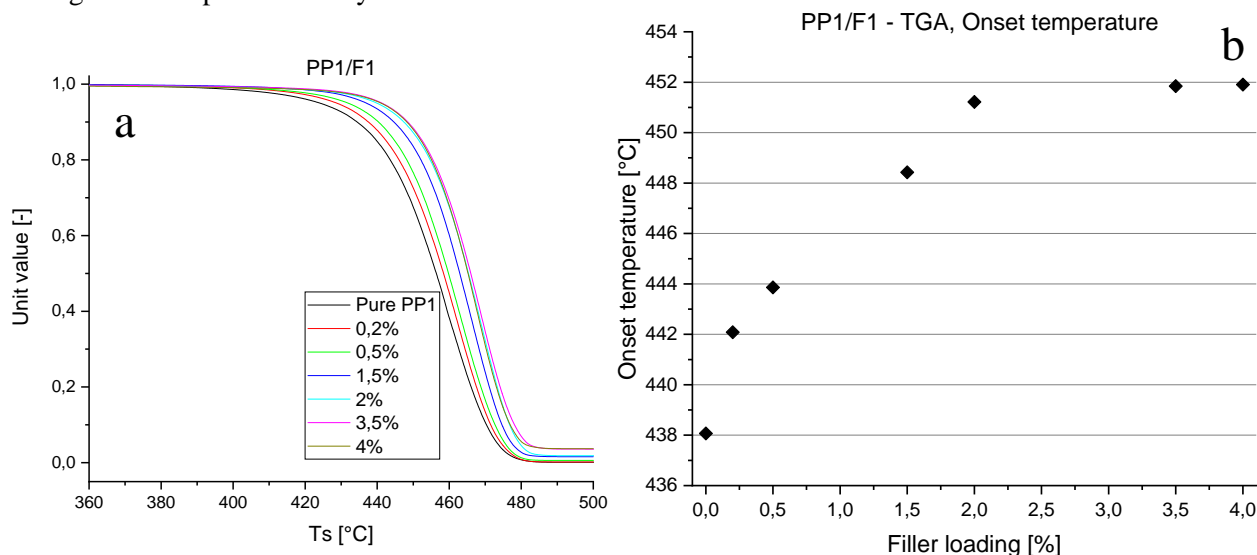


Figure 36, (a) TGA curves of the degradation of different compositions of PP1 with filler F1, (b) Onset temperature calculated from the TGA of the different compositions of PP1/F1.

Table 3, Table of calculated residue from TGA of PE1 with F1 compared to desired filler loading of F1

PP1/F1 TGA Results							
Filler loading (wt.%)	0	0.25	0.5	1.5	2	3.5	4
Residue @ 550 °C (wt.%)	~0	~0.14	0.57	1.54	1.79	3.54	3.6
Onset temperature (°C)	438.1	442.1	443.9	448.4	451.2	451.8	451.9

A thermogravimetric analysis was done to estimate the amount of filler that was desired for each concentration. Each compound showed that the compounding of the filler material and the polymer matrix was done in a correct manner by calculating residue that was left over from the degradation of the composites in an inert atmosphere. In Table 5, we can see that the calculated residue from the composites had a sufficiently accurate value except for perhaps the highest concentration that deviated by a small amount.

The thermal degradation as seen in figure 36 of the different composites of PP1/F1 shows that there is an increase in thermal stability with increased filler content.

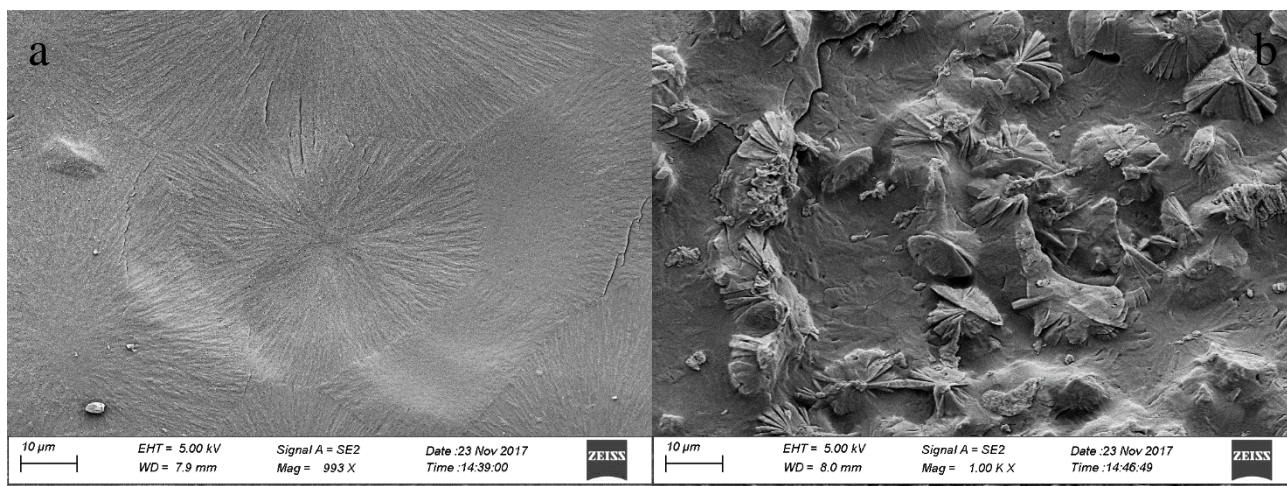


Figure 37, (a) SEM picture of pure PP1 at a magnification of 993x, (b) SEM picture of PP1/0,5%F1 at a magnification of 1000x.

Figure 37a shows an SEM picture of pure PP1 where we can see clearly the spherulites forming grains and grain boundaries with neighbouring grains. We can also see that there are little irregularities of crystalline structures on the surface of the pure PP1. While in figure 37b we can see that there are distinctively more crystalline structures protruding from the surface.

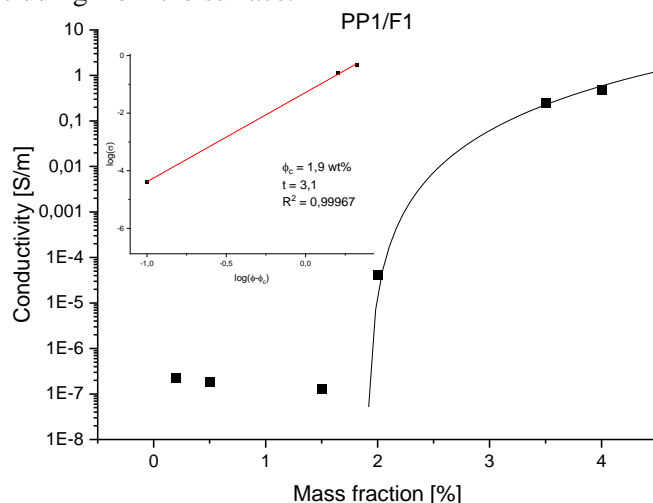


Figure 38, Electrical conductivity as a function of filler loading of PP1 with filler F1.

Figure 38 shows electrical conductivity for the composite PP1/F1 as a function of filler amount of F1. The linear fitting of the logarithmic values of the conductivity as a function of the percolation powerlaw equation was calculated to be  $m_c = 1.9$  wt.%. The accuracy of this fitting may be disputable since there are only three values of conductivity above the percolation threshold. Additionally, two of the values are in the conductive region while the third initial lower values are almost exactly on the calculated percolation. As mentioned before, without the real values of the lower concentrations, an accurate calculating is hard to achieve. The lower concentration values are simply noise from the oscilloscope that was used to measure the current through the specimen.

#### 4.2.2 PP2/F1

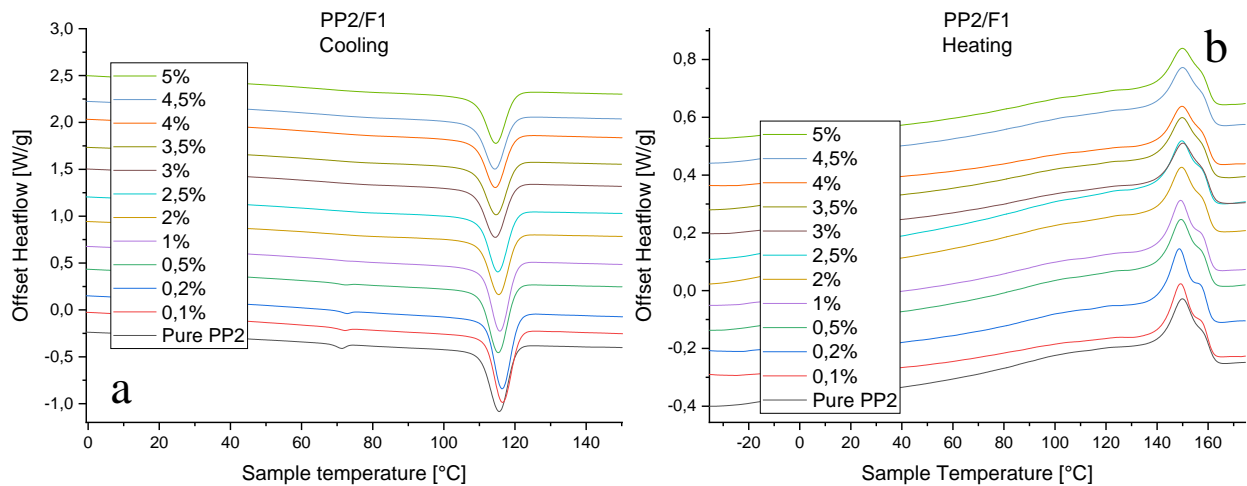


Figure 39, (a) DSC curve of crystallization peaks of different compositions of PP2 with filler F1, (b) DSC curve of melting peaks of different compositions of PP2 with filler F1.2

In figure 39a, we can see the crystallization peaks of the polymer PP2 with filler F1. There are two distinctive peaks that are observable in the lower filler concentrations. This is the secondary crystallization temperature, and as we can see in figure 39a, the peak becomes smaller with increased filler amount. At 2 wt.% of F1 it is not observable at all. The primary crystallization peak was observed to initially increase and then decrease the crystallization temperature.

In figure 39b, we can see the melting peaks of the same composite in different compositions. There was a small observable of decreased melting temperature in the lower filler concentrations, as we can see closer in Figure 42, and later increase in melting temperature with higher filler loadings. Comparing the melting and crystallization temperature with the degree of crystallinity for PP2/F1 seen in Figure 41, we can conclude that the filler acts as a nucleating agent but inhibits the crystallization kinetics more than nucleating it after a certain filler loading. The secondary crystallization peak indicates that no distinctive secondary melting point is formed due to the filler having such high activation energy that the peak simply blends in to the crystallization curve.

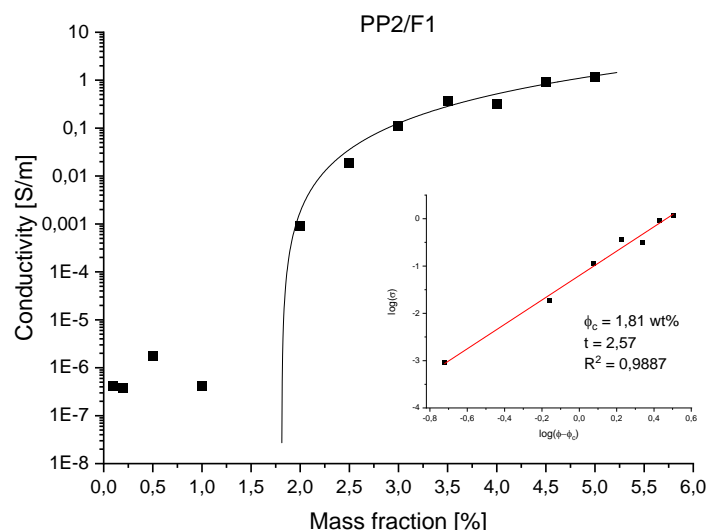


Figure 40, Electrical conductivity as a function of filler loading of PP2 with filler F1

Figure 40 shows us a graph of the electrical conductivity of PP2 with filler F1. The lower conductivity values at filler loading from and below 1 wt.% is the background noise that was detected from the measuring instrument. As we can see on the graph, the fitted percolation threshold was calculated to be  $m_c = 1.81$  wt.% with a  $R^2 = 0.9887$ .

### 4.2.3 Summary of polypropylene composites

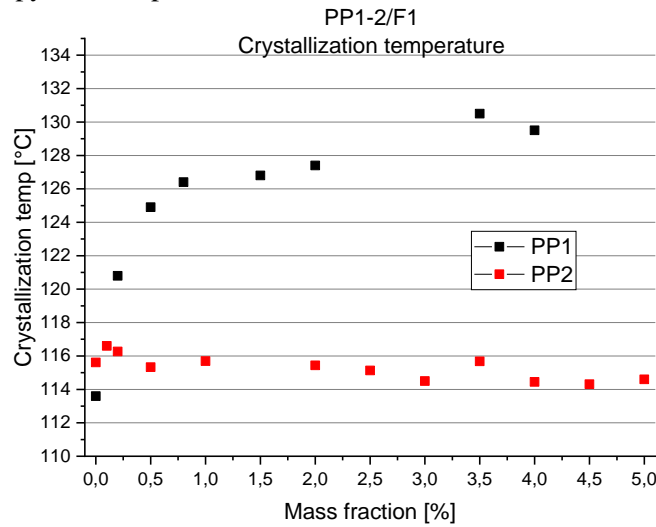


Figure 41, Crystallization temperature as a function of filler of polypropylene composites with filler F1.

In Figure 41, we can see that the crystallization temperatures differ a lot between the PP1 and PP2. This is due to PP2 having a different polymer architecture than that of PP1. We can clearly see that in the case of PP1/F1 that the filler is increasing the crystallization temperature, while PP2/F1 is barely affected. There might be some initial increase in lower filler amounts, but the evidence is rather inconclusive.

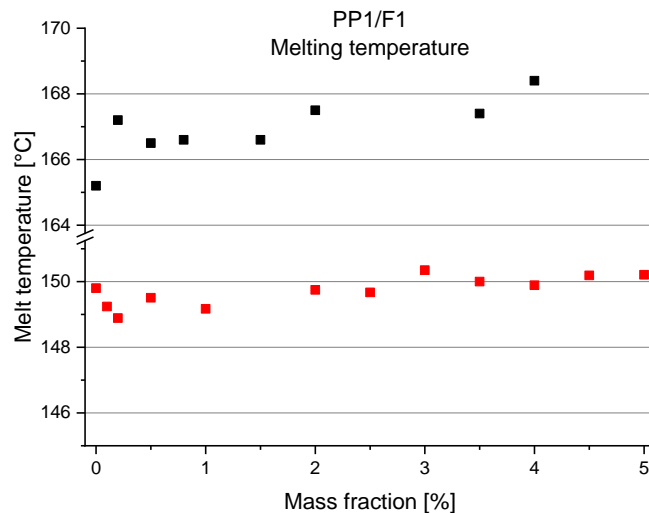


Figure 42, Melting temperature as a function of filler of polypropylene composites with filler F1.

Figure 42 above, shows a similar trend for the melting temperature of PP1 and PP2 as the case with the crystallization temperature. The average trend for PP1/F1 is that its melting temperature increases with increased filler loading, while PP2/F1 seems to initially lower then stay constant within 1 °C.

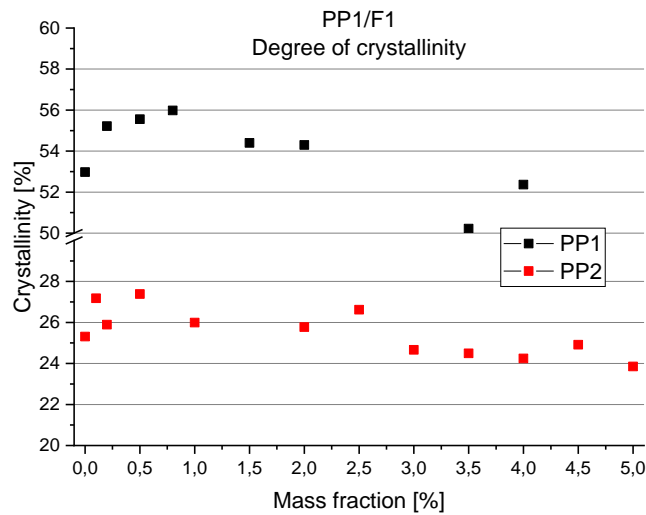


Figure 43, Degree of crystallinity as a function of filler of polypropylene composites with filler F1.

The degree of crystallinity, as seen in Figure 43, we can see that similarly to polyethylene composites, the polypropylene composites with filler F1 has the same trend of initially increased crystallinity in lower filler contents, while decreasing with higher filler content. This indicates yet again, that the filler F1 is acting as a nucleating agent while in the same time inhibiting the crystallization kinetics.

### 4.3 Electrical properties of PE and PP nanocomposites

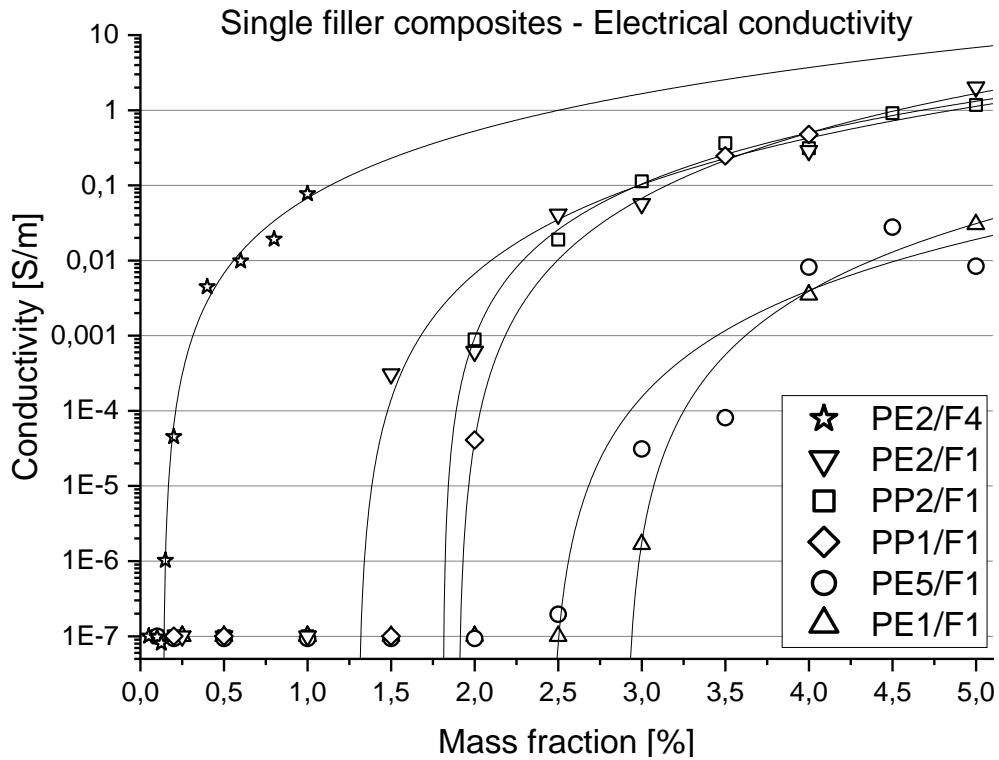


Figure 44, Electrical conductivity of all single filler and single polymer composites

Figure 44 shows the graph of all composites measured for electrical conductivity. The composite PE2/F4 had the lowest percolation threshold while PE1/F1 had the lowest. Comparing the different composites electrical properties can tell one something about the fillers interaction with the different polymers.

We can see that the filler F1 has a similar effect on the polypropylene composites. PP1 and PP2 has very similar percolation threshold.

The PE composites show very different results depending on what type of PE was used as a matrix for the filler F1. PE2 had the lowest percolation threshold of the polyethylene composites while PE1 had the highest.

Table 4, A table of all single filler composites of PE and PP showing the percolation threshold of each composite tested for electrical properties.

Composite	PE2/F4	PE2/F1	PP2/F1	PP2/F1	PE5/F1	PE1/F1
Percolation Threshold (wt.%)	0.136	1.3	1.81	1.9	2.45	2.9
t-exponent	2.67	3.08	2.57	3.1	3.15	3.21

The t-exponent's standard deviation  $s$ , was calculated to be approximately 0.272 with a mean value of 2.964. This value in reality would perhaps change to either a lower or higher value for the composites with different polymer matrices and different fillers if the measurements were made in a more sensitive machine. The conductivity values for pure polymer components that were used in this project are around  $10^{-12}$  S/m, while the DC setup only could measure down to  $10^{-7}$  S/m. The nanoparticles in the nanocomposites may have actually started to percolate below the calculated percolation threshold because there was a potential inaccuracy of 5 order of magnitude. In the same way the t-exponent may vary for these composites as well in actuality.

## 4.4 Hybrid composites

### 4.4.1 PP1/F1/F2

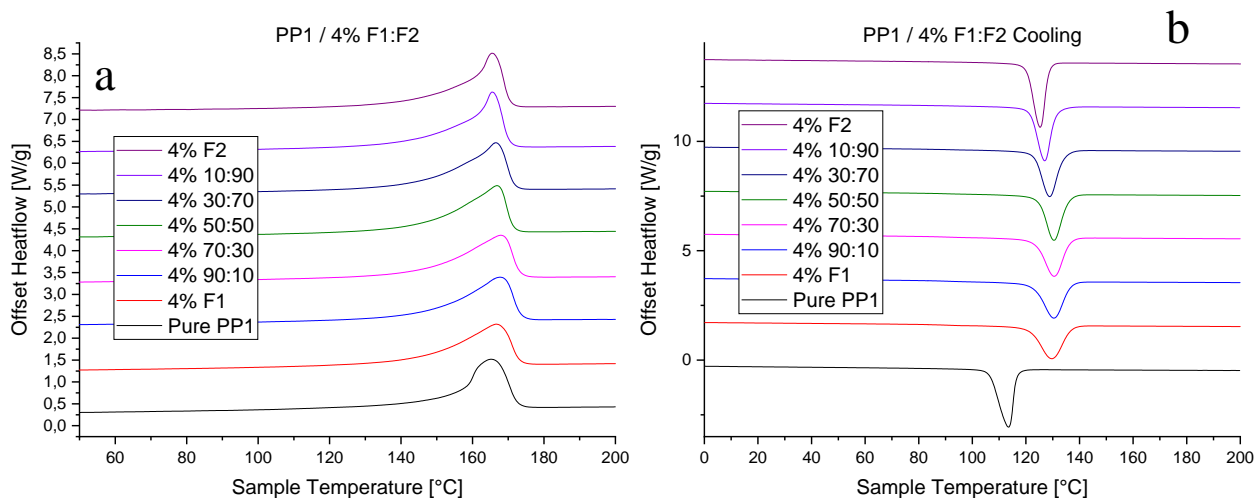


Figure 45, (a) DSC curve of melting peaks of different compositions of PP1 with fillers F1&F2, (b) DSC curve of melting peaks of different compositions of PP1 with fillers F1&F2.

We can see in figure 45a the melting temperatures of the hybrid composite PP1 with fillers F1 and F2. All curves except for the pure PP1 have a total filler concentration of 4wt% but in different filler ratios. Looking at the melting temperatures of the different filler ratios we can see that there is a change in the step height and broadening or narrowing of the peak width. Comparing the melting and crystallization peaks with the degree of crystallinity seen in Figure 50 we can see that there is a correlation between the maximum degree of crystallinity and the maximum crystallization temperature at a 50:50 ratio between fillers F1&F2. The degree of crystallinity and crystallization temperature seems to follow the same parabolic trend towards a maximum value at 50:50.

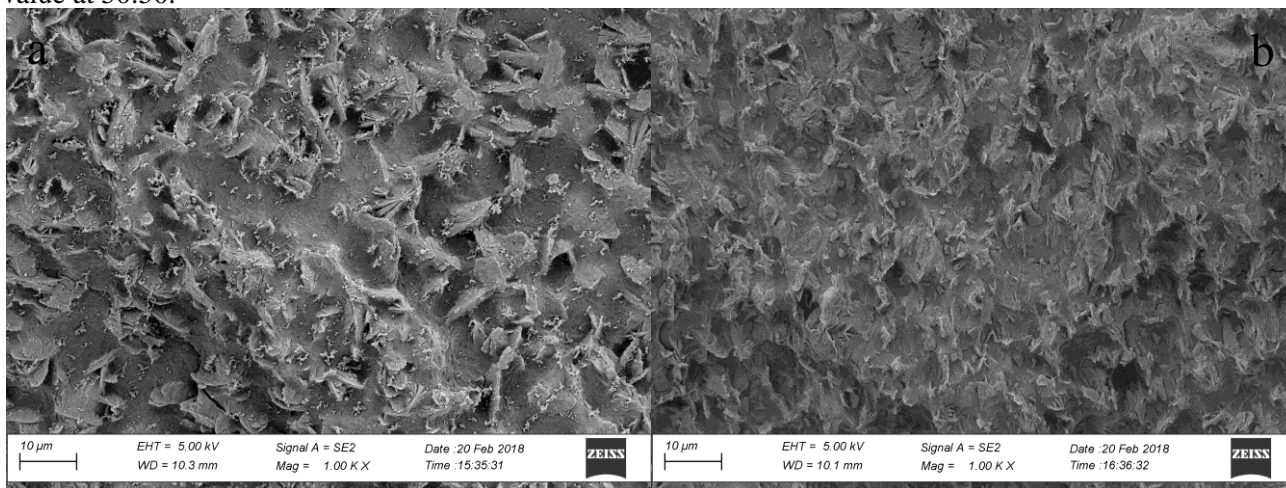


Figure 46, (a) SEM picture of PP1 with 4wt.% of filler F2 at a magnification of 1000x, (b) SEM picture of PP1 with 4wt.% of fillers 90wt.%F1 & 10wt.%F2 at a magnification of 1000x.

The figure 46 above shows an SEM of the hybrid composite which consists of filler F1 and F2 in polymer PP1 matrix. Figure (a) to the left consists only of filler F2 while figure (b) on the right has a filler ratio of 90%F1 and 10%F2. This composition showed to have the highest conductivity of the hybrid composites. We can see that the figure on the left has more visible crystalline structures protruding from the surface while the figure on the right has a lower degree of visibility of crystalline structures. There are a few reasons why this might be. One reason that the crystalline structure is much denser in the picture to the right making it hard to see individual crystalline structures. A second reason might be that the etching of the composite sample when prepared for the SEM was not executed properly. The latter case seems to be the most reasonable cause of observable difference.

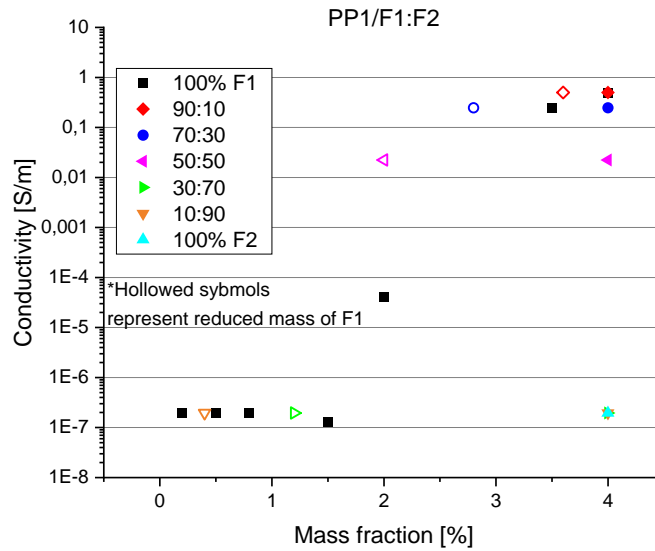


Figure 47, Electrical conductivity as a function of filler loading of PP2 with filler F1 & F2 and reduced mass fraction of F1 represented as hollow symbols.

Figure 47 above shows us the electrical measurement of the hybrid material PP1 with fillers F1 and F2 in different proportions. The hollowed symbols of respective colour is the reduced mass fraction of filler F1. This is to show when compared with PP1 with F1 how the filler F2 is affecting the percolation curve. In this case there seems to be a mixture of the two fillers that has an increase in overall conductivity. It is not by much and perhaps due to the vastly different ratios there might be a specific ratio value that has the most optimal mix of the two. In this study it observable that a ratio of 90%F1 and 10%F2 had a slightly more increased conductivity. This however might just be within the error bar of the conductivity. The value would have to be considerably higher or reproduced to see if the trend remains with other attempts. One thing that can be concluded is that it is possible to substitute filler F1 with filler F2 up to a mixture of 70% and 30% respectively without affecting the conductivity much of the composite at 4wt% filler loading.

#### 4.4.2 PP1/F1/F3

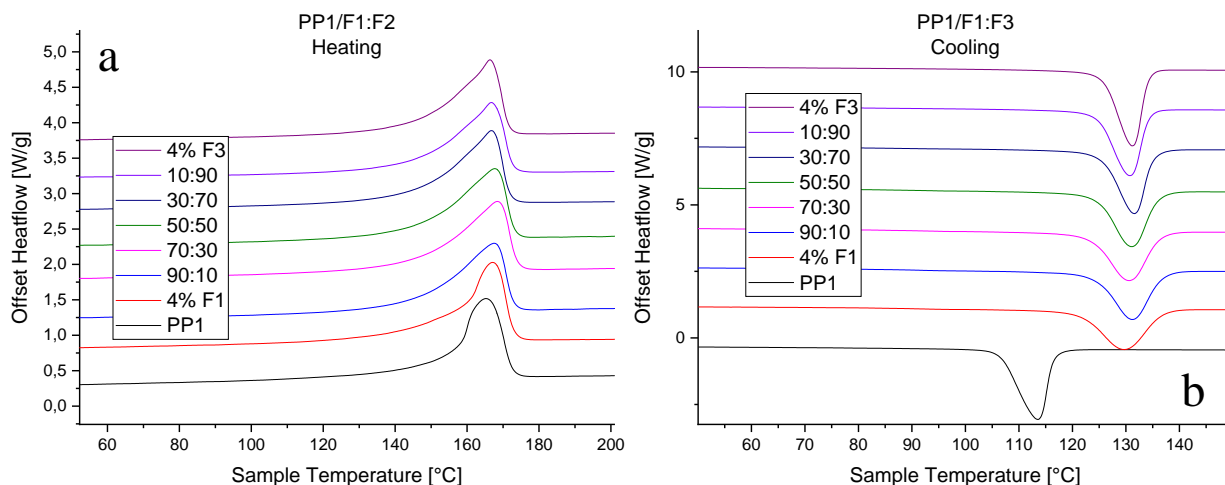


Figure 48, (a) DSC curve of melting peaks of different compositions of PP1 with fillers F1&F3, (b) DSC curve of crystallization peaks of different compositions of PP1 with fillers F1&F3.

In Figure 48a above we can see that the melting temperature is barely affected by the filler ratios, however when looking closer at Figure (a) which shows the melting temperatures of composite PP1 with fillers F1 and F3 we can see that there is a maximum melting temperature as a function of filler loading in the composite PP1 with 70%F1, 30%F3. The temperature difference of the different filler loading is just slight, but there seems to be a parabolic trend of the melting temperature where 70%F1 30%F3 is the maximum. Another remark that can be made is how the shape of the melting curve changes with different filler ratios. We can see that the peaks are sharper and steeper when its melting temperature has reached. Looking at the crystallization temperature we can see that there is no observable trend in the different filler ratios except for the peak height and width. As there was more of the filler F3 in the hybrid systems it is observable that the peak height increased and the width narrowed. This suggests that crystallization occurs more rapidly when the filler F3 is present in the polymer matrix. Looking at the degree of crystallinity in figure 50b we can see that there is as a parabolic trend as a function of the filler ratios. At 50:50 of F1:F3 there is an observable maximum in the degree of crystallinity.

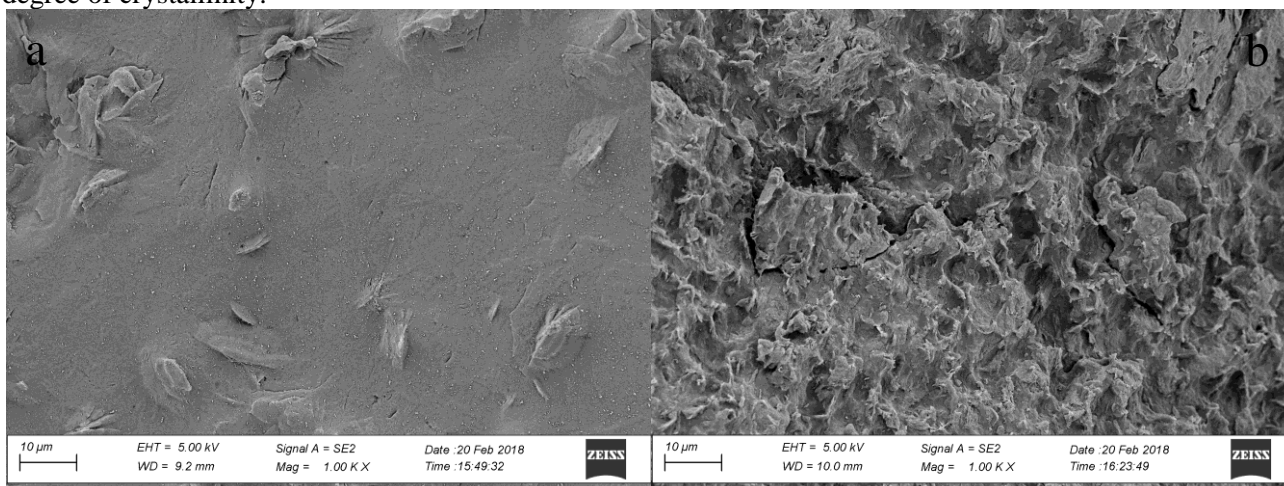


Figure 49, (a) SEM picture of PP1 with 4wt% of filler F3 at a magnification of 1000x, (b) SEM picture of PP1 with 4wt% of fillers 90wt.%F1 & 10wt.%F3 at a magnification of 1000x..

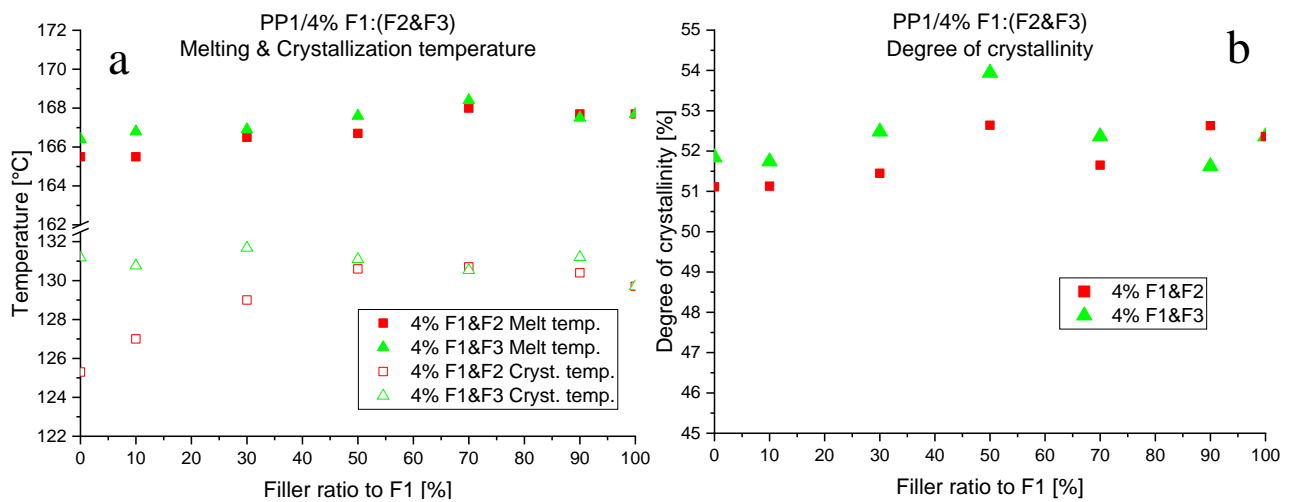


Figure 50, (a) Melting and crystallization temperatures as a function of filler ratio between the fillers F1&F2&F3, (b) Degree of crystallinity as a function of filler ratio between the fillers F1&F2&F3.

Figure 50 (a) above shows the melting and crystallization temperatures of composites PP1/F1/F2 and PP1/F1/F3. The graph is plotted temperature vs. filler loading of filler F1. For e.g. 70:30 F1:F2 is shown at 70% on the graph. The can see that the crystallization temperatures of the two different hybrid composites differ in their trend. F1&F2 composites was observed to have slightly lower values overall and especially in the ratios where F2 was dominant there was a considerable decrease in crystallization temperature compared to the other F1&F3 composites. This suggests that the crystallization process is different for the fillers F2 and F3 when incorporated into PP1 matrix.

The degree of crystallinity, seen in figure 50 (b), shows a similar trend of the two different hybrid composites. They both have a maximum degree of crystallinity at 50:50 filler ratio mixes and follow a parabolic trend which was a lower degree of crystallinity when more of either filler was the dominating filler proportion. It seems that the 50:50

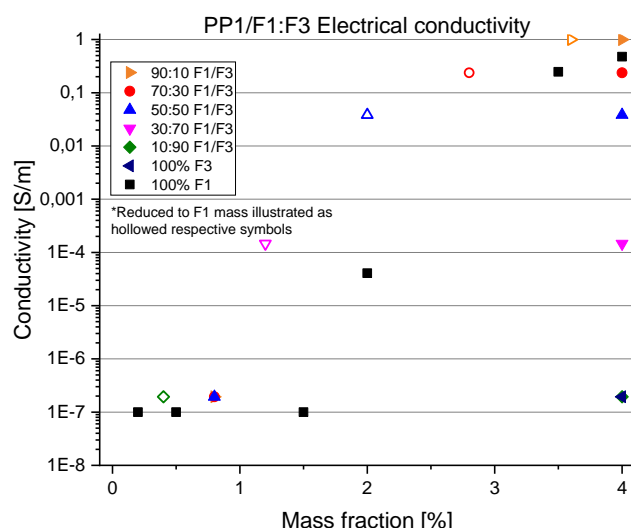


Figure 51, Electrical conductivity as a function of filler loading of PP2 with filler F1 & F3 and reduced mass fraction of F1 represented as hollow symbols.

Figure 51 above shows us the electrical measurement of the hybrid material PP1 with fillers F1 and F3 in different proportions. The hollowed symbols of respective colour are the reduced mass fraction of filler F1. In this case there seems to be a mixture of the two fillers that has an increase in overall conductivity. In this study it observed that a ratio of 90%F1 and 10%F3 had the highest conductivity of the filler ratios. The conductivity had increased in the factor of 2 compared filler F1 in the same filler concentration. Since this increase is considerably high it was deemed not to be an artefact. One thing that can be concluded is that it is possible to substitute filler F1 with filler F2 up to a mixture of 70% and 30% respectively without affecting the conductivity much of the composite at 4wt% filler loading. The filler ratio 30:70 was not able to measure any conductivity, however this is not a correct assessment since the instrument that was used could only measure the conductivity up to  $1 \times 10^{-7}$  S/m. In reality the values are lower but due to the measuring method they were not detected.

We can see that the filler F3 affects the percolation curve more than filler F2 hybrid composites in the way that the reduced filler proportion of F1 was more shifted to the left. This suggests that filler F3 is better at forming conductive pathways with filler F1 than filler F2 is with filler F1. This might be due to filler F3 having higher aspect ratio than that of filler F2.

Finally, the conductivity of both hybrid systems showed an increase in conductivity in filler ratios of 90%F1 and 10%F2/F3. This might be a bridging effect where the filler F3 connects the pathways of filler F1 in such a way that there are more connected pathways globally in the nanocomposite.

#### 4.4.3 PE2/F1/F4

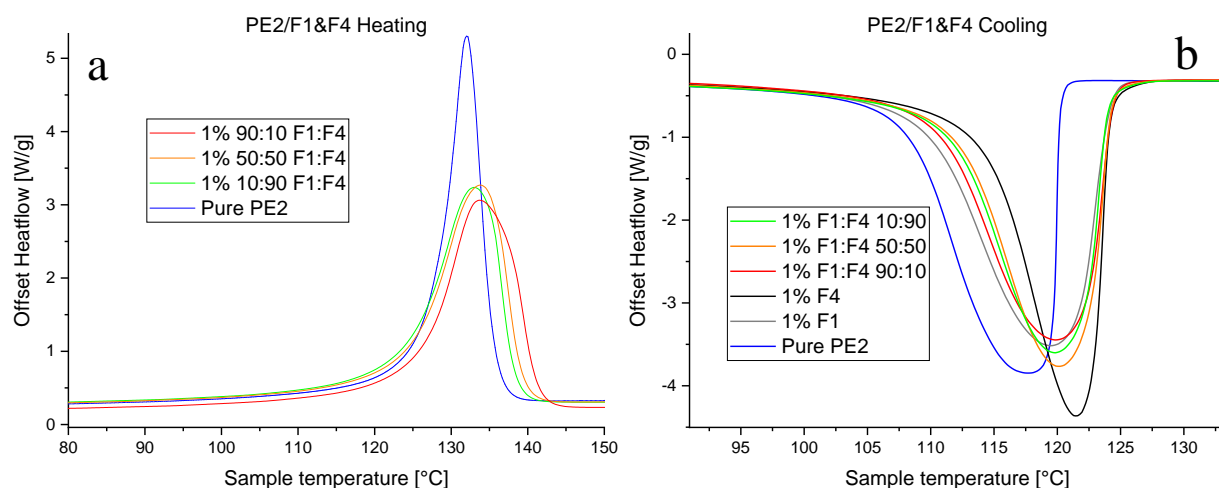


Figure 52, (a) DSC curve of melting peaks of different filler ratios of PE2 with 1 wt.% of fillers F1&F4, (b) DSC curve of crystallization peaks of different filler ratios of PE2 with 1 wt.% of fillers F1&F4.

The figures 52 above shows the melting and crystallization temperature of PE2 with fillers F1 and F4 in different filler ratios at a 1 wt.%. We can see in figure 44a that the melting temperature does not change depending in the filler ratio. The crystallization temperatures in figure 44b does not show any change either except for 1 wt.% of F4. This was deemed to be an artefact since it is the only concentration that differs in the visual aspect in the DSC analysis. This was mentioned before from Figure 24.

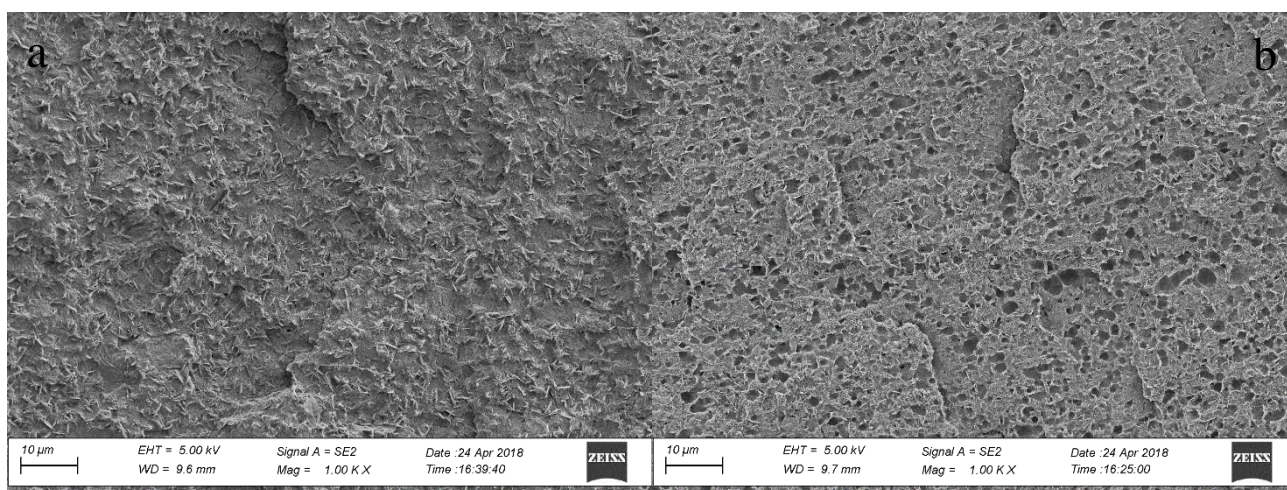


Figure 53, (a) SEM picture of PE2 with 1 wt.% of fillers 90%F1 & 10%F4, (b) SEM picture of PE2 with 1 wt.% of fillers 10%F1 & 90%F4.

Figure 53 above shows an SEM picture of PE2/1wt% of filler F1 and F4 in compositions 90:10 and 10:90 respectively. We can see in figure (a) that the surface contains more globular crystalline structure than that of figure (b) where more lamellar crystalline structure extends throughout the surface of the fractured sample. Looking back at figure 34 we can see that the degree of crystallinity of 1 wt.% F1 and 1 wt.% F4 has a difference of 5% in crystallinity. Comparing these values with the observed SEM pictures suggests that filler F1 has a higher influence of the degree in crystallinity proportionally to the same filler concentration. This might be that F1 creates spherulitic crystalline structures which are more densely packed crystals than that filler F4 that creates more lamellar crystal structures.

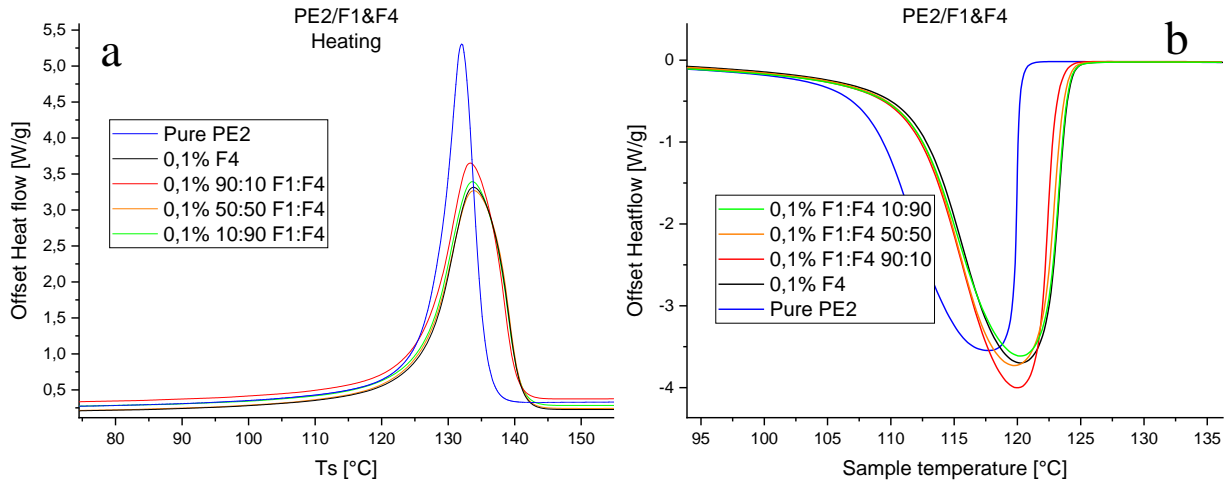


Figure 54, (a) DSC curve of melting peaks of different filler ratios of PE2 with 0.1 wt.% of fillers F1&F4, (b) DSC curve of crystallization peaks of different filler ratios of PE2 with 0.1 wt.% of fillers F1&F4.

The figure 54 above shows the melting and crystallization temperatures of the composite PE2/F1&F4 at a total filler concentration of 0.1 wt.%. The melting peaks decreased in step height but broadened significantly and shifted to a higher temperature. This results in a higher degree of crystallinity which we can see in figure 34. The crystallization peaks did not show a significant change in step height however, the peak was shifted and narrowed which in turn suggests that the filler gives the polymer a nucleating activation energy. As concluded earlier, this suggests that the filler acts as a nucleating agent.

The degree of crystallinity between the different filler ratios had a small but inconclusive change depending on what filler proportion was present in the polymer matrix.

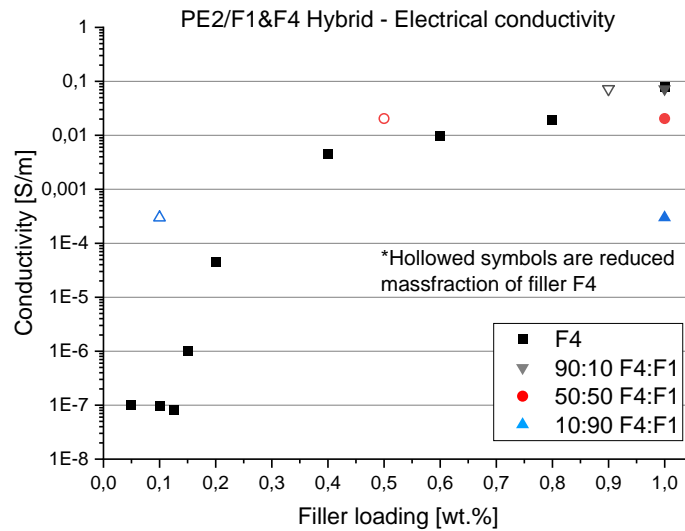


Figure 55, Electrical conductivity as a function of filler loading of PE2 with filler F1 & F4 and reduced mass fraction of F4 represented as hollowed symbols.

The conductivity of the hybrid composite of the fillers of F1 and F4 in PE2 matrix maintained the same conductivity as the single filler composite PE2/F4 when replaced 10 wt.% of its total filler loading with filler F1. As seen in figure 55 we can see that the 50:50 filler ratio also has considerably high conductivity as it is in the same order of magnitude in electrical conductivity even though half of its mass fraction has been replaced with filler F1. The ratio of 10:90 of filler F4 and F1 had a decrease in almost 2 orders of magnitude in electrical conductivity.

## 4.5 Blend composites

### 4.5.1 PE1/PP1/F1 Method A

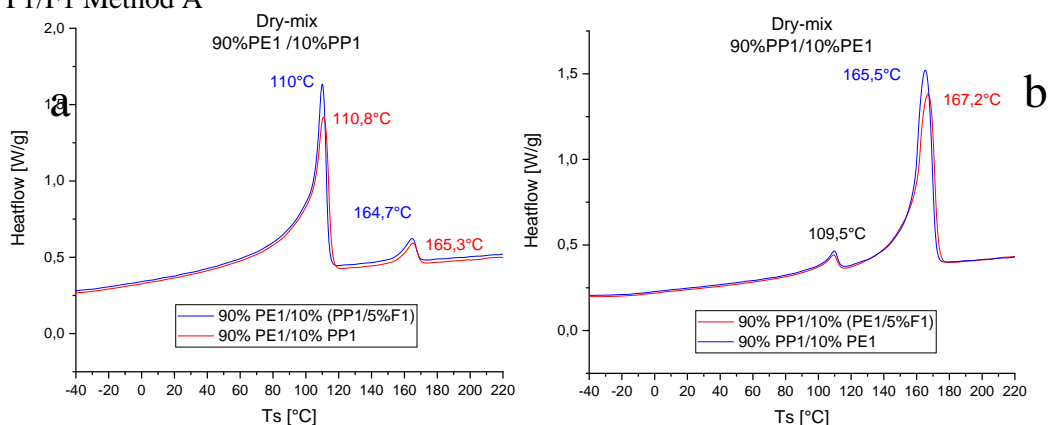


Figure 56, (a) DSC of a two polymer blend composites where one consisting of 90% PE1 and 10% PP1 and the other has 5 wt.% of filler F1 in the 10% PP1 phase. (b) DSC of a two polymer blend composites where one consisting of 90% PP1 and 10% PE1 and the other has 5 wt.% of filler F1 in the 10% PP1 phase. The manufacturing method was Method A

The Figure 56 above shows the melting peaks of polymer blends of 90:10 of both polymers PP1 and PE1 with and without filler F1 present in the 10% phase of respective polymer blend. We can see when comparing the pure polymer blends to the blends containing the filler F1 that the melting temperature does not change. Comparing the melting temperature with the pure components of each polymer phase we can see that they do not correspond to the 5 wt.% fraction of the 10% phase. The reason is that we would see a higher step height of the melting peak in the 10% phase if all of the filler remained in that smaller phase. Instead we see values that correspond to a composite which contains a 0.5 wt% filler concentration which is the total filler fraction of the blend. This makes sense since Method A preparation method mixes all components at the same time.

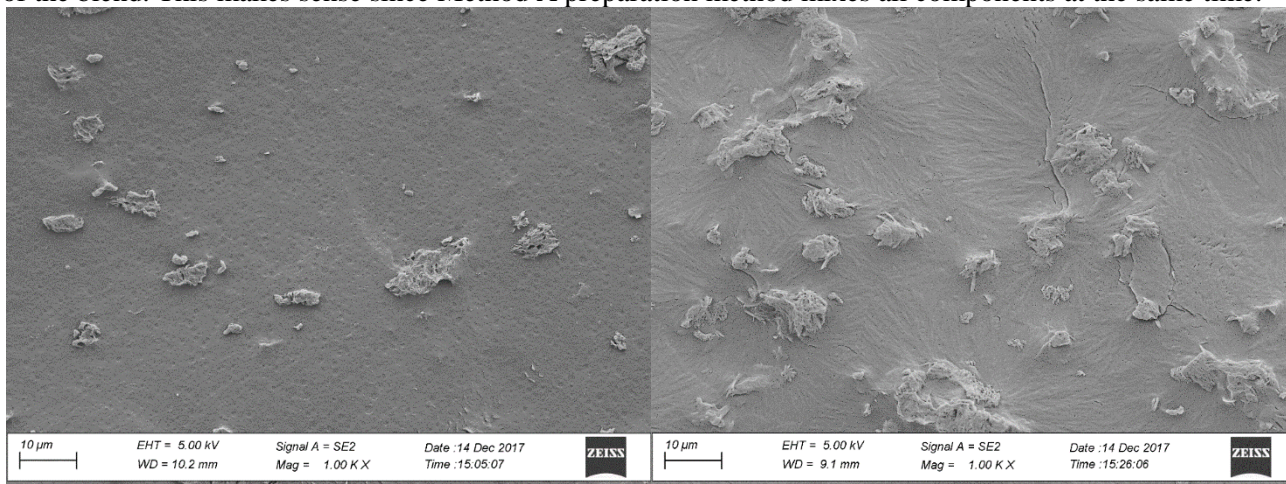


Figure 57, (a) SEM picture of a polymer blend of 90% PE1 10% (PP1/5wt% F1). The manufacturing was Method A, (b) SEM picture of a polymer blend of 90% PP1 10% (PE1/5wt% F1). The manufacturing method was Method A.

#### 4.5.2 PE1/PP1/F1 Method B

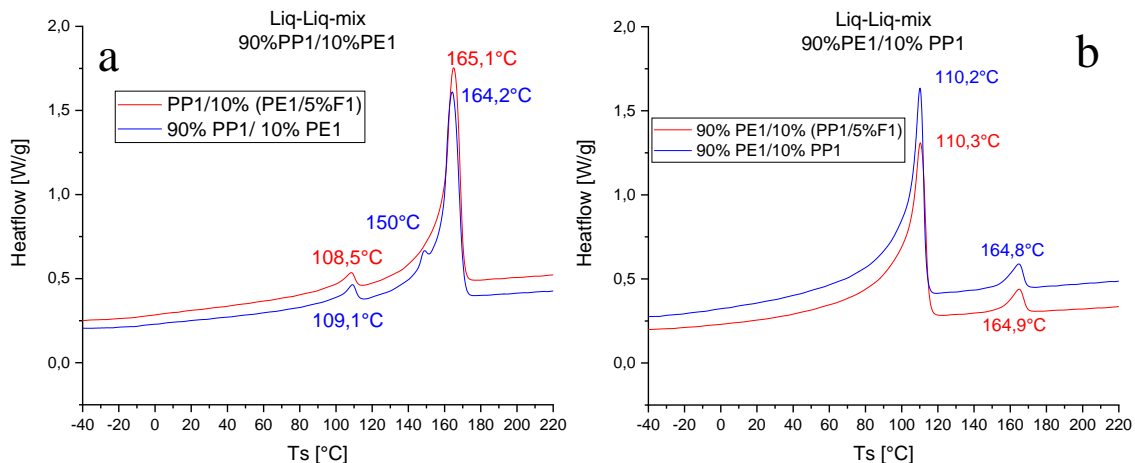


Figure 58, (a) DSC of a two polymer blend composites where one consisting of 90% PP1 and 10% PE1 and the other has 5wt% of filler F1 in the 10% PE1 phase. The manufacturing method was Method B  
 (b) DSC of a two polymer blend composites where one consisting of 90% PP1 and 10% PE1 and the other has 5wt% of filler F1 in the 10% PE1 phase. B. The manufacturing method was Method B

The figures above show the polymer blends of the same compositions as last time, however in this case the manufacturing method was different. In this case a single polymer was compounded together with filler F1 at a loading of 5 wt.%. Later the compounded composite was mixed together with the other pure polymer component in an extruder with a mixing screw to achieve a good liquid phase mixing of the two components. Looking at figure 58a we see the polymer blends of 90%PP1 and 10%PE1 and another blend that contains 5 wt.% of filler F1 in the PE1 phase. We can see that there is no change in melting temperature when the filler is present in the blend. There is a small peak at 150 °C that was later discovered to be an artefact, possible by some contamination from the compounding of the starting material.

In figure 49b we see the respective polymer blends of PE1/PP1 with a polymer ratio of 90:10. Similarly as the latter case there was no change in melting temperature when the filler F1 was present in the smaller phase. Neither the width nor the peak height changed for either polymer blend with the filler F1 present.

#### 4.5.3 PE1/PP1/F1 Method C

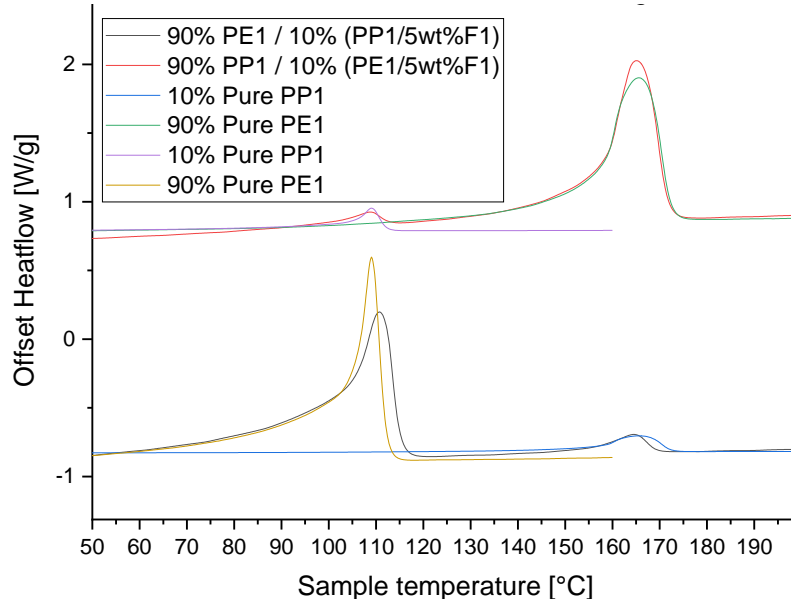


Figure 59, DSC curves of 90:10 and 10:90 blends of PE1 and PP1 with 5wt% of F1 in the 10% of respective phase. The manufacturing method was Method C.

In figure 59 we can see the polymer blends of PE1 and PP1 in different compositions and with the pure components of the respective polymer. The 90%PE/10%(PE1/5wt%F1) we can see that the pure polymer component of PP1 fits very well with the blend. The only difference is the peak height. The melting temperature remains the same for that blend. The smaller 10% of PE1 with 5wt% of F1 is a little broader and step height is lower than that of the pure component of PE1. The other blend is 90%PP1/10%(PE1/5wt%F1) and we can see that the pure component of PE1 is different than that of the PE1 component in the blend. The PE1 peak in the blend shifts by 1°C in melting temperature and the peak height is reduced. The peak has also broadened but the degree of crystallinity remains roughly the same.

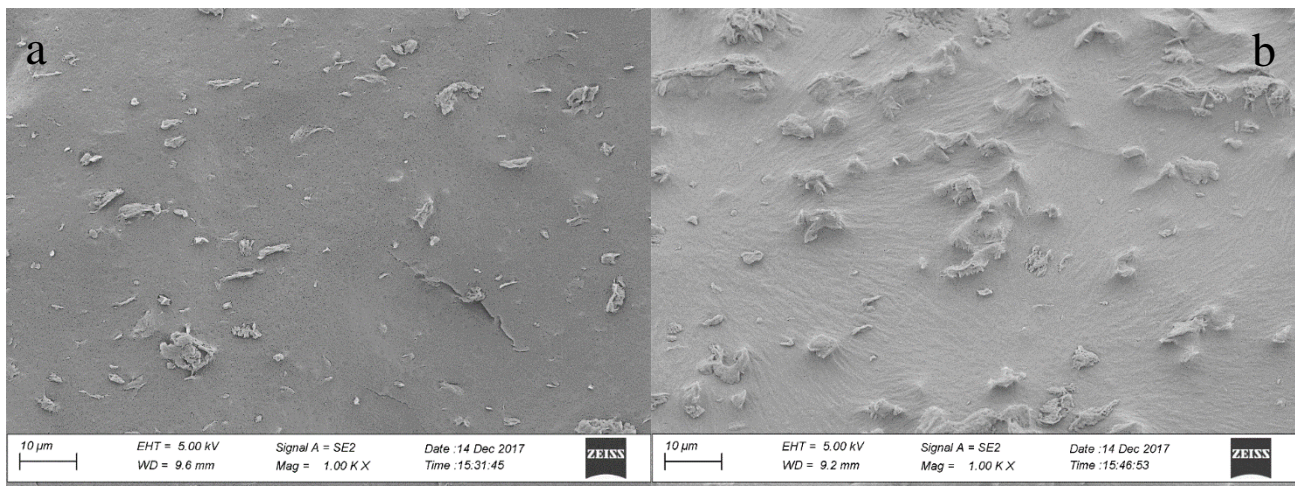


Figure 60, (a) SEM picture of a polymer blend of 90%PE1 10% (PP1/5wt% F1). The manufacturing method was Method., (b) SEM picture of a polymer blend of 90%PP1 10% (PE1/5wt% F1). The manufacturing method was chunk mixing.

Figure 60 shows two different blends of PE1 and PP1 where 5wt% of the 10% phase in each compound was present. When looking in a magnified picture of the composites we can see yet again that the filler particles tend to stay in the phase it was introduced in. It was observed from the SEM analysis that the filler seems to prefer to stay in the phase it was introduced in. When looking at SEM picture at a higher magnification we can see on several pictures that smaller particles are encapsulated in the introduced polymer phase. This occurs to respective polymer blend which suggests that the particles are not thermodynamically driven to a lower state of energy, rather driven effect of shear mixing.

## Sources of error

Generally, internal mixing chambers are regarded as equipment that easily get contaminated since they are usually used for many different polymers by different people. After each compounding, it is inevitable that some small traces will be left in the chamber nevertheless how well the instrument was cleaned. This residue will probably be introduced to the next compounding session in small traces which can affect the properties of the desired nanocomposite. The compounding time was found to be different depending on the type of filler that was used and also the amount that was added into the chamber through the use of the burette dispenser. Some fillers came in the form of powders while some other were already introduced into a masterbatch which greatly varied the compounding time. It was also found that at the higher filler loadings, the fillers that were in powder form were more difficult to incorporate towards the end. This is probably due to the change in viscosity of the polymer melt when the filler is incorporated, which makes it harder to mix with the remaining filler. This difference in time can affect the amount of degradation of the polymer since it is not in an oxygen free environment.

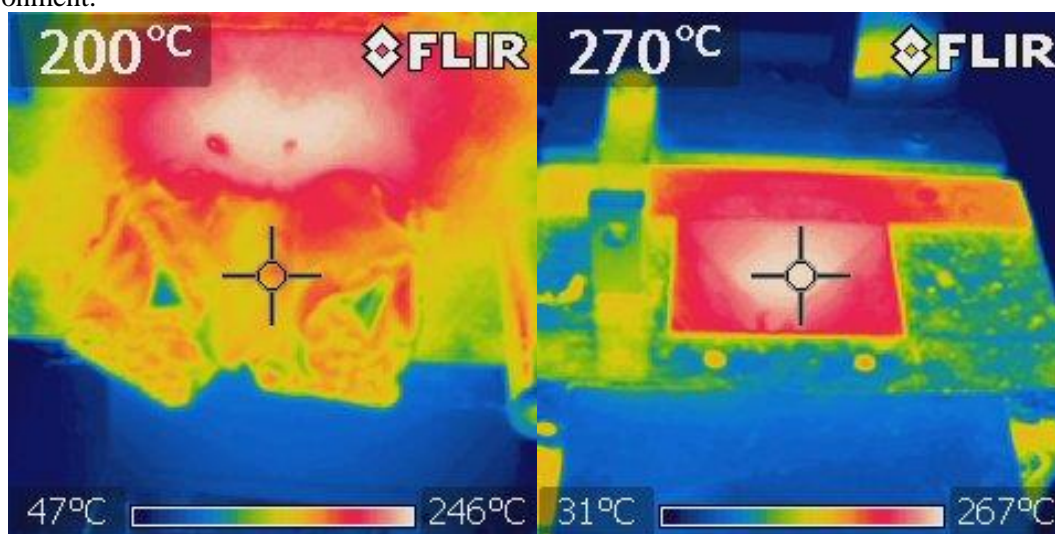


Figure 61, Thermal pictures of compounder. (a) Measurement of the melt directly after removal of chamber, (b) measurement of the backwall while compounding.

As seen in Figure 61 above, we can see in (a) that the direct temperature measurement after the removal of the chamber was precisely at the set temperature. However, in figure (b) we can see a hotspot of the backwall of the chamber which had a significant increase in temperature compared to the set temperature. Luckily the hotspot is a bit above the chamber, but when adding the polymer pellets into the mixer, some pellets will come in contact with this hotspot and the risk of degradation will be higher which can result as a contaminated composite.

As mentioned before, the measurement of electrical conductivity was done by using a precision multimeter, however it could only measure to a certain accuracy. This inaccuracy of measurement could affect the fitting of the percolation equation.

The thermogravimetric analysis was observed to only be able to measure filler contents down to 0,5wt.% which was expected. There is however more sensitive instrument that could be used for a more accurate reading for lower filler loadings.

When doing the DSC analysis, it was reported on different occasions that the instrument was not properly calibrated at some points. This has been observed in few samples, but some samples may have been overlooked and will give an inaccurate result.

The etchant that was used to etch the polymer samples was prepared with a potassium permanganate which was a bit outdated. It was observed in some SEM picture that the salt had not properly diluted which could result that the composite sample were not equally etched homogeneously.

## 5. Conclusion

The overall conclusion of the polyethylene-based composites is that the melting temperature increases slightly with increased filler content. While some PE composites show inconclusive trends, it is evident that most PE composites got affected in the same manner.

The composites with filler F1 had a trend of initially increased crystallization temperature at low filler content and then a decreased with increased filler loading. It was also observed that the polymers differ in their morphological structure even though they are all polyethylene-based composites. This is due to the difference of the matrices' different molecular structure.

The composite PE2/F4 had a more noticeable trend compared to the composites with filler F1. This is due to the filler F4 having a higher aspect ratio in respect to its density.

Alignment of filler F4 due to shear and elongational flow produced during the hot pressing was present in the PE2/F4 composite which might affect the electrical conductivity depending on the direction the electrical samples were cut.

The melting temperature of the polypropylene composites showed different results for the two different polypropylene matrices. PP1 showed an increase in melting temperature as a function of filler F1 loading while PP2's melting temperature initially decreased then increased with higher filler loading. The crystallization temperature ended up being different as well for the two polypropylene composites. PP1 with F4 increased substantially in crystallization temperature while PP2 had approximately the same crystallization temperature regardless of filler loading. This suggests that the two polymer matrices are very different in their molecular structure. The degree of crystallinity however showed similar results for both composites where the crystallinity initially increased and later decreased with increased amount of fillers present.

For single filler systems, it was evident that all fillers acted as a nucleating agent, however impaired the chain conformation of the polymer which in turn locally inhibited the crystallization kinetics which resulted as higher degree in crystallinity in low filler content but later lowered the crystallinity with higher filler content.

Hybrid systems of filler F1 with fillers F2 and F3 showed a synergetic effect where in both cases the electrical conductivity increased when 10 wt.% of filler F1 was replaced with either filler F2 or F3.

The crystallinity of the hybrid composites of PP1 with fillers F1, F2 and F3 had a parabolic trend in the degree of crystallinity as a function of filler ratio where the ratio of 50:50 of F1 with F2 or F3 reached a maximum degree of crystallinity.

Combining filler F1 with F4 in a polyethylene matrix can substantially reduce the electrical percolation threshold in respect to filler F1 alone. The filler ratio of 90:10 the maintained the same electrical conductivity as the single filler composite of PE2 with F4.

The electrical conductivity decreased only by 72% when substituting 50% of filler F4 with filler F1 which means that in respect to filler F1 the percolation threshold could decrease significantly compared to the single filler systems of F1.

The processing technique of chunk mixing was found to affect the dispersion and distribution of filler F1 in polyethylene/polypropylene blends. It was found that the composites had smaller agglomerates which suggests that the repeated mixing procedure seems to break up the filler agglomerates and more homogeneously disperse the particles than the other processing techniques.

There was no visible difference in morphology between the composites manufactured made by Method A nor Method B, however Method C showed an increase in filler dispersion. This may be due to the repeated process of compounding where the fillers have been under shearing for the double amount of time.

## Future work

For further development of this project, it would be interesting to see how well the theoretical predictions of the percolation threshold coincide with the real values. A suggestion would be to have a known filler with well-known properties combined with certain kinds of polymers and the use of a simulation program to predict the percolation threshold.

Hybrid composites showed very promising results which should perhaps be more focused in a future project. Tweaking the ratios and the types of filler by having smaller intervals of different concentrations could perhaps improve the composites' electrical conductivity which could be beneficial for the industry.

In literature, blend composites show great potential to significantly lower the electrical percolation threshold. By doing more extensive literature review one could perhaps find a study to improve upon by incorporating new types of filler such as those which were used in this project.

Method C showed that dispersiveness of the fillers increased when the composites were re-compounded. Perhaps further studies on the dispersiveness by initially incorporating the fillers to one of the two polymer components of a blend composite should focus on the mixing parameters.

## Bibliography

- [1] D. R. Paul and L. M. Robeson, "Polymer nanotechnology: Nanocomposites," *Polymer (Guildf)*, vol. 49, no. 15, pp. 3187–3204, 2008.
- [2] A. Tojeira, S. S. Biscaia, R. Q. Viana, I. S. Sousa, and G. R. Mitchell, *Controlling morphology in 3D printing: in "Controlling the morphology of polymers."* 2016.
- [3] P. J. S. G. Ashby, M. F. Schodek, Daniel L; Ferreira, *Nanomaterials, nanotechnologies and design: an introduction for engineers and architects*. Butterworth-Heinemann, 2009.
- [4] G. Nichols *et al.*, "A review of the terms agglomerate and aggregate with a recommendation for nomenclature used in powder and particle characterization," *J. Pharm. Sci.*, vol. 91, no. 10, pp. 2103–2109, 2002.
- [5] J. K. Nelson *et al.*, *Dielectric Polymer Nanocomposites*. Springer New York Dordrecht Heidelberg London.
- [6] P. Article, "Nmat1849-2 the Rise of Graphene," pp. 183–191.
- [7] M. Bhattacharya, "Polymer nanocomposites-A comparison between carbon nanotubes, graphene, and clay as nanofillers," *Materials (Basel)*, vol. 9, no. 4, pp. 1–35, 2016.
- [8] A. A. Vasileiou, M. Kontopoulou, and A. Docoslis, "A noncovalent compatibilization approach to improve the filler dispersion and properties of polyethylene/graphene composites," *ACS Appl. Mater. Interfaces*, vol. 6, no. 3, pp. 1916–1925, 2014.
- [9] G. Mittal, V. Dhand, K. Y. Rhee, S. J. Park, and W. R. Lee, "A review on carbon nanotubes and graphene as fillers in reinforced polymer nanocomposites," *J. Ind. Eng. Chem.*, vol. 21, pp. 11–25, 2015.
- [10] J.-B. Donnet, R. C. Bansal, and M.-J. Wang, *Carbon Black: Science and Technology*, Second edi. MARCEL DEKKER, INC, 1993.
- [11] I. J. Sanders and T. L. Peeten, *Carbon Black*. Nova Science Publishers, Incorporated, 2011.
- [12] J. B. Donnet, T. K. Wang, and J. C. M. Peng, *Carbon fibers*. 1998.
- [13] T. A. Osswald and G. Menges, *Materials Science of Polymers for Engineers, 3rd ed.* 2012.
- [14] "4.3 Mechanical Behavior - Knovel." [Online]. Available: <https://app.knovel.com/web/view/khtml/show.v/rcid:kt009AJ955/cid:kt009AJ9Y2/viewerType:khtml/r?id:pdf?page=11&view=collapsed&zoom=1>. [Accessed: 14-Mar-2018].
- [15] N. G. McCrum, C. P. Buckley, and C. B. Bucknall, *Principles of Polymer Engineering*, 2nd ed. 1997.
- [16] Ulf W. Gedde, *Polymer physics*. 1995.
- [17] P. Cebe *et al.*, "Heat of fusion of polymer crystals by fast scanning calorimetry," *Polym. (United Kingdom)*, vol. 126, pp. 240–247, 2017.
- [18] Y. Kong and Y. N. Hay, "The measurement of cristalinity of polymers by DSC," *Polymer (Guildf)*, vol. 43, no. 1, pp. 3873–3878, 2002.
- [19] M. Pyda, Ed., "Polypropylene (PP) Heat Capacity, Enthalpy, Entropy, Gibbs Energy: Datasheet from 'The Advanced THERMAL Analysis System (ATHAS) Databank – Polymer Thermodynamics' Release 2014 in SpringerMaterials (<https://materials.springer.com/polymerthermodynamics/docs>)." Springer-Verlag Berlin Heidelberg & Marek Pyda.
- [20] F. Lux, "Models proposed to explain the electrical conductivity of mixtures made of conductive and insulating materials," *J. Mater. Sci.*, vol. 28, no. 2, pp. 285–301, 1993.
- [21] Z. Rubin, S. A. Sunshine, M. B. Heaney, I. Bloom, and I. Balberg, "Critical behavior of the electrical transport properties in a tunneling-percolation system," *Phys. Rev. B*, vol. 59, no. 19, pp. 12196–12199, 1999.
- [22] C. Grimaldi and I. Balberg, "Tunneling and nonuniversality in continuum percolation systems," *Phys. Rev. Lett.*, vol. 96, no. 6, pp. 15–18, 2006.
- [23] I. Balberg, "Percolation Theory and Its Application in Electrically Conducting Materials," *Semicond. Polym. Compos. Princ. Morphol. Prop. Appl.*, pp. 145–169, 2012.
- [24] G. Ahmed and J. Blackman, "On theories of transport in disordered media," *J. Phys. C Solid State Phys.*, vol. 12, no. 1979, pp. 837–853, 1979.
- [25] Derek L. Ho, Robert M. Briber, and Charles J. Glinka, *Polymer Nanocomposites*, vol. 804. 2001.
- [26] G. Ambrosetti, C. Grimaldi, I. Balberg, T. Maeder, A. Danani, and P. Ryser, *Solution of the tunneling–percolation problem in the nanocomposite regime*, vol. 81, no. 15. p. 1–12.
- [27] I. Balberg, *Percolation Theory and Its Application in Electrically Conducting Materials*. p. 145–169.

- [28] G. Ambrosetti, C. Grimaldi, I. Balberg, T. Maeder, A. Danani, and P. Ryser, "Solution of the tunneling-percolation problem in the nanocomposite regime," *Phys. Rev. B - Condens. Matter Mater. Phys.*, vol. 81, no. 15, pp. 1–12, 2010.
- [29] C. W. Nan, "Physics of inhomogeneous inorganic materials," *Prog. Mater. Sci.*, vol. 37, no. 1, pp. 1–116, 1993.
- [30] A. Celzard, E. McRae, C. Deleuze, and M. Dufort, "Critical concentration in percolating systems containing a high-aspect-ratio filler," *Phys. Rev. B - Condens. Matter Mater. Phys.*, vol. 53, no. 10, pp. 6209–6214, 1996.
- [31] T. Gkourmpis, "Carbon-Based High Aspect Ratio Polymer Nanocomposites," *Nanosci. Comput. Chem.*, no. May, pp. 85–123, 2013.
- [32] A. Dasari, Y. Zhong-Zhen, and Y.-W. Mai, *Polymer Nanocomposites: Towards Multi-Functionality*. 2016.
- [33] H. Deng, L. Lin, M. Ji, S. Zhang, M. Yang, and Q. Fu, "Progress on the morphological control of conductive network in conductive polymer composites and the use as electroactive multifunctional materials," *Prog. Polym. Sci.*, vol. 39, no. 4, pp. 627–655, 2014.
- [34] R. M. Mutiso and K. I. Winey, "Electrical properties of polymer nanocomposites containing rod-like nanofillers," *Prog. Polym. Sci.*, vol. 40, no. 1, pp. 63–84, 2015.
- [35] J. R. Potts, D. R. Dreyer, C. W. Bielawski, and R. S. Ruoff, "Graphene-based polymer nanocomposites," *Polymer (Guildf.)*, vol. 52, no. 1, pp. 5–25, 2011.
- [36] "Ohm's Law," *Edited 2 April 2018, at 08:41. Referenced 8 May 2018*. [Online]. Available: [https://en.wikipedia.org/wiki/Ohm%27s\\_law](https://en.wikipedia.org/wiki/Ohm%27s_law).
- [37] M. M. Shahin, R. H. Olley, and M. J. Blissett, "Refinement of etching techniques to reveal lamellar profiles in polyethylene banded spherulites," *J. Polym. Sci. Part B Polym. Phys.*, vol. 37, no. 16, pp. 2279–2286, 1999.